Studies on the development of a new type of heterogeneous photocatalysis(Dissertation_全文)

AUTHOR(S):

Teramura, Kentaro

Studies on the Development of a New Type of Heterogeneous Photocatalysis

KENTARO TERAMURA

2004

Studies on the Development of a New Type of Heterogeneous Photocatalysis

KENTARO TERAMURA

Department of Molecular Engineering
Graduate School of Engineering
Kyoto University

2004

Preface

The progress of "photocatalyst and photocatalysis" has realized commercialization of "TiO_2 photocatalyst" as an air purifier, a deodorization filter, a refrigerator, walls and window glass of a room, a soundproofed wall of highway, a side mirror of automobiles, etc. Although the photocatalyst is now familiar to the science society as well as the general public, we should be aware of the fact of no establishment of either chemical plants or processes using "photocatalyst and photocatalysis". This is due to the limitation of the intrinsic function of "TiO_2 photocatalyst". It can catalyze only the complete oxidation of extremely dilute organic compounds and its absolute activity is very poor.

It was since 1970 that the photocatalyst and photocatalysis has been of the scientific interest. The first attention was paid to photoassisted electrolysis of water with a TiO_2 photoelectrode reported by Honda and Fujishima. The water photoelectrolysis could be understood by regarding the titania as a photochemical micro-cell. This is an application of semiconductor band theory. After that, the principle of photocatalysis has been explained in terms of electrochemistry. It is donated by the flat band potentials of titania semiconductor where photoformed electrons and holes lie. In other words, it can be described by the thermodynamical quantity called chemical potentials although it deals with kinetic phenomena like catalytic reactions. The photoelectrolysis of water can be explained electrochemically and has been developed by understanding the band structure of the semiconductors. However, to develop the other chemical reactions like chemical synthesis, complete oxidation, etc., the kinetic considerations and the geometrical knowledge of the reaction sites are required. The photocatalytic reaction is always under the control of rates of adsorption of substrate, formation of intermediate and desorption of product. The difference of photocatalysis from ordinary catalysis is that a photoformed pair of electron and positive hole participates in some elementary steps. The author would like to insist that important is the deep understanding and the insight of the mechanism of photocatalyses and the design of the photocatalytic system on its basis. On this stance, the author commenced the study of photocatalyses.

The main themes in the present thesis are the elongation of a lifetime of charge separation for the realization of the high photocatalytic activity and the specification of active species for the design of the elegant catalytic selectivity.

The studies presented in this thesis were carried out at Department of Molecular Engineering, Graduate School of Engineering, Kyoto University from 2001 thorough 2004 under the supervision of Professor Takuzo Funabiki. The author wishes to express his sincere gratitude to Professor Takuzo Funabiki for his guidance, philosophical suggestion and continual encouragement throughout this work. In addition, the author should make special acknowledgements to Associate Professor Tsunehiro Tanaka for his grateful guidance, valuable suggestions, fruitful discussions, strict but heartwarming advices and careful reviewing of the manuscripts. Grateful thanks should be made to Dr. Yutaka Hitomi for his helpful advices and pointed suggestions. The author is deeply grateful to two seniors of his laboratory, Dr. Takashi Yamamoto at Tokyo Institute of Technology and Dr. Yoshiumi Kohno at Shizuoka University for their useful advices to experiment, instructive suggestions, and exact discussions concerned to this study, in addition to continual encouragement throughout this work. Special thanks should be made to Associate Professor Kohki Ebitani at Osaka University, Associate Professors Hisao Yoshida and Tomoko Yoshida at Nagoya University, Mr. Yasutaka Nagai at Toyota Central R&D Labs., Inc., Associate Professor Tetsuya Shishido at Tokyo Gakugei University, Lecturer Hirofumi Aritani at Saitama Institute of Technology and Dr. Sakae Takenaka at Tokyo Institute of Technology for their encouragement and valuable discussions at the conferences, and helpful suggestions and assistance for measurements and analyses of XAFS spectra. The author shows gratitude to the staffs of Photon Factory at KEK in Ibaraki prefecture and of Spring-8 at JASRI in Hyogo prefecture for measurement of XAFS although XAFS studies are not published in this thesis. The author wishes to express his sincere gratitude to Professor Yuan Kou at Peking Unversity in China for his heartwarming hospitality and valuable discussion when I stayed in Beijing, China to analyze XAFS spectra. Lecturer Hiroshi Kominami at Kinki Unversity, and Dr. Shinji Iwamoto and Professor Masashi Inoue at Kyoto Unversity are acknowledged for their kind

offer of HYCOM sample and high surface area TiO_2, respectively. In addition, the author is deeply grateful to Catalysis Society of Japan, Ishihara Sangyo Kaisya Ltd., TAYCA Co., Zeon Co. and Fuji Silysia Chemical Ltd. for offering samples. Special acknowledgement must be made to Professor emeritus of Kyoto University Satohiro Yoshida for his continual encouragement throughout this work.

The author is also indebted to Ms. Kyoko Arakaki and Mr. Seiji Yamazoe who have cooperated the photo-SCR described in part I, Messrs. Masaya Kani, Tomohiro Hosokawa and Tai Ohuchi who have cooperated the selective photo-oxidation of hydrocarbons described in part II and Ms. Haruka Ishikawa who has cooperated the photocatalytic reduction of CO_2 described in part III for their collaboration and instructive discussions about this work. Thanks should be made to Secretary Ms. Ayako F. Matsuoka for her kind official supports. The author is grateful to all the members of the group of catalysis research led by Professor Funabiki.

Finally, the author sincerely thanks his parents Hidenori and Mayumi, his grandparents Kohjiro and Michiko, and his younger brother Shintaro for their understanding and heartwarming encouragement.

Kentaro Teramura

Kyoto,

October, 2003

CONTENTS

Preface
Contents
General introduction ---------- 1

Part I **Photoassisted selective catalytic reduction of NO with NH_3 in the presence of O_2 over heterogeneous catalysts**

Introduction of Part I ---------- 12

Chapter 1. Photoassisted selective catalytic reduction of NO with NH_3 in the presence of O_2 over Rb_2O-V_2O_5/SiO_2 ---------- 17
Chapter 2. Reaction and kinetic study for photoassisted selective catalytic reduction of NO over TiO_2 ---------- 25
Chapter 3. Identification of surface intermediate on TiO_2 by FT-IR spectroscopy ---------- 41
Chapter 4. Photoinduced electron transfer between adsorbent and adsorbed species ---------- 61

Part II **Selective photo-oxidation of hydrocarbons in the liquid phase over supported vanadium oxides**

Introduction of Part II ---------- 74

Chapter 5. Selective photo-oxidation of cyclohexane over various supported vanadium oxide catalysts ---------- 81
Chapter 6. Identification of reaction mechanism of selective photo-oxidation of cyclohexane over V_2O_5/Al_2O_3 ---------- 89
Chapter 7. Selective photo-oxidation of hydrocarbons over V_2O_5/Al_2O_3 ---------- 109

Part III **Photocatalytic reduction of CO_2 to CO in the presence of H_2 or CH_4 as a reductant over MgO** ---------- 123

Summary ---------- 153
List of publications ---------- 161

General introduction

Historical consideration of photocatalyst and photocatalysis

Nowadays, it might be generally understood that the historic curtain of "photocatalyst and photocatalysis" was raised by Honda and Fujishima in 1971. In particular, those who are occupied in the development of water electrolysis over photocatalyst tend to state this strongly.[1-3] This is only a one-sided view of "photocatalyst and photocatalysis". The author does not doubt that the breakthrough by Honda and Fujishima, so called "Honda-Fujishima effect"[4,5], promotes a progress of "photocatalyst and photocatalysis"; i.e., irradiation of a titanium dioxide (TiO_2) electrode connected with Pt as a counter electrode produces O_2 and H_2 from water by applying very low bias voltage. Thus, at first, Honda and Fujishima mentioned this phenomenon from an electrochemical standpoint. After that, this system was applied to the TiO_2 powder loading Pt, which was recognized as that the Pt-TiO_2 photocatalyst is equivalent to the micro-photoelectrochemical cell. Using this micro-electrochemical cell, numerous photocatalytic systems have been contrived and attempted so far as an application of electrochemistry. However, recently, central matter of interest and concern returned again to the photocatalytic capability of bare TiO_2 itself. Before the discovery of Honda-Fujishima effect, many catalysis researchers have uncovered and developed some semiconductor photocatalysts. Actually, in some reviews dealing with semiconductor photocatalysts, the reviewers did not attach importance to Honda-Fujishima effect.[6-8] In particular, the effect does not relate to the application for abatement and removal of pollutants in the environmental atmosphere and waters although this application is a main theme of semiconductor photocatalyst.

The history of "photocatalyst and photocatalysis" goes back to the 1920's. In 1927, Baur[9] reported the formation of hydroperoxide over irradiated ZnO. During 1950's when the semiconductor band theory had risen to be popular, some research groups investigated that inorganic gases such as O_2 are adsorbed on and desorbed from semiconductor materials under photoirradiation.[10,11] As mentioned above, Honda and Fujishima[4,5] found out the water electrolysis by use of the Pt and TiO_2 photoelectrodes in 1971 when it was the age of oil crisis.

After that, many extensive studies on "photocatalyst and photocatalysis" have been carried out and reported. A characteristic point is that the water electrolysis over photocatalysts has been developed mainly in Japan. Bart et al.[12] and Sato et al.[13,14] found the water electrolysis over Pt/TiO_2 photocatalyst under a special condition. Domen et al.[15,16] first designed and realized the photocatalytic system for splitting water to H_2 and O_2 stoichiometrically. At the present time, the development of visible-light-driven photocatalysts is the main theme for the water electrolysis and it is led by the Japanese research groups.[17-21] On the other hand, some research groups have investigated to apply the semiconductor photocatalysts to various reactions. From 1970's to 1980's, the photocatalytic reduction of CO_2[22,23] and NOx[24] were widely investigated. In addition, some groups proposed the ammonia photosynthesis from N_2 and H_2 although no one has been confirmed the reaction until now.[25-27] These reactions exhibit too little activity, that is highly disadvantageous. Accordingly, a limited number of reports has appeared recently. In 1980's, some research groups applied TiO_2 photocatalyst to the selective oxidation of various hydrocarbons. However, many researchers understand currently that over TiO_2, hydrocarbons are oxidized deeply to CO_2 under photoirradiation. Therefore, it is well-known that TiO_2 photocatalyst is applied to the total oxidation of harmful organic compounds (i.e., dioxin compounds, endocrine disrupters and volatile organic compounds (VOCs)). Consequently, nowadays, the two streams of the water electrolysis over visible-light-driven photocatalysts and the removal of harmful compounds by oxidative mineralization over TiO_2 almost occupy the field of "photocatalyst and photocatalysis".

Excitation mechanism

The photocatalytic reaction mechanism has been seldom clarified in detail although many photocatalytic reactions have been reported up to the present. The reaction mechanism is often explained according to the classical electron transfer theory, a formation of excited electron (e^-) in the conduction band and the positive hole (h^+) in the valence band; i.e., electron transfer involved in various photocatalytic reactions from lattice oxygen to metal cation (for example, in the case of TiO_2, from lattice oxygen to Ti^{4+}). The author believes that the electron transfer caused by band gap irradiation is only a first order approximation of the

reaction mechanism. It is not always necessary that the electron transfer takes place between metal and lattice oxygen. Adsorbed species may play a role as an electron source or a positive hole source. In this thesis, the author focuses on clarification of the reaction schemes in the photocatalytic reactions and on control of the electron transfer brought about by photoirradiation. But before summarizing this thesis, the author will discuss on the disadvantages of TiO_2 photocatalyst and describe how the problems are solved when TiO_2, alternative supported photocatalysts and insulators are used as photocatalysts.

Diagnostics of disadvantage of TiO_2 as a photocatalyst

(1) No capability of selective oxidation

Here, the author tries to describe the possible elementary steps proceeding over TiO_2 in the presence of oxygen and discusses what is the disadvantage of TiO_2 when it is used for selective oxidation. The initial reaction is the formation of an electron and a positive hole in TiO_2. Of the both, elementary steps which the electron concerns are three consecutive processes. Each of the process is accompanied with the formation of active oxygen species. The first reaction is the reduction of an oxygen molecule by electron to form ionosorbed O_2^- species. The second is the cleavage of O_2^- by the reaction with the positive hole resulting in the formation of neutral atomic oxygen. The last is the reaction between atomic oxygen and the electron. The various active oxygen species are generated in each process. These are represented by the following formulae;

$$h\nu \longrightarrow h^+ + e^- \quad (1)$$

$$O_2 + e^- \longrightarrow O_2^-(ads) \quad (2)$$

$$O_2^-(ads) + h^+ \longrightarrow 2O(ads) \quad (3)$$

$$O(ads) + e^- \longrightarrow O^-(ads) \quad (4)$$

Subsequent consideration is on the reactions brought about by positive holes. The positive hole is trapped by a surface hydroxyl group or a lattice oxygen atom to produce a hydroxyl radical or O^-(lattice), respectively. In addition, O^-(lattice) is easily interacted with O_2 molecule to form O_3^-(ads). The elementary steps are described below;

$$h^+ + OH \longrightarrow \cdot OH(ads) \quad (5)$$

$$h^+ + O^{2-}(\text{lattice}) \longrightarrow O^-(\text{lattice}) \quad (6)$$

$$O^-(\text{lattice}) + O_2 \longrightarrow O_3^-(\text{ads}) \quad (7)$$

As described above, many kinds of active oxygen species with quite different reactivity are generated on TiO_2 under photoirradiation in the presence of O_2, and therefore, selective oxidation of organic compounds can not be realized. Moreover, a somewhat large organic molecule should be adsorbed on TiO_2 at multiple sites and the multi-centered adsorption causes the multi-electronic oxidation and the consecutive oxidation. The photo-oxidation process is destined to proceed consecutively and/or non-selectively. We can assert that TiO_2 is suitable for the oxidative decomposition of organic compounds (the deep oxidation to CO_2). Consequently, it is impossible to realize the selective photo-oxidation process over TiO_2 at all.

(2) Restriction of excitation wavelength by band-gap energy.

It is well-known that the band-gap energies of anatase and rutile are 3.2 and 3.0 eV, respectively. This means that anatase and rutile can not utilize the light with wavelength longer than 388 and 413 nm, respectively. Therefore, we can utilize only a trace amount of wavelength of sunlight as long as TiO_2 is used. Recently, it was reported that N-doped TiO_2 exhibits the absorption in visible light domain.[28] Some research groups claimed that a new donor band consisting of N 2p orbitals is located at higher energy level than the original valence band consisting of O 2p orbitals, resulting in the reduction in band gap energy. However, we can not tell the change of electronic band structure by N-doping from the spectral feature. The appearance of a shoulder peak at the absorption edge by N-doping suggests the formation of the new donating impurity level. There is no evidence that the N-level is delocalized. Actually, there have been no reports yet that visible light illumination of N-doped TiO_2 causes a high quantum yield.

(3) Extremely low activity

Ibusuki et al.[29-32] reported that benzene as a model VOCs (volatile organic compounds) in the feed stream can be abated by total oxidation over TiO_2 photocatalyst very effectively. However, they also reported that 120 ppm of benzene can not be removed over

irradiated TiO_2 although 80 ppm of benzene is efficiently decomposed to form CO_2 (selec., 93 %) and CO (7 %) in the presence of water vapor. This suggests that specific activity of TiO_2 is absolutely small. This result is caused by the insufficient charge separation in TiO_2. The photoformed electrons and holes are consumed by recombination much more rapidly than by the photocatalytic reaction. The recombination is the main reason of too short lifetime of the excited state and poor activity of TiO_2. Ohtani et al.[33,34] investigated the recombination step in detail with a fsec-pulse laser irradiation to TiO_2 and found that the decay curve of consumption of electron-hole pairs can be fitted with a quadratic function. Although the decay curve is different from an exponential function, the half life could be estimated to be in the order of nsec. They also found that the recombination takes place at the defect site of lattice oxygen. In order to enhance the activity, some research groups prepared the TiO_2 with high crystallinity to suppress the formation of defect sites at minimum and the others synthesized the TiO_2 with high specific surface area to increase the active surface.[35] However, the limit of the extended lifetime of the excited state is only several tens of nsec despite the careful efforts.

Tactics of the evolution of photocatalyst and photocatalysis

(1) Realization of selective photooxidation of hydrocarbons

The author applied highly dispersed metal oxide catalyst supported on insulating carrier to selective oxidations in place of TiO_2. It is known that supported mononuclear oxo metalate exhibits photocatalytic activity.[36] The so-called excited mechanism is initiated by the formation of electron-hole pair in the specific metal-oxo bond. The oxo metalate ions are also isolated and work as active sites where the substrate is adsorbed like a ligand of complex. In this case, multi-electronic oxidation hardly occurs and therefore, it is difficult that the consecutive oxidation proceeds over highly dispersed supported transition metal oxides. In addition, because the energy does not get scattered or lost between metalates and insulating carrier and between each metalate ions, the excited states exhibit the long lifetime, more than msec which is 10^6 times longer than that observed for TiO_2. The stability of the excited state of surface metalate compensates the low density of the active sites sufficiently. Furthermore,

addition of some ingredients alters the electronic structure of the metalate anion and consequently controlling the effective wavelengths are expected to be possible.

(2) Controlling the effective wavelengths

Because the photocatalytic process must include adsorption and excitation of substrate, the author thinks that the adsorbate itself can act as a donor or an acceptor. To prove this, the author selected the reduction of carbon dioxide as a model reaction. The reduction potential of carbon dioxide is more negative than that of H^+/H_2 and therefore even single-electron reduction is quite difficult. This means that lowest unoccupied molecular orbital (LUMO) of carbon dioxide lies at high energy side. But, if the O-C-O bond angle is less than 180 degree, the LUMO level becomes stabilized. It is known that the O-C-O bond angle is bent when carbon dioxide is adsorbed on solid base. We adopted MgO and ZrO_2 as an adsorbent for carbon dioxide and irradiated UV-ray to the sample. Very clear CO_2^-. radical was observed by EPR experiment. The radical species is fairly stable and it can be readily reacted with H_2. The signal of the CO_2^-. radical can be observed after the illumination of the UV light with the wavelength at 330 nm, which corresponds to much lower photon energy than the band gap energy of MgO and ZrO_2. In this case, the LUMO level of adsorbed carbon dioxide lies between conduction and valence band flat potentials and carbon dioxide itself works as an electron acceptor. Thus, in situ doping of CO_2 to insulator or semiconductor can take off the restriction of the band gap energy irradiation.

(3) Enhancement of activity by improvement of charge separation

An NH_2 radical on TiO_2 was used for the present purpose. It is known that UV-illumination to various metal oxides having adsorbed NH_3 brings about the formation of NH_2 radical.[37-40] This may suggest that the adsorbed NH_3 captures the positive hole and release the proton under photoirradiation. In the case of TiO_2, EPR spectrum of the irradiated sample shows the formation of not only the NH_2 radical but also the Ti^{3+} radical. These signals are very stable and are not decayed for an hour at 100 K. Contact of NO with the catalyst quenched the signal of the NH_2 radical leaving the Ti^{3+} signal. The presence of the

long-lived NH_2 radical shows that the recombination of electrons and holes is suppressed by fixation of holes on the amide species resulting in the improvement of charge separation. In the present case, we observed that 1000 ppm of NO was consumed per a min by contact with the NH_2 radicals. Taking into account that the results of Ibusuki et al., the reaction rate of our photocatalytic system is 100 times faster than the ordinary oxidation over TiO_2 photocatalyst.

Survey of the present thesis

In this thesis, the author adopted three reactions to attempt to clarify and solve the problems which TiO_2 photocatalyst exhibits.

In part I, photo-SCR of NO with NH_3 in the presence of O_2 will be dealt with. The author shows that the activity of TiO_2 can be enhanced to be high enough for practical use. To develop and optimize the reaction system more, the detailed mechanism is inspected and verified. As a result, the NH_2 radicals which are formed by capturing photo-formed positive holes by adsorbed ammonia play a significant role in the long-lived charge separation. The utilization of the active species could be a great hint for development of a new type of photocatalytic systems.

In part II, chapters concerning photo-assisted liquid phase oxidation of hydrocarbons over supported oxo-metalate ions will be compiled. Highly dispersed metal oxide over insulator metal oxide with high specific surface area exhibits high activity for selective oxidation. Because the surface metalate anion used in this part is monomeric and isolated, the excited state like an excitation arising in TiO_2 semiconductor has very long lifetime as energy does not get scattered or lost. Therefore, the supported oxo-metalate ions exhibit high catalytic activity. In addition, since only a single electron excitation takes place, consecutive oxidations which usually proceed over TiO_2 photocatalyst hardly occur and promote the selective oxygenation of hydrocarbons. Here, the author will discuss the detailed mechanism.

In part III, the new type of "photocatalytic reaction" will be discussed. The in situ acceptor level can be created in the forbidden band by adsorption of CO_2. The reduction potential of CO_2 is found at very low level but the LUMO gets lower as the OCO angle becomes less than 180 degrees. A CO_2 molecule is known to be bent when an acidic CO_2

molecule is adsorbed on the solid base. Consequently, the adsorbed CO_2 acts as an electron acceptor over the solid base. The author shows that alkaline earth metal oxides and ZrO_2 oxide doped by CO_2 can work as "photocatalyst" active against 330 nm irradiation for reduction of CO_2. This chapter suggests the possibility of control of the limit of band-gap energy and the importance of electron transfer.

References

(1) Mills, A.; Davies, R. H.; Worsley, D. *Chem. Soc. Rev.* **1993**, *22*, 417.

(2) Linsebigler, A. L.; Lu, G.; Yates Jr., J. T. *Chem. Rev.* **1995**, *95*, 735.

(3) Fujishima, A.; Rao, T. N.; Tryk, D. A. *J. Photochem. Photobiol. C-Photochem. Rev.* **2000**, *1*, 1.

(4) Fujishima, A.; Honda, K. *Bull. Chem. Soc. Jpn.* **1971**, *44*, 1148.

(5) Fujishima, A.; Honda, K. *Nature* **1972**, *238*, 37.

(6) Fox, M. A.; Dulay, M. T. *Chem. Rev.* **1993**, *93*, 341.

(7) Pichat, P. *Catal. Today* **1994**, *19*, 313.

(8) Hoffmann, M. R.; Martin, S. T.; Choi, W. Y.; Bahnemann, D. W. *Chem. Rev.* **1995**, *95*, 69.

(9) Baur, E. *Helv. Chim. Acta* **1927**, *22*, 261.

(10) Freund, T.; Gomes, W. P. *Catal. Rev.* **1969**, *3*, 1.

(11) Wolkenstein, T. *Adv. Catal.* **1973**, *23*, 157.

(12) Bart, A. J. *J. Photochem.* **1979**, *10*, 59.

(13) Sato, S.; White, J. M. *Chem. Phys. Lett.* **1980**, *72*, 83.

(14) Sato, S.; White, J. M. *J. Am. Chem. Soc.* **1980**, *102*, 7206.

(15) Domen, K.; Naito, S.; Onishi, T.; Tamaru, K. *Chem. Phys. Lett.* **1982**, *92*, 433.

(16) Domen, K.; Naito, S.; Onishi, T.; Tamaru, K. *J. Phys. Chem.* **1982**, *86*, 3657.

(17) Takata, T.; Tanaka, A.; Hara, M.; Kondo, J. N.; Domen, K. *Catal. Today* **1998**, *44*, 17.

(18) Domen, K.; Kondo, J. N.; Hara, M.; Takata, T. *Bull. Chem. Soc. Jpn.* **2000**, *73*, 1307.

(19) Zou, Z. G.; Arakawa, H. *J. Photochem. Photobiol. A-Chem.* **2003**, *158*, 145.

(20) Kato, H.; Kudo, A. *Catal. Today* **2003**, *78*, 561.

(21) Kudo, A. *Catal. Surv. Asia* **2003**, *7*, 31.

(22) Hemminger, J. C.; Carr, R.; Somorjai, G. A. *Chem. Phys. Lett.* **1978**, *57*, 100.

(23) Inoue, T.; Fujishima, A.; Konishi, S.; Honda, K. *Nature* **1979**, *277*, 637.

(24) Courbon, H.; Pichat, P. *J. Chem. Soc., Faraday Trans. 1* **1984**, *80*, 3175.

(25) Schrauzer, G. N.; Guth, T. D. *J. Am. Chem. Soc.* **1977**, *99*, 7189.

(26) Dickson, C. R.; Nozik, A. J. *J. Am. Chem. Soc.* **1978**, *100*, 8007.

(27) Miyama, H.; Fujii, N.; Nagae, Y. *Chem. Phys. Lett.* **1980**, *74*, 523.

(28) Asahi, R.; Morikawa, T.; Ohwaki, T.; Aoki, K.; Taga, Y. *Science* **2001**, *293*, 269.

(29) Einaga, H.; Futamura, S.; Ibusuki, T. *J. Jpn. Petrol. Inst.* **1999**, *42*, 363.

(30) Einaga, H.; Futamura, S.; Ibusuki, T. *PCCP Phys. Chem. Chem. Phys.* **1999**, *1*, 4903.

(31) Einaga, H.; Futamura, S.; Ibusuki, T. *Syokubai* **2000**, *42*, 145.

(32) Einaga, H.; Futamura, S.; Ibusuki, T. *Appl. Catal. B-Environ.* **2002**, *38*, 215.

(33) Ikeda, S.; Sugiyama, N.; Pal, B.; Marci, G.; Palmisano, L.; Noguchi, H.; Uosaki, K.; Ohtani, B. *Phys. Chem. Chem. Phys.* **2001**, *3*, 267.

(34) Ikeda, S.; Sugiyama, N.; Murakami, S.; Kominami, H.; Kera, Y.; Noguchi, H.; Uosaki, K.; Torimoto, T.; Ohtani, B. *Phys. Chem. Chem. Phys.* **2003**, *5*, 778.

(35) Kominami, H.; Murakami, S.; Kato, J.; Kera, Y.; Ohtani, B. *J. Phys. Chem. B* **2002**, *106*, 10501.

(36) Maldotti, A.; Molinari, A.; Amadelli, R. *Chem. Rev.* **2002**, *102*, 3811.

(37) Vansant, E. F.; Lunsford, J. H. *J. Phys. Chem.* **1972**, *76*, 2716.

(38) Brotikovskii, O. I.; Zhidomirov, G. M.; Kazanskii, V. B.; Mashchenko, A. I.; Shelimov, B. N. *Kinet. Katal.* **1971**, *12*, 616.

(39) Nagai, S. *Bull. Chem. Soc. Jpn.* **1973**, *46*, 1144.

(40) Shimamoto, N.; Hatano, K.; Katsu, T.; Fujita, Y. *Bull. Chem. Soc. Jpn.* **1975**, *48*, 18.

Part I

Photoassisted selective catalytic reduction of NO with NH_3 in the presence of O_2 over heterogeneous catalysts

Introduction of Part I

NO*x* exhausted from the stationary emission source and the mobile emission source has been warned to be a possible agent of town smog and acid rain. Of the NO*x* emission sources, the main one is a combustion system such as a boiler, an engine, *etc.* because combustion of N_2 at high temperature results in the formation of NO*x*. Therefore, NO*x* should be eliminated at outlet of the combustion system although the presence of water and air obstructs the achievement. However, two catalytic NO*x* removal systems are operated under cruel conditions. One is the three-way catalyst system equipped in the mobile emission source and the other is selective catalytic reduction of NO with NH_3 (NH_3-SCR) system located in the stationary source. In the case of these systems, NO*x* removal rate is more than 90 %. However, it is desirable to develop a new catalyst system fulfilled the recent strict environmental standard.

In this part, the author kept his eyes on the NH_3-SCR system. In the stationary emission sources such as power stations, waste incinerators and industrial boilers, NO*x* in the exhaust gases are removed ordinarily by the selective catalytic reduction system with NH_3 (NH_3-SCR) in the presence of O_2 from 573 K to 673 K over V_2O_5-WO_3/TiO_2 or MoO_3-WO_3/TiO_2 catalysts.[1-4] In 1967, Markvart and Pour reported firstly that the presence of O_2 makes the operation temperature of catalyst (Pt/Al_2O_3) fall down in the NO reduction with NH_3.[5] They predicted that O_2 promotes desorption of adsorbed NH_3 species. After that, V_2O_5/TiO_2 catalyst uncovered in 1970's achieved practical NO conversion and N_2 selectivity.[6,7] The NH_3-SCR system was established by three Japanese corporations (Hitachi, Ltd., Babcock-Hitachi K.K., Mitsubishi Petrochemical Corp.). It was confirmed that O_2 also participates in the NH_3-SCR over V_2O_5/TiO_2 as another oxidant. The reaction stoichiometry in the typical NH_3-SCR condition was determined as follows;

$$4NO + 4NH_3 + O_2 \longrightarrow 4N_2 + 6H_2O \qquad (1)$$

Many research reports supported that the typical NH_3-SCR system proceeds according to Eley-Rideal mechanism. Therefore, NO in the gas phase attacks the adsorbed NH_3 species. Two research groups proposed different adsorbed NH_3 species and reaction

schemes based on Eley-Rideal mechanism. Ramis et al.[8,9] proposed that Lewis acid sites of the vanadium centers are the active sites and that the NH_2NO species is formed as an intermediate in these sites. On the other hand, Topsøe et al.[10-12] proposed that acid site (V^{5+}-OH) and redox sites (V^{5+}=O) are concerned in essentially two separate catalytic functions, and the NH_2NO species was identified by infrared spectroscopy. However, the definitive mechanism has not been reported yet.

The requested feature of the NH_3-SCR system at the present stage is described as follows;

1. NO*x* must be removed at high conversion rate (more than 90 %).
2. Compounds including N atoms are hardly formed except N_2.
3. Catalysts must have strong durability to SO*x*.
4. Catalysts must have considerable durability to H_2O.
5. The system must be operated in the presence of excess O_2.

In the case of the waste incinerators, the exhaust gas contains SO*x*, halogen compounds, particulate materials (PM) and fly ash as well as NO*x*. The de-NO*x* process is often located at downstream of de-halogen and/or de-SO*x* processes to prevent catalysts from rapid deactivation by strong adsorption of halogen compounds and highly concentrated SO*x*. However, most de-halogen and de-SO*x* processes are operated on the bases of wet absorption method which was carried out by spraying $Ca(OH)_2$ and/or $Mg(OH)_2$ solution(s). Consequently, the outlet temperature of these processes falls down below 453 K. In the de-NO*x* process, it is necessary to heat the catalyst bed and the inlet gas in order to activate catalyst. Therefore, the development of low temperature SCR system is a pressing need. Many research groups are now carrying out to research this problem.[13-18]

It is known that photocatalysts can promote reactions under mild condition, at an ambient temperature and an atmospheric pressure. Above all, TiO_2 is the most well-known photocatalyst and many studies have been done.[19,20] There are some reports about NO*x* removal over TiO_2 photocatalyst. Courbon and Pichat[21] reported that photoadsorption of NO, photoexchange of oxygen of NO with lattice oxygen and photodecomposition of NO take place over irradiated TiO_2 at room temperature. $N^{18}O$ was adsorbed on TiO_2 rapidly and $N^{16}O$

was produced by isotopic exchange. In addition, $N^{18}O$ was decomposed to produce N_2, $N_2{}^{16}O$ and $N_2{}^{18}O$. Illumination of TiO_2 with UV light urges the detachment of surface oxygen atoms. Recently, the direct NO removal over photocatalyst has attracted attention for a practical use like SCR.[22-25] But there are serious and fatal problems that the activity to remove NO is too low and NO converts to nitrate ion in the presence of O_2. From the different viewpoint, Cant et al.[26] reported that NO reduction proceeds in the presence of NH_3 over irradiated TiO_2. Their work inspires the author with new development to innovate photo-SCR with NH_3 in the presence of excess O_2.

The present part is devoted to the description of the NH_3-SCR over photocatalysts and to the discussion of the reaction mechanism of photo-SCR over TiO_2. In chapter 1, the author reports the photo-SCR over Rb-ion-modified silica-supported vanadium oxide under irradiation. In chapter 2, the author indicates that photo-SCR with NH_3 in the presence of excess O_2 proceeds over irradiated TiO_2 at a practical rate. In addition, the reaction mechanism was investigated by kinetic study and discussed on the basis of Eley-Rideal mechanism. Chapter 3 describes identification of intermediate in photo-SCR over TiO_2 by FT-IR spectroscopy. The generation of NH_2NO intermediate was confirmed on TiO_2. In Chapter 4, the author discusses the electron transfer from adsorbed species (N atom of NH_3 adsorbed on TiO_2) to adsorbent (Ti atom of TiO_2) relevant to the reaction mechanism of the photo-SCR with NH_3 in the presence of O_2.

References

(1) Bosch, H.; Janssen, F. *Catal. Today* **1988**, *2*, 369.

(2) Cho, S. M. *Chem. Eng. Prog.* **1994**, *90(I)*, 39.

(3) Forzatti, P.; Lietti, L. *Heterogeneous Chem. Rev.* **1996**, *3*, 33.

(4) Busca, G.; Lietti, L.; Ramis, G.; Berti, F. *Appl. Catal. B: Environ.* **1998**, *18*, 1.

(5) Markvart, M.; Pour, V. *J. Catal.* **1967**, *7*, 279.

(6) Kato, A.; Matsuda, S.; Nakajima, F.; Imanari, M.; Watanabe, Y. *J. Phys. Chem.* **1981**, *85*, 1710.

(7) Kato, A.; Matsuda, S.; Kamo, T.; Nakajima, F.; Kuroda, H.; Narita, T. *J. Phys. Chem.* **1981**, *85*, 4099.

(8) Ramis, G. G.; Busca, G.; Lorenzelli, V.; Forzatti, P. *Appl. Catal.* **1990**, *64*, 243.

(9) Ramis, G.; Busca, G.; Bregani, F.; Forzatti, P. *Appl. Catal.* **1990**, *64*, 259.

(10) Topsøe, N. Y. *Science* **1994**, *265*, 1217.

(11) Topsøe, N. Y.; Topsøe, H.; Dumesic, J. A. *J. Catal.* **1995**, *151*, 226.

(12) Topsøe, N. Y.; Dumesic, J. A.; Topsøe, H. *J. Catal.* **1995**, *151*, 241.

(13) Smirniotis, P. G.; Pena, D. A.; Uphade, B. S. *Angew. Chem.-Int. Edit.* **2001**, *40*, 2479.

(14) Long, R. Q.; Yang, R. T.; Chang, R. *Chem. Commun.* **2002**, 452.

(15) Qi, G. S.; Yang, R. T. *Chem. Commun.* **2003**, 848.

(16) Qi, G. S.; Yang, R. T. *J. Catal.* **2003**, *217*, 434.

(17) Qi, G. S.; Yang, R. T.; Chang, R. *Catal. Lett.* **2003**, *87*, 67.

(18) Marban, G.; Antuna, R.; Fuertes, A. B. *Appl. Catal. B-Environ.* **2003**, *41*, 323.

(19) Linsebigler, A. L.; Lu, G.; Yates Jr., J. T. *Chem. Rev.* **1995**, *95*, 735.

(20) Fujishima, A.; Rao, T. N.; Tryk, D. A. *J. Photochem. Photobiol. C-Photochem. Rev.* **2000**, *1*, 1.

(21) Courbon, H.; Pichat, P. *J. Chem. Soc., Faraday Trans. 1* **1984**, *80*, 3175.

(22) Hashimoto, K.; Wasada, K.; Toukai, N.; Kominami, H.; Kera, Y. *J. Photochem. Photobiol. A-Chem.* **2000**, *136*, 103.

(23) Hashimoto, K.; Wasada, K.; Osaki, M.; Shono, E.; Adachi, K.; Toukai, N.; Kominami, H.; Kera, Y. *Appl. Catal. B-Environ.* **2001**, *30*, 429.

(24) Yamashita, H.; Ichihashi, Y.; Anpo, M.; Hashimoto, M.; Louis, C.; Che, M. *J. Phys. Chem.* **1996**, *100*, 16041.

(25) Zhang, J. L.; Ayusawa, T.; Minagawa, M.; Kinugawa, K.; Yamashita, H.; Matsuoka, M.; Anpo, M. *J. Catal.* **2001**, *198*, 1.

(26) Cant, N. W.; Cole, J. R. *J. Catal.* **1992**, *134*, 317.

Chapter 1

Photoassisted selective catalytic reduction of NO with NH_3 in the presence of O_2 over Rb_2O-V_2O_5/SiO_2

Abstract

Rb-ion-modified V_2O_5/SiO_2 (Rb-VS) was found to be an effective catalyst for photoassisted selective catalytic reduction (SCR) of NO with NH_3 in the presence of oxygen at room temperature. V_2O_5/SiO_2 and SiO_2 did not promote the reaction either in the dark or with irradiation. The reaction mechanism over irradiated Rb-VS is different from the conventional NO SCR with ammonia. NO*x* is firstly adsorbed over irradiated Rb-VS in the presence of O_2, followed by adsorption of NH_3.

Introduction

The selective catalytic reduction (SCR) of NO*x* with ammonia in the presence of oxygen at ambient temperature is now of great interest.[1] We here proposed an alternative method aided by the used of light. The NO SCR with ammonia is an established method[2] for the reduction of NO from the fixed emission source using the catalyst V_2O_5/TiO_2, WO_3/TiO_2, etc. the important requirement is that NO SCR with ammonia is performed at lower temperatures than the conventional technique. In the conventional case, an ammonia molecule is protonated to an ammonium cation which reacts with NO and this can be realized at a temperature above 573 K. In 1975, Kazansky et al. reported that the hydrogen radical might be abstracted by photoexcited V=O species of silica-supported vanadium oxide to form V-OH and NH_2 at ambient temperature.[3,4] The NH_2 radical is a likely reagent to react with an iso-spin state molecule such as NO. This work hinted at using supported vanadium oxide as a catalyst for the NO*x* SCR with ammonia and we have developed the catalyst by modification of the alkali ions which improves the photocatalytic capability.[5-8] In the present paper, we report the photoassisted NO*x* SCR with ammonia.

Experimental

The catalyst sample used here was Rb-modified vanadium oxide supported on silica (Rb-VS) which was prepared by impregnation of silica-supported vanadium oxide (VS) with an evaporated to dryness, followed by calcination with a dry air flow at 773 K. The loading amount of vanadium in VS was 2.5 wt.% as V_2O_5 and the ratio (Rb/V) of Rb cations to vanadium cations in Rb-VS was adjusted to be 1.5. VS was prepared as described elsewhere.[9] The reaction was carried out in a conventional closed circulating system made of glass tube (dead space, 225 cm^3) and the catalyst sample, 0.2 g, was spread over the flat bottom (12 cm^2) of the catalyst bed. Prior to reaction, the catalyst was evacuated at 673 K for 30 min, and then treated at 673 K at 80 Torr of oxygen for 1.5 h, followed by evacuation at the same temperature for 30 min. The reaction gases (20 mmol ^{15}NO corresponding to 0.2 kPa, 20

μmol NH_3 corresponding to 0.2 kPa, 0-40 μmol O_2 corresponding to 0-0.4 kPa, and 255 μmol Ar, a diluent) were mixed for 30 min before contact with the catalyst and then admitted into the reactor. During the gas mixing in the presence of oxygen, the homogeneous reaction, NO + $1/2O_2$ = NO_2; ΔG^0 = -8.89 kcal·mol^{-1}, quickly takes place and almost all the NO is converted to NO_2. Therefore, the actual reaction proceeds between NO_2 and NH_3 in the presence of oxygen, the initial pressure of which exceeds 10 μmol. The catalyst sample was irradiated from the flat bottom of the reactor with a 250 W ultra high pressure Hg lamp supplied from USHIO Co. the gas composition at a given time was determined by a quadrupole-type mass spectrometer calibrated by Ar^{2+} internal standard. The 10 μmol of molecular amount in the reaction apparatus corresponds to 1000 ppm concentration against an atmospheric pressure.

Results and Discussion

Figure 1(a) shows the time course of evolution of nitrogen and conversion of NH_3 and NO*x* in the absence of catalyst sample after 30 min homogeneous reaction with the mixture of 19.6 μmol ^{15}NO, 19.6 μmol NH_3, 19.6 μmol O_2 and 255 μmol Ar. Because the free energy of the reaction, NO_2 + NH_3 → NH_2 + $3/2H_2O$ + $1/4O_2$ at room temperature is negative, the reaction proceeds spontaneously. Therefore, NO and NH_3 gradually decreased. In the presence of VS and Rb-VS, as shown in Figure 1(b) and (c), NO consumption and N_2 evolution curves were similar to those found in the homogeneous reaction except for the acceleration of NH_3 uptake. NH_3 was thought to be adsorbed on the acid sites of the sample as well as on the silica surface with the reaction : Si-O-Si + NH_3 → Si-OH + NH_2-Si.[10] Ammonia uptake rate over Rb-VS is faster than that over VS. But these adsorbed ammonia species did not react with NO readily at such a low temperature. As found in the blank test, N_2 evolution is accompanied by NO uptake. Although we omit the data in Figure 1, the reaction curve on SiO_2 was almost the same as those found in Figure 1(b) and (c). Photoirradiation of VS or SiO_2 did not change the reaction profile and we could not confirm the formation of NH_2 radicals as proposed by Kazansky et al. On the other hand, photoirradiation of Rb-VS

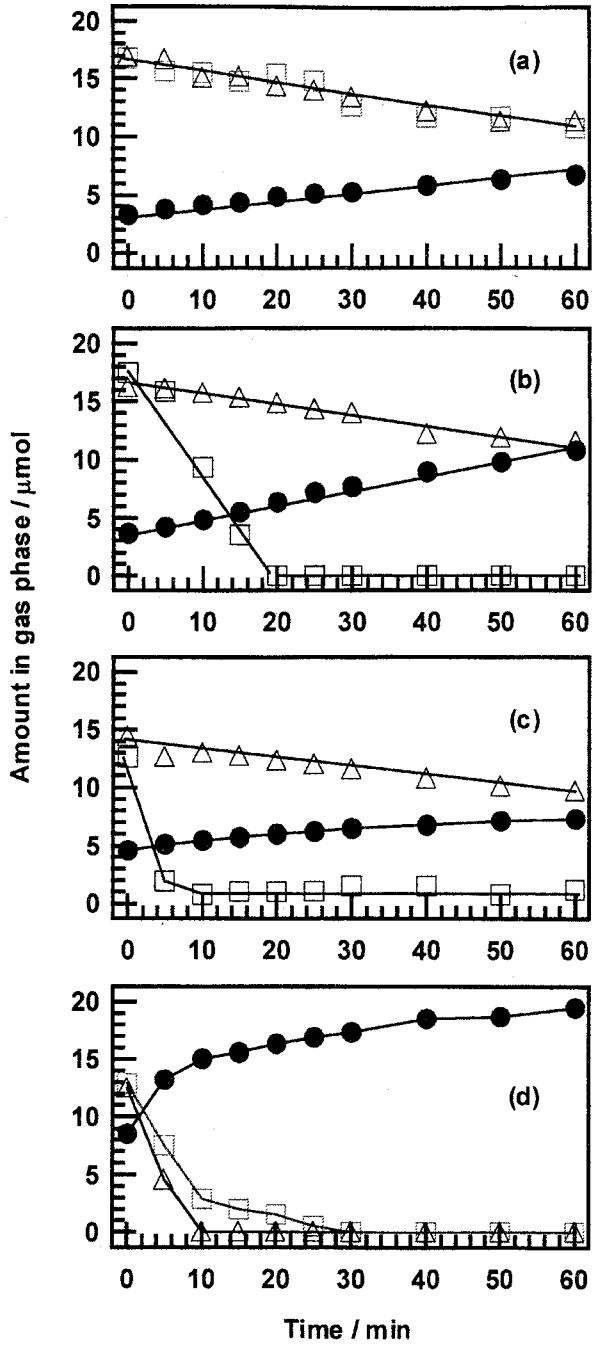

Figure 1 Time course of N_2 (circle), NO*x* (triangle), and NH_3 (square) in the gas phase for the NO-NH_3-O_2 reaction (a) without catalyst in the dark, (b) over VS in the dark, (c) over Rb-VS in the dark (d) over irradiated Rb-VS.

greatly enhances the evolution of N_2 and accelerates NO*x* and NH_3 uptake as shown in Figure 1(d). The NO*x* uptake rate during the first 5 min was calculated to be 7.2 $\mu mol \cdot min^{-1} g\text{-}cat^{-1}$ and faster than that of NH_3, 5.4 $\mu mol \cdot min^{-1} g\text{-}cat^{-1}$. We found that Rb-VS is the most effective

of the samples for NO*x* photo-SCR with ammonia. On the irradiated Rb-VS, ammonia uptake follows the NO*x* uptake while in the dark ammonia is firstly adsorbed. Therefore, the reaction mechanism is quite different from that of the conventional NO*x* SCR with ammonia. We carried out the reactions at 373 and 473 K over Rb-VS and found the same reaction time course, indicating that NO reduction with ammonia in the presence of oxygen can be operated in the temperature range 300-473 K.

Table 1 summarizes the reaction results for 10 min irradiation over Rb-VS together with those of the blank test, run 1 and a run in the dark, run 2. As already mentioned above, the presence of Rb-VS (run 2) enhances the adsorption of ammonia greatly but N_2 formation is not so different from that observed in the case of the homogeneous reaction (run 1). Form ran 3 through 7, the initial amount of oxygen was changed from 0.0 to 39.5 μmol over irradiated Rb-VS. In the absence of oxygen, the reaction is scarcely accelerated from the homogeneous reaction. Interestingly, ammonia adsorption is suppressed in comparison with a run in the dark. Addition of oxygen to the system enhances the reaction rate greatly. The

Table 1 Initial conditions and reaction results for 10 min irradiation[a]

Run No.	Initial stage Introduced amount / μmol			After 10 min Amount of gas phase / μmol		
	NO	NH_3	O_2	N_2	NO*x*	NH_3
1[b]	19.6	19.6	19.6	4.2	15.1	15.5
2[c]	19.6	19.6	19.6	9.0	13	0.8
3	24.3	20.0	0	5.3	16.3	10.6
4	21.4	20.4	5.5	13.9	0	3.4
5	23.9	20.6	9.4	13.9	0	3.3
6	19.6	19.6	19.6	15.0	0	2.9
7	23.9	20.6	39.5	17.9	0	1.8
8	22.5	0	20.3	0	2.3	0
9	196	198	196	147	0	17.3

[a] Rb-VS: 0.2 g. The values involve error within ±15 %.

[b] No catalyst in the dark. [c] In the dark

removal rate of NO*x* is higher than that of NH_3. The amount of evolved N_2 for 10 min irradiation increased with increasing partial pressure of oxygen. These results suggest that oxygen plays an important role in this reaction. NO is oxidized in a gas phase reaction and thus formed NO_2 is photoadsorbed on Rb-VS. This adsorbed species presumably reacts with NH_3. Actually, as shown in run 8, NO_2 which is thought to be formed by homogeneous oxidation of NO was adsorbed on irradiated Rb-VS and removed from the gas phase. In run 8, N_2 formation was not observed, suggesting that direct decomposition of NOx does not take place. After run 8, ammonia was admitted into the system. N_2 formation was not observed in the dark but as the catalyst was irradiated, N_2 was evolved. Therefore, both adsorption of NO*x* and rection with NH_3 are promoted by irradiation of the catalyst. In the presence of oxygen as shown in run 3, NO still remained in the gas phase after 10 min irradiation. Therefore, we concluded that NO itself is not adsorbed on Rb-VS but NO_2 is adsorbed on irradiated Rb-VS. On the other hand, although initial amounts of oxygen were not sufficient for the formation of NO_2 in run 4, the reaction still proceeded and NO*x* was removed from the gas phase within 10 min irradiation. We can not help proposing that not only NO_2 but also NO is adsorbed on Rb-VS. We speculate the reaction mechanism in the case of oxygen-poor conditions as follows: NO is homogeneously converted to NO_2 and subsequently NO_2 is photoadsorbed on Rb-VS. The adsorbed NO_2 reacts with NH_3 to form an oxygen-rich precursor consisting of N_2, H_2O and (OH). The NO molecule may attack the precursor. This is only speculation and more information is needed. A further study is now in progress. The amount of vanadium cations in the system was 55 μmol and therefore the reaction might be conjectured a stoichiometric. To investigate whether the reaction is catalytic or not, we carried out the reaction with the gases of ten times larger amount as shown in run 9. NO*x* was completely removed from the gas phase within 10 min irradiation. Judging from the amount of evolved N_2, the turnover number of vanadium cations was three. The so-called oxygen-rich precursor of ca. 50 μmol may remain on the surface at 10 min irradiation time.

References

(1) Zhu, Z. P.; Liu, Z. Y.; Liu, S. J.; Niu, H. X.; Hu, T. D.; Liu, T.; Xie, Y. N. *Appl. Catal. B: Environ.* **2000**, *26*, 25.

(2) Pârvulescu, V. I.; Grange, P.; Delmon, B. *Catal. Today* **1998**, *46*, 233.

(3) Gritscov, A. M.; Shvets, V. A.; Kazansky, V. B. *Kinet. Katal.* **1973**, *14*, 1062.

(4) Gritscov, A. M.; Shvets, V. A.; Kazansky, V. B. *Chem. Phy. Lett.* **1975**, *35*, 511.

(5) Tanaka, T.; Takenaka, S.; Funabiki, T.; Yoshida, S. *Chem. Lett.* **1994**, 1585.

(6) Takenaka, S.; Kuriyama, T.; Tanaka, T.; Funabiki, T.; Yoshida, S. *J. Catal.* **1995**, *155*, 196.

(7) Tanaka, T.; Takenaka, S.; Funabiki, T.; Yoshida, S. *J. Chem. Soc., Faraday Trans.* **1996**, *92*, 1975.

(8) Takenaka, S.; Tanaka, T.; Funabiki, T.; Yoshida, S. *Catal. Lett.* **1997**, *44*, 67.

(9) Tanaka, T.; Nishimura, Y.; Kawasaki, S.; Ooe, M.; Funabiki, T.; Yoshida, S. *J. Catal.* **1989**, *118*, 327.

(10) Morrow, B. A.; McFarlan, A. J. *J. Phys. Chem.* **1992**, *96*, 1395.

Chapter 2

Reaction and kinetic study for photoassisted selective catalytic reduction of NO over TiO_2

Abstract

It was found that 83 % of NO conversion and 96 % of N_2 selectivity are achieved in the photo-SCR system over TiO_2 photocatalyst (JRC-TIO-4 equivalent to Degussa P-25). N_2 was evolved in the gas phase when NO was flowed over TiO_2 pretreated by NH_3 under photoirradiation. The photo-SCR reaction proceeds according to the Eley-Rideal mechanism. NO in the gas phase attacks NH_3 adsorbed on the Lewis acid site. The strength and/or quantity of the Lewis acid site related to NH_3 adsorption had an influence on the N_2 evolution. Therefore, the surface acid property of TiO_2 is an important factor to control the N_2 evolution. In addition, the reaction orders of gases (NO, NH_3 and O_2) and light intensity were determined by the kinetic studies. The results supported the reaction mechanism which we have proposed in the previous works (Scheme1). The time-determining step of the photo-SCR over TiO_2 is the process of decomposition of a NH_2NO intermediate under excess O_2 concentration or re-oxidation of Ti^{3+} to Ti^{4+} below 2 % O_2 concentration.

Introduction

It is desirable to remove NO*x* exhausted in the stationary emission source and the mobile emission source because the emission of NO*x* which is causative of town smog and acid rain is brought under control strictly.[1,2] In the stationary emission sources such as a power station, a waste incinerator and an industrial boiler, NO*x* in the exhaust gas removed ordinarily by the selective catalytic reduction system with NH_3 (NH_3-SCR) in the presence of O_2 from 573 K to 673 K over V_2O_5-WO_3/TiO_2 or MoO_3-WO_3/TiO_2 catalyst.[3-6] The NH_3-SCR system was uncovered by three Japanese corporations (Hitachi, Ltd., Babcock-Hitachi K.K., Mitsubishi Petrochemical Corp.).[7,8] It is interesting that O_2 make the driving temperature of catalyst fall down in the NH_3-SCR system.[9] Therefore, the reaction rate of the NH_3-SCR enlarges in the presence of O_2. The reaction stoichiometry in the typical NH_3-SCR condition had been determined as follows;

$$4NO + 4NH_3 + O_2 \longrightarrow 4N_2 + 6H_2O \qquad (1)$$

It is a common understanding that the typical NH_3-SCR system proceeds according to Eley-Rideal mechanism. Therefore, NO in the gas phase attacks the adsorbed NH_3 species. The two research groups proposed different adsorbed NH_3 species and reaction schemes based on the Eley-Rideal mechanism. Ramis et al.[10,11] proposed that Lewis acid sites of the vanadium center are active sites and that the NH_2NO species is formed as an intermediate in these sites. On the other hand, Topsøe et al.[12-14] proposed that V^{5+}-OH and V^{5+}=O are acid site and redox site as active sites, respectively, and the NH_2NO species was identified by infrared spectroscopy. However, the reasonable mechanism is now under discussion.

Nowadays, almost stationary emission sources are loaded with the NH_3-SCR system such as a strong de-NO*x* process. The exhaust gas contains various polluted gases and materials, for example, NO*x*, SO*x*, halogen compounds, PM and fly ash etc. The several removal systems are arranged in outlet of industrial plants to eliminate these materials efficiently. In the case of the waste incinerators which exhaust the high concentration of SO*x* and halogen compounds, the de-NO*x* process is often located downstream of the de-halogen and/or de-SO*x* processes because the catalysts used in the de-NO*x* process (V_2O_5-WO_3/TiO_2

or MoO_3-WO_3/TiO_2) are deactivated rapidly by halogen compounds and highly concentrated SO*x*. However, most de-halogen and de-SO*x* processes are based on wet mixed shotcrete which was carried out by spray of $Ca(OH)_2$ and $Mg(OH)_2$ solution. Consequently, the outlet temperature of these processes falls below 453 K. In the de-NO*x* process, it is necessary to re-heat the catalyst bed and gas in order to activate catalyst. Recently, some authors found new catalysts activated at low temperatures.[15-23] We have reported that photo-SCR with NH_3 in the presence of O_2 proceeds at room temperature over Rb-ion-modified silica supported vanadium oxide (Rb_2O-V_2O_5/SiO_2)[24], silica-supported titanium oxide (TiO_2/SiO_2)[25] and titanium dioxide (TiO_2)[26,27] under photoirradiation. In the case of TiO_2, 83 % of NO conversion and 96 % of N_2 selectivity were achieved in the conventional fixed bed flow system.[26] It has been confirmed that these catalysts work from 300 K to 473 K.

The reasonable reaction mechanism of the photo-SCR with NH_3 over TiO_2 was demonstrated by various spectroscopies and determined as shown in Scheme 1.[27] In Step 1, NH_3 is adsorbed on Lewis acid site of TiO_2 in the dark. NH_3 in the gas phase was diminished

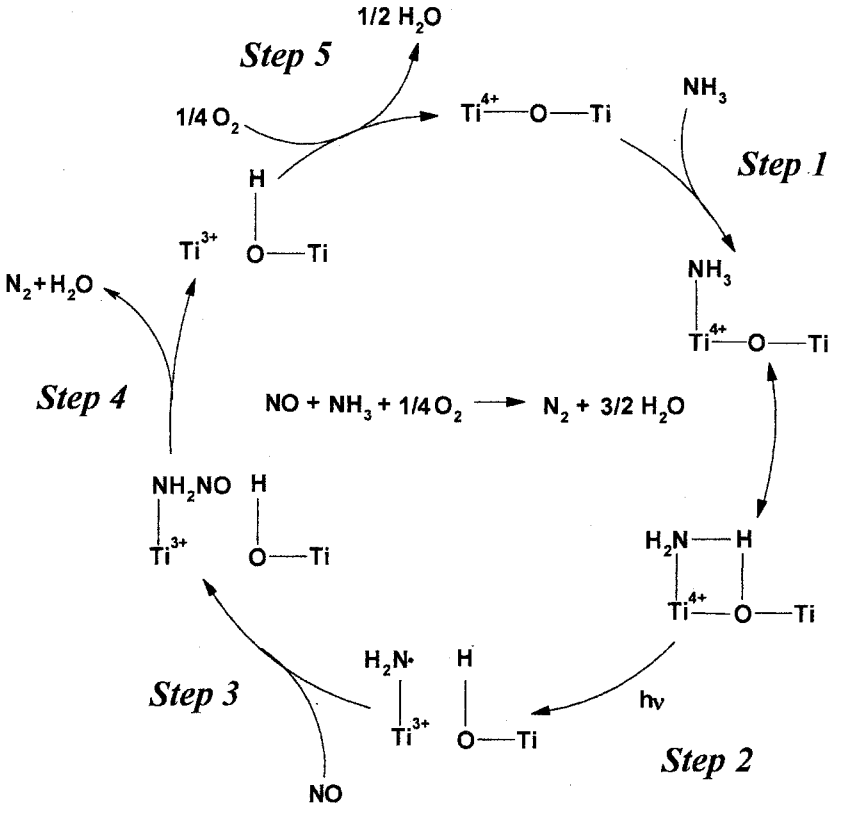

Scheme 1 Reaction mechanism of photo-SCR with NH_3 over TiO_2.

rapidly on introducing to TiO_2. And, the bands assigned to NH_3 adsorbed on the Lewis acid sites (1599 and 1215 cm^{-1}) were confirmed by FT-IR spectroscopy. One hydrogen atom of the adsorbed NH_3 species interacts with a lattice oxygen atom. In Step 2, an electron derived from N-atom of NH_3 adsorbed on TiO_2 transfers to Ti^{4+} under photoirradiation. Accordingly, electron transfer takes place between adsorbent and adsorbed species. The photoformed hole is captured by the NH_2^- species evolved from adsorbed NH_3 to produce a NH_2 radical. The OH stretching vibration band of TiO_2 (3675 cm^{-1}) increased in intensity under photoirradiation after NH_3 treatment according to FT-IR spectroscopy. In addition, the NH_2 radical and the Ti^{3+} species were detected by EPR spectroscopy after illumination to TiO_2 adsorbing NH_3. The signals assigned to the NH_2 radical were quite stably present even after more than one hour at 123 K when the irradiation was ceased. This indicates that the electron transfer takes place from an N atom of adsorbed NH_3 to a Ti^{4+} atom of TiO_2 efficiently. In Step 3, the formed NH_2 radical is attacked by NO in the gas phase to produce a NH_2NO intermediate. It was confirmed by EPR spectroscopy that the lines assigned to the NH_2 radicals vanish away as soon as NO is introduced to TiO_2 adsorbing NH_3 in the dark. The bands derived from the NH_2NO intermediate were monitored by FT-IR spectroscopy when TiO_2 adsorbing NH_3 was irradiated in the presence of NO. These bands were not observed in the dark. In Step 4, the NH_2NO intermediate is decomposed to N_2 and H_2O. Needless to say, we observed the formation of N_2 in the photo-SCR reaction. The detected N_2 gas was only $^{15}N^{14}N$ on using ^{15}NO and $^{14}NH_3$. This indicates that N atoms of N_2 molecule consist of one N atom derived from NH_3 and one N atom derived from NO. In Step 5, the Ti^{3+} species is re-oxidized to the first Ti^{4+} species by O_2. It was affirmed by UV-Vis spectroscopy that the Ti^{3+} species of TiO_2 reduced by H_2 was reoxidized to the Ti^{4+} species. In this way, the photo-SCR reaction proceeds catalytically. Accordingly, the reaction stoichiometry in the photo-SCR is same as that in the conventional NH_3-SCR (Reaction 1). In the present study, we carried out screening of various TiO_2 photocatalysts in the photo-SCR with NH_3. In addition, the kinetic study of the photo-SCR was investigated to clarify the reaction mechanism as shown in Scheme 1.

Experimental

TiO_2 samples used in this study were supplied from the Japan Catalysis Society (JRC-TIO-1, 2, 3, 4, 5), Ishihara Sangyo Kaisha, Ltd. (ST-01, 21, 30L, 31, 41), and TAYCA Co. (TKP-101, 103). The TiO_2 samples were hydrated in distilled water for 2 h at 353 K and filtered with a pump. After that, the sample was kept at 383 K for 24 h in an oven, followed by calcinations in air at 873 K for 2 h. The sample was ground to a powder from 26 to 50 mesh after calcination. Table 1 shows the specific surface area evaluated by BET method using N_2 adsorption isotherm at 77 K and crystal phase determined by XRD.

Amount of adsorbed NH_3 on TiO_2 was determined by the adsorption equilibrium method as follows. 0.2 g of TiO_2 was evacuated at 673 K as a pretreatment. NH_3 was introduced to TiO_2 and measured an adsorption isotherm at room temperature in a conventional closed static system connected to a vacuum pump at room temperature.

The reaction was carried out in a conventional fixed bed flow system at atmospheric pressure. TiO_2 samples were packed in the glass reactor equipped with a flat facet (50 x 15 x 1 mm^3). The amount of each TiO_2 catalyst used in the photo-SCR reaction was shown in Table 1. Prior to a reaction, each catalyst sample was treated at 673 K by passing 5 % O_2 diluted with Ar at a flow rate of 50 cm^3min^{-1} for 1 h. The composition of the reaction gas was NO: 1000 ppm, NH_3: 1000 ppm, O_2: 2 - 10 %, and the balance Ar and the flow rate was 100 cm^3min^{-1} corresponding to the gas hourly space velocity (GHSV) 4000-16000 h^{-1}. The catalyst sample was irradiated from the flat side face of the reactor with a 300 W ultra-high Xe lamp (Perkin-Elmer). The gas composition at given time was determined by TCD gas chromatograph (Shimazu GC-8A) equipped with a column packed with Molecular Sieve 5A and Porpack Q using Ar as a carrier gas.

The reaction kinetics was also investigated in the conventional fixed bed flow system, however, TiO_2 sample (ST-41) was packed in the smaller reactor (10 x 13 x 1 mm^3) to put a differential condition into practice. The concentration of NO, NH_3 or O_2 was converted at 250 - 1250 ppm, 250 - 1250 ppm or 0.5 – 3.5 %, respectively. On the other hand, the light intensity could be changed by current value of the light source because the light intensity is in

proportion to the current value. In our case, the current value of the Xe lamp was converted at 14 – 20 A. When one concentration or light intensity was changed to determine this reaction order, the others kept constant. Accordingly, the logarithms of the N_2 evolutions were plotted and approximated by a straight line to determine the reaction orders.

Results and Discussion

Table 1 indicates the NO conversion and the N_2 selectivity in the photo-SCR with NH_3 over various TiO_2 photocatalysts. JRC-TIO-1, JRC-TIO-3 and ST-01 exhibited the better activity (ca. 75 % conversion) in comparison with the other TiO_2 samples. The surface area of three samples used in the photo-SCR is almost same as ca. 40 m^2. However, the surface area

Table 1 Results of photo-SCR with NH_3 over various TiO_2 photocatalysts

catalyst	Amount / g	Phase	SA / m^2	Production (ppm)		NO conv. (%)	N_2 selec. (%)
				N_2	N_2O		
JRC-TIO-1	0.60	A	43.0	770	20	79.0	97.5
JRC-TIO-2	0.81	A	12.6	200	0	20.0	100.0
JRC-TIO-3	0.91	R	41.5	760	0	76.0	100.0
JRC-TIO-4	0.66	A+R	31.5	550	10	56.0	98.2
JRC-TIO-5	1.14	R	3.96	440	16	45.6	96.5
ST-01	0.50	A	44.8	710	23	73.3	96.9
ST-20	0.82	A	40.3	620	0	62.0	100.0
ST-30L	0.57	A	68.7	650	0	65.0	100.0
ST-31	0.57	A	54.3	130	0	13.0	100.0
ST-41	0.84	A	7.98	320	0	32.0	100.0
TKP-101	0.66			655	0	65.5	100.0
TKP-103	0.58			260	0	26.0	100.0

GHSV = 16000 h^{-1}

NO : 1000 ppm, NH_3 : 1000 ppm, O_2 : 5 %

is not the factor which control the activity of the photo-SCR because ST-31 exhibits very low activity despite of high surface area. On the other hand, recently, it is uncovered that the crystal phase of TiO_2 (anatase or rutile) make the activity control in various reactions.[28-31] The crystal phase of JRC-TIO-3 was rutile although that of JRC-TIO-1 and ST-01 was detected as anatase by XRD. Therefore, the crystal phase is not an important factor to affect the activity of the photo-SCR. Another factor except the surface area and the crystal phase would control the activity. The results of the photo-SCR over TKP-101 and 103 suggests new concept to us. TAYCA Co. published that the acid-base properties of TKP-101 and 103 exhibit weak acidity and weak bascity, in addition, TKP-101 and 103 specialize in the adsorption of NH_3 and NOx, respectively. In the present study, the performance of TKP-101 concerning NO conversion was two and half times larger than that of TKP-103. Consequently, the surface acidity has an influence on the activity in the photo-SCR. We proposed that the strength and/or quantity of the Lewis acid site are important factors to determine the activity of the photo-SCR. However, the factor in detail is now under discussion.

Figure 1 shows the time course of the photo-SCR with NH_3 in the presence of O_2 over JRC-TIO-4 (equivalent to Degussa P-25) photocatalyst (NO and NH_3 : 1000 ppm, O_2 : 10 %, Ar dilute, SV = 4000 h^{-1}). N_2O was produced only in trace amounts although N_2 and

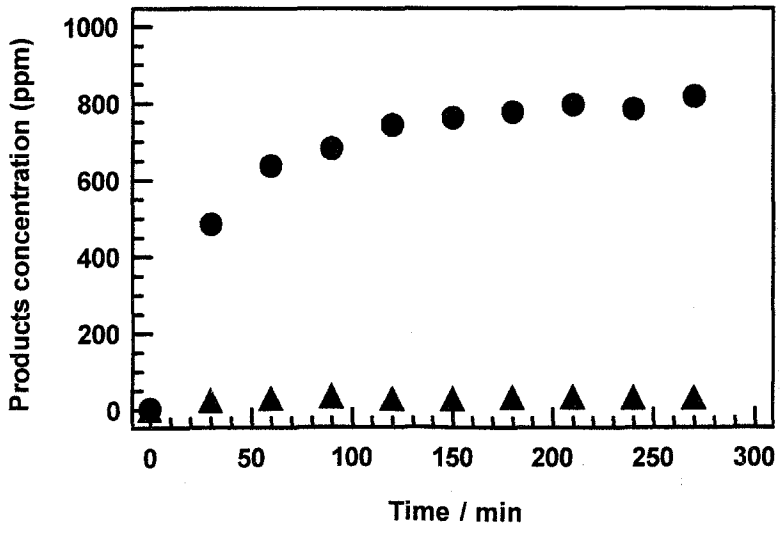

Figure 1 Outlet concentration of N_2 (circle) and N_2O (triangle) in the SCR of NO with ammonia at 323 K under photoirradiation. GHSV = 4000 h^{-1} NO : 1000 ppm, NH_3 : 1000 ppm, O_2 : 10 %.

N_2O were detected in this reaction. Accordingly, the produced gas is almost N_2. The NH_3-SCR reaction is a down hill reaction and therefore it proceeds in the dark at low

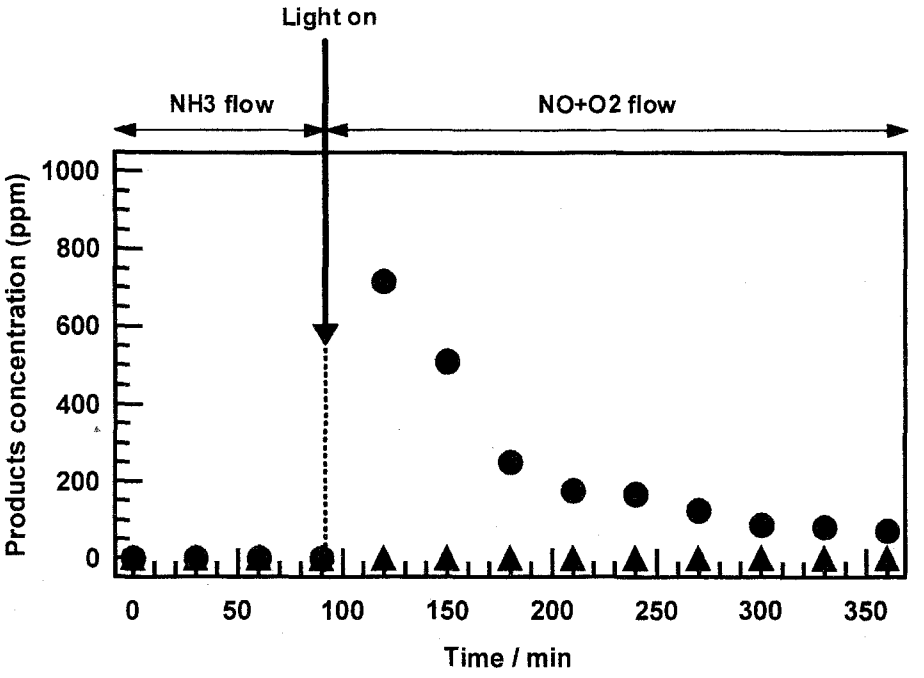

Figure 3 Outlet concentration of N_2 (circle) and N_2O (triangle) during varying experimental conditions. In the first 90 min, NH_3 was flowed in the dark and at 90 min, NH_3 flow was switched to NO and O_2 and the lamp was turned on. GHSV = 4000 h^{-1} NO : 1000 ppm, NH_3 : 1000 ppm.

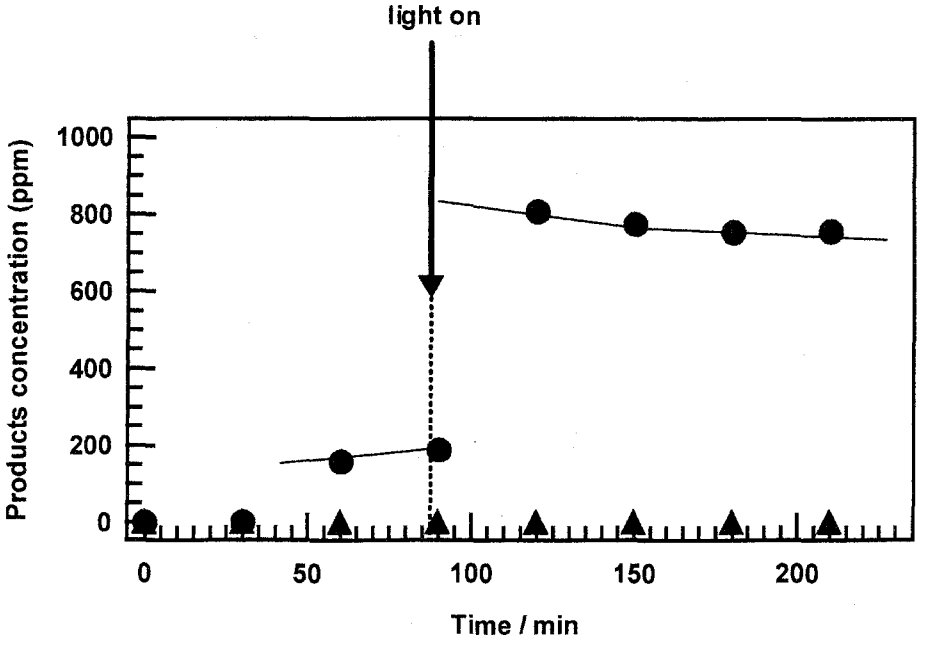

Figure 2 Outlet concentration of N_2 (circle) and N_2O (triangle) in the SCR of NO with ammonia at 323 K. GHSV = 4000 h^{-1} NO : 1000 ppm, NH_3 : 1000 ppm.

temperature at 20 % of NO conversion. Photoirradiation caused remarkable enhancement of activity. When the reaction gas was passed under photoirradiation, the N_2 evolution rate gradually increased and attained a steady rate, 83 % of NO conversion after 120 min photoirradiation. Then, 96 % of N_2 selectivity was achieved. The induction period may be due to the time for saturation of the adsorption equilibrium of the reactant molecules. To examine this behavior, in the first 90 min, the reaction gas was passed in the dark and after 90 min, photoirradiation was started as shown in Figure 2. In the dark, N_2 was evolved at 20 % conversion as mentioned above. The NO conversion jumped remarkably to the level of the steady rate (83 %) as soon as the photoirradiation was started and became constant quickly. This clearly shows that the induction period is the time for equilibrium adsorption of reactant molecules. In order to find which NO or NH_3 molecule is adsorbed first, we carried a couple of experiments. In the first experiments, NO and O_2 were passed in the first 90 min and then the feed gas was switched to NH_3. Neither N_2 or N_2O was detected in the outlet flow during the whole reaction time and NO was not detected after switching the feed gas, suggesting that NO is very weakly adsorbed as a nitrate on TiO_2.[27] In the second experiments NH_3 was passed in the first 90 min in the dark and then the feed was changed to NO and O_2 at the same time as irradiation was started as shown in Figure 3. N_2 was evolved at a steady rate the moment that the gas feed composition was changed and the photoirradiation was started. However, the N_2 evolution was not observed in the dark. After that, the N_2 evolution rate gradually decreased. This shows that NH_3 was firstly adsorbed on TiO_2 and consumed by the contact with NO. The NO total amount formed N_2 was determined to be 0.23 mmol·g-cat^{-1} by integrating the evolution rate of N_2, and the value was consistent with the amount of adsorbed NH_3 over TiO_2. Figure 4 shows the adsorption isotherm of NH_3 on TiO_2 at room temperature. The partial pressure of NH_3 was 0.76 Torr because the mixture gas prepared in this reaction contained 1000 ppm of NH_3. The amount of adsorbed NH_3 over TiO_2 was 0.24 mmol·g-cal^{-1} at 0.76 Torr from Figure 4. In conclusion, the NH_3 species adsorbed on Lewis acid site of TiO_2 is excited by photoirradiation of TiO_2 and reacts with NO in the gas phase to produce N_2. Therefore, the photo-SCR with NH_3 proceeds according to the Eley-Rideal mechanism.

The kinetic study was carried out to verify the reaction mechanism proposed by us.

The reaction rate is shown as a following formula:

$$r = kC_{NO}^{\alpha} C_{NH_3}^{\beta} C_{O_2}^{\chi} I^{\delta} \quad (2)$$

We carried out the photo-SCR under the condition of the various concentration of NO, NH_3 or O_2, or the different light intensity to determine each reaction order. Figure 5 – 7 (a) shows the N_2 evolution in the photo-SCR under condition of various concentration of NH_3, NO or O_2. In addition, Figure 5 – 7 (b) plots the logarithms of Figure 5 – 7 (a). In the case of NO (Figure 5) and NH_3 (Figure 6), the logarithms of the N_2 evolutions were approximated by a straight line as follows:

$$\ln C_{N_2} = 0.86 + 0.51 \ln C_{NO} \quad (3)$$

$$\ln C_{N_2} = 4.6 + (-0.05) \ln C_{NH_3} \quad (4)$$

We have already confirmed that NH_3 is adsorbed quickly on the Lewis acid site of TiO_2.[26,27] It is an adequate result that the reaction order of NH_3 is zeroth. On the other hand, if NO in the gas phase attacks NH_3 adsorbed on TiO_2 as described in Scheme 1, the reaction order of NO is first. However, in this study, that was 0.5th order. This suggests that NO physorbed on TiO_2 weakly as well as diffused in the gas phase reacts with the adsorbed NH_3 species. In the case

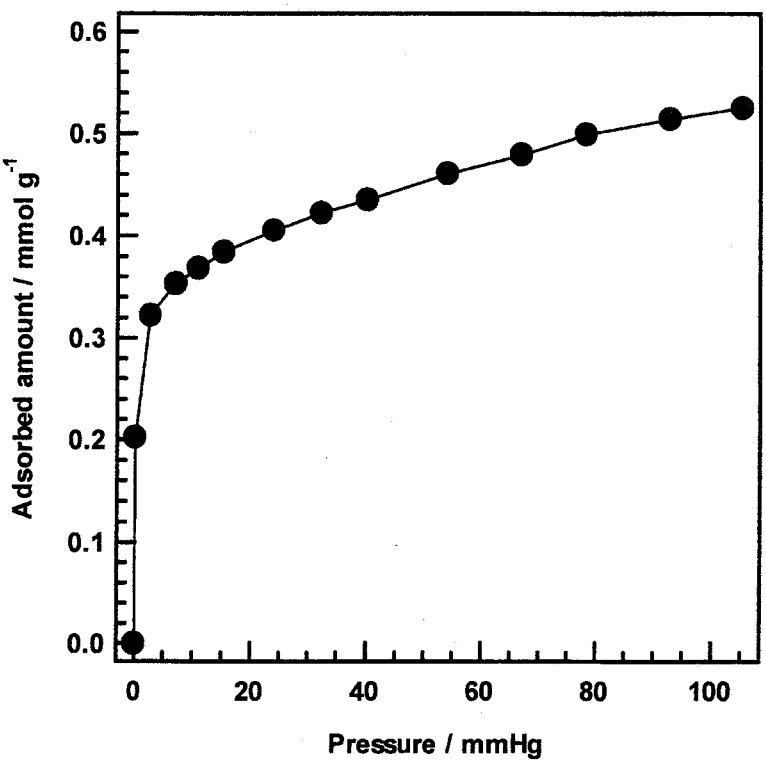

Figure 4 Adsorption isotherm of NH_3 on TiO_2 at room temperature.

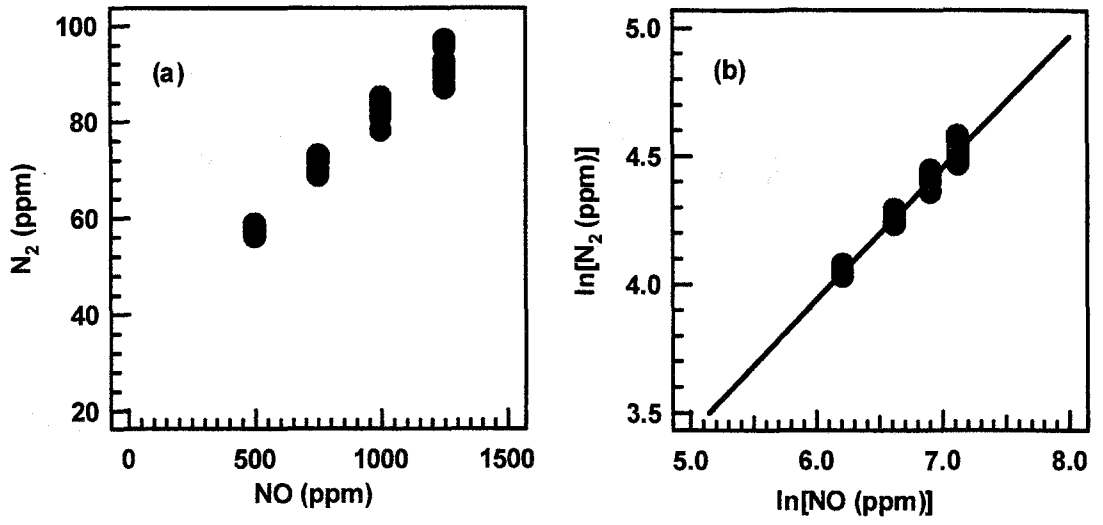

Figure 5 (a) N_2 evolution in the photo-SCR under condition of various NO concentrations and (b) logarithm of (a).

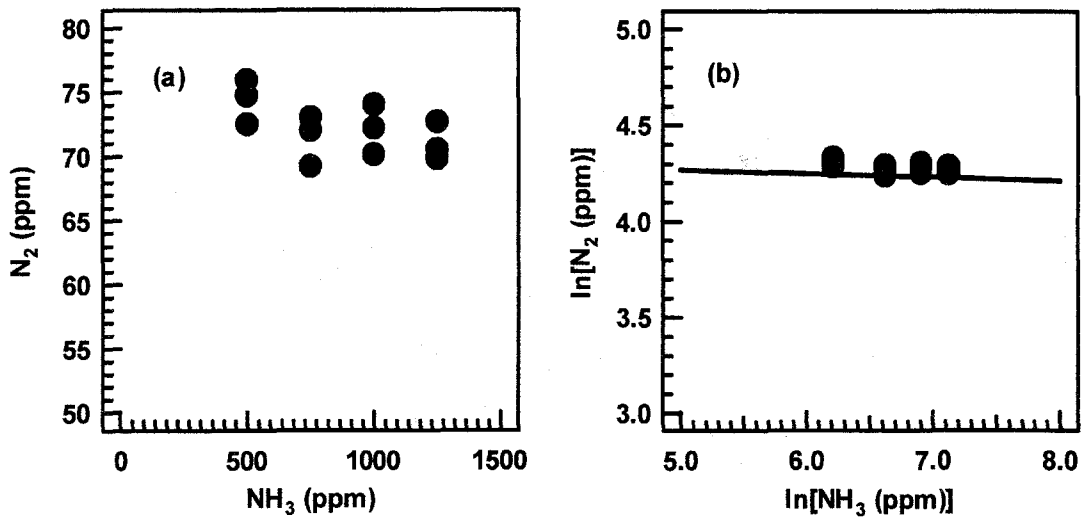

Figure 6 (a) N_2 evolution in the photo-SCR under condition of various NH_3 concentrations and (b) logarithm of (a).

of O_2 (Figure 7), the logarithms of the N_2 evolutions could be fitted by two lines (below and above 2 % O_2 concentration).

$$\ln C_{N_2} = 4.2 + 0.23 \ln C_{O_2} \quad \text{(below 2 \%)} \tag{5}$$

$$\ln C_{N_2} = 4.3 + 0.07 \ln C_{O_2} \quad \text{(above 2 \%)} \tag{6}$$

It was proposed in Scheme 1 that O_2 have a role of re-oxidation of Ti^{3+} to Ti^{4+}. In the case of low O_2 concentration, the re-oxidation step has an influence on the reaction rate. On the other hand, the re-oxidation step in high O_2 concentration does not affect the reaction rate because this step proceeds quickly. Finally, we need to investigate the reaction order against the light

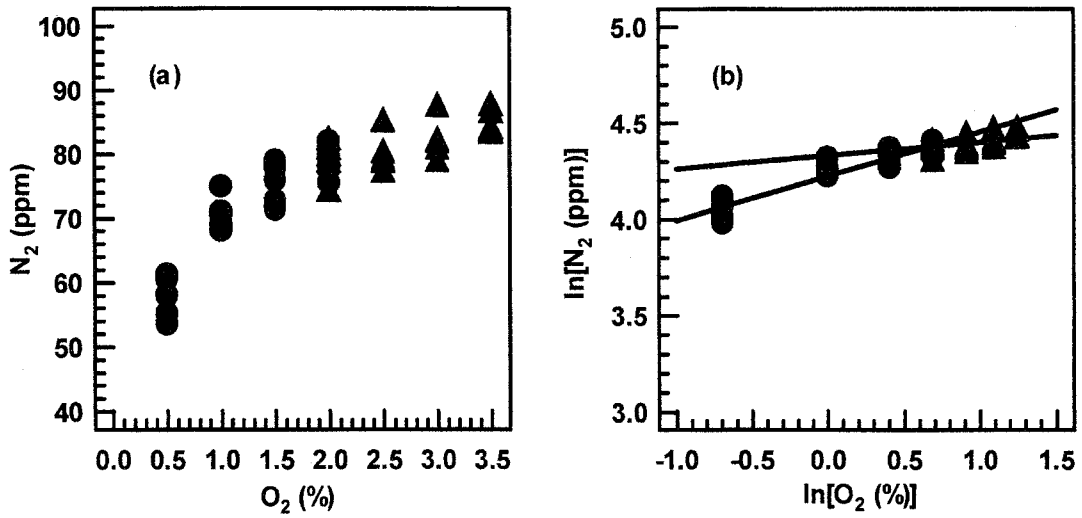

Figure 7 (a) N_2 evolution in the photo-SCR under condition of various O_2 concentrations and (b) logarithm of (a).

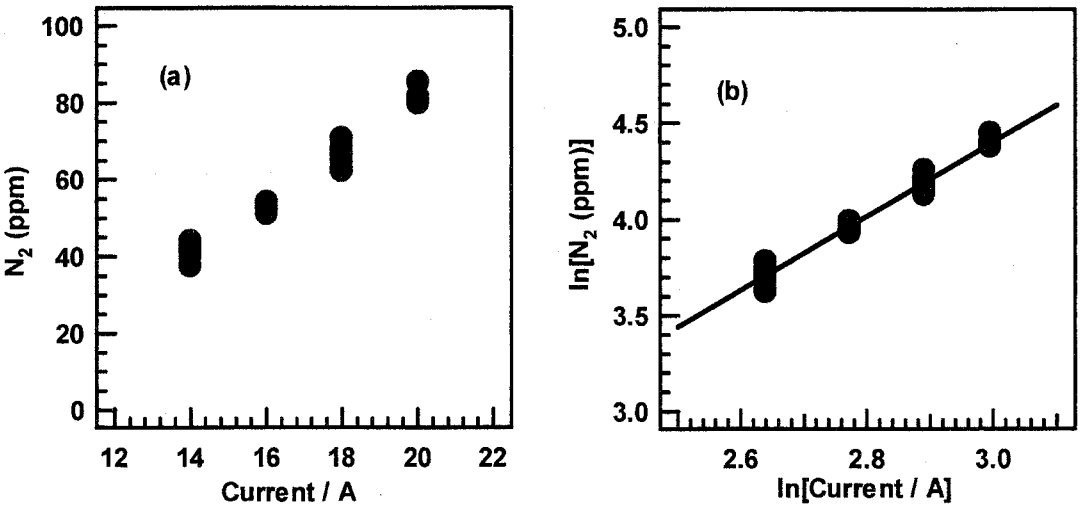

Figure 8 (a) N_2 evolution in the photo-SCR under photoirradiation of various light intensities and (b) logarithm of (a).

intensity because photocatalysis depends on the illuminated light intensity. As mentioned above, the light intensity of the Xe lamp used in this study is in proportion to the current. Figure 8(a) shows the N_2 evolution in the photo-SCR under condition of various current values. In addition, Figure 8(b) plots the logarithm of Figure 8(a). The logarithms of the N_2 evolutions were also approximated by a straight line.

$$\ln C_{N_2} = (-1.4) + 1.9 \ln A \qquad (7)$$

In scheme 1, the reaction mechanism of the photo-SCR is related to only one electron transfer in Step 2. In this study, it was clarified that the reaction rate is second order against the light

intensity. This suggests that an electron affects another step as well as the electron transfer from the NH_2 species to the Ti^{4+} species. We have found out that some reaction steps in Scheme 1 proceed in the dark. It is a common knowledge that NH_3 is adsorbed on the Lewis acid site of TiO_2 in the dark quickly. Actually, NH_3 in the gas phase was diminished rapidly on introducing to TiO_2. Next, we have already confirmed by EPR spectroscopy that the signal assigned to a NH_2 radical vanishes as soon as NO is introduced to the reactor in the dark. In addition, it was detected by UV-Vis spectroscopy that O_2 made a Ti^{3+} species of TiO_2 treated by H_2 re-oxidize to a Ti^{4+} species in the dark. These are summarized as follows. Step 1, 3 and 5 proceed in the dark, therefore, the light intensity is also related to Step 4, decomposition of a NH_2NO species. It is well-known that the NH_2NO species is decomposed easily by heat treatment.[10,11] In the present study, heat of the infrared light would have an influence on the reaction rate.

The results are summarized as a following formulae:

$$r = kC_{NO}^{0.5}C_{NH_3}^{0}C_{O_2}^{0.23}I^{1.9} \quad \text{(below 2 \%)} \tag{8}$$

$$r = kC_{NO}^{0.5}C_{NH_3}^{0}C_{O_2}^{0.07}I^{1.9} \quad \text{(above 2 \%)} \tag{9}$$

We compared these reaction rate obtained in the reaction to that calculated from Scheme 1 to clarify whether Scheme 1 is a reasonable mechanism or not. Each reaction rate was calculated due to assume that each step of Scheme 1 is time-determining step as follows.

$$r = k_1 P_{NH_3} \quad \text{(Step 1)} \tag{10}$$

$$r = k_2 I \quad \text{(Step 2)} \tag{11}$$

$$r = \frac{k_3 K_2 P_{NO} I}{1 + K_2 I} \quad \text{(Step 3)} \tag{12}$$

$$r = \frac{k_4 K_2 K_3 P_{NO} I^2}{1 + K_2 I + K_2 K_3 P_{NO} I} \quad \text{(Step 4)} \tag{13}$$

$$r = \frac{k_5 K_2 K_3 K_4 P_{NO} P_{O_2}^{0.25} I^2}{1 + K_2 I + K_2 K_3 P_{NO} I + K_2 K_3 K_4 P_{NO} I^2} \quad \text{(Step 5)} \tag{14}$$

Reaction rate constant and equilibrium constant of each step represents k_x and K_x, respectively (x = step number). These formulae were compared with the formulae obtained in the present

study (8 and 9). The reaction order of the formula 10, 11 and 12 is not compatible with that of the formula 8 or 9. Consequently, Step 1, 2 and 3 are not time-determining step of the photo-SCR. The formula 13 is consistent with the formula 9 (at low O_2 concentration), whereas the formula 14 agrees with the formula 8 (at high O_2 concentration). In conclusion, Step 4, the decomposition of the NH_2NO species, conducts as time-determining step under condition of excess O_2 concentration. On the other hand, at low O_2 concentration, Step 5, re-oxidation of Ti^{3+} to Ti^{4+}, is time-determining step because O_2 is concerned to Step 5 critically.

Conclusion

TiO_2 is a reasonable photocatalyst for the photo-SCR with NH_3. The reaction mechanism of the photo-SCR is based on the Eley-Rideal mechanism. It was clarified that NH_3 adsorbed on TiO_2 reacts with NO in the gas phase. The surface acid property of TiO_2 has an influence on NH_3 adsorption, therefore, is an important factor to determine NO conversion. The photo-SCR reaction mechanism proposed from the spectroscopic results was also demonstrated by the kinetic study. The process of the decomposition of the NH_2NO intermediate conducts as time-determining step under condition of excess O_2 concentration. On the other hand, re-oxidation step is time-determining step below 2 % O_2 concentration.

List of Symbols

r : reaction rate

k : reaction rate constant

K : equilibrium constant

C : gas concentration

I : light intensity

A : current value of lamp

P : partial pressure of gas

Acknowledgement

We would like to thank Ishihara Sangyo Kaisha, Ltd. for offering the TiO_2 sample, ST-01, 21, 30L, 31, 41. In addition, we show gratitude to supply TKP-101 and 103 by TAYCA Co.

References

(1) Wood, S. C. *Chem. Eng. Prog.* **1994**, *90(I)*, 32.

(2) Parvulescu, V. I.; Grange, P.; Delmon, B. *Catal. Today* **1998**, *46*, 233.

(3) Bosch, H.; Janssen, F. *Catal. Today* **1988**, *2*, 369.

(4) Cho, S. M. *Chem. Eng. Prog.* **1994**, *90(I)*, 39.

(5) Forzatti, P.; Lietti, L. *Heterogeneous Chem. Rev.* **1996**, *3*, 33.

(6) Busca, G.; Lietti, L.; Ramis, G.; Berti, F. *Appl. Catal. B: Environ.* **1998**, *18*, 1.

(7) Kato, A.; Matsuda, S.; Nakajima, F.; Imanari, M.; Watanabe, Y. *J. Phys. Chem.* **1981**, *85*, 1710.

(8) Kato, A.; Matsuda, S.; Kamo, T.; Nakajima, F.; Kuroda, H.; Narita, T. *J. Phys. Chem.* **1981**, *85*, 4099.

(9) Markvart, M.; Pour, V. *J. Catal.* **1967**, *7*, 279.

(10) Ramis, G. G.; Busca, G.; Lorenzelli, V.; Forzatti, P. *Appl. Catal.* **1990**, *64*, 243.

(11) Ramis, G.; Busca, G.; Bregani, F.; Forzatti, P. *Appl. Catal.* **1990**, *64*, 259.

(12) Topsoe, N. Y. *Science* **1994**, *265*, 1217.

(13) Topsoe, N. Y.; Topsoe, H.; Dumesic, J. A. *J. Catal.* **1995**, *151*, 226.

(14) Topsoe, N. Y.; Dumesic, J. A.; Topsoe, H. *J. Catal.* **1995**, *151*, 241.

(15) Zhu, Z. P.; Liu, Z. Y.; Liu, S. J.; Niu, H. X. *Appl. Catal. B-Environ.* **1999**, *23*, L229.

(16) Zhu, Z. P.; Liu, Z. Y.; Liu, S. J.; Niu, H. X.; Hu, T. D.; Liu, T.; Xie, Y. N. *Appl. Catal. B: Environ.* **2000**, *26*, 25.

(17) Zhu, Z. P.; Liu, Z. Y.; Liu, S. J.; Niu, H. X. *Appl. Catal. B-Environ.* **2001**, *30*, 267.

(18) Smirniotis, P. G.; Pena, D. A.; Uphade, B. S. *Angew. Chem.-Int. Edit.* **2001**, *40*, 2479.

(19) Long, R. Q.; Yang, R. T.; Chang, R. *Chem. Commun.* **2002**, 452.

(20) Qi, G. S.; Yang, R. T. *Chem. Commun.* **2003**, 848.

(21) Qi, G. S.; Yang, R. T. *J. Catal.* **2003**, *217*, 434.

(22) Qi, G. S.; Yang, R. T.; Chang, R. *Catal. Lett.* **2003**, *87*, 67.

(23) Marban, G.; Antuna, R.; Fuertes, A. B. *Appl. Catal. B-Environ.* **2003**, *41*, 323.

(24) Tanaka, T.; Teramura, K.; Funabiki, T. *Phys. Chem. Chem. Phys.* **2000**, *2*, 2681.

(25) Tanaka, T.; Teramura, K.; Yamamoto, T.; Takenaka, S.; Yoshida, S.; Funabiki, T. *J. Photochem. Photobiol. A-Chem.* **2002**, *148*, 277.

(26) Tanaka, T.; Teramura, K.; Arakaki, K.; Funabiki, T. *Chem. Comm.* **2002**, 2742.

(27) Teramura, K.; Tanaka, T.; Funabiki, T. *Langmuir* **2003**, *19*, 1209.

(28) Torimoto, T.; Nakamura, N.; Ikeda, S.; Ohtani, B. *Phys. Chem. Chem. Phys.* **2002**, *4*, 5910.

(29) Ohno, T.; Sarukawa, K.; Tokieda, K.; Matsumura, M. *J. Catal.* **2001**, *203*, 82.

(30) Ohno, T.; Sarukawa, K.; Matsumura, M. *J. Phys. Chem. B* **2001**, *105*, 2417.

(31) Ohno, T.; Sarukawa, K.; Matsumura, M. *New J. Chem.* **2002**, *26*, 1167.

Chapter 3

Identification of surface intermediate on TiO_2 by FT-IR spectroscopy

Abstract

Selective catalytic reduction (SCR) of NO with NH_3 in the presence of O_2 takes place over titanium oxide under photoirradiation at low temperature. The active site of TiO_2 is suggested to be the Ti^{4+} Lewis acid site. TiO_2 exhibits the weak Lewis acid property. NH_3 is adsorbed easily on the Lewis acid site as compared with NO. It is conceivable that NO in the gas phase attacks NH_3 adsorbed on the Lewis acid site. N_2 and H_2O are generated via a nitrosamide intermediate. Consequently, the reduced Ti^{3+} species is formed and is reoxidized to the Ti^{4+} species by oxygen. NO can be also adsorbed directly on the Lewis acid site which is unoccupied by NH_3 and transformed to inactive the nitrate species. In the absence of oxygen, NO re-oxidizes the Ti^{3+} species and N_2O was produced.

Introduction

It is well-known that NO*x* is a causative agent of acid rain and town smog. To abate the NO*x* emission, various de-NO*x* technologies have been developed and improved.[1,2] In the case of the stationary emission source such as a power station, waste incinerator, and industrial boiler, NO*x* in exhaust gas is removed ordinarily by the selective catalytic reduction (SCR) process with NH_3 in the presence of O_2 at high temperature (from 573 to 673 K) over V_2O_5-WO_3/TiO_2 and V_2O_5-MoO_3/TiO_2.[3-7] It was concluded that NO is the actual reactant and that oxygen participates in the reaction.[4] Today, most authors agree that the reaction stoichiometry in typical SCR condition is the following:

$$4NO + 4NH_3 + O_2 \longrightarrow 4N_2 + 6H_2O \qquad (1)$$

De-halogen and/or de-SO*x* processes are often located at upstream of de-NO*x* process, in particular in the case of the waste incinerator because V_2O_5-WO_3/TiO_2 and V_2O_5-MoO_3/TiO_2 used in the de-NO*x* process are deactivated easily by halogen compounds and highly concentrated SO*x*. However, most of de-SO*x* processes are based on wet mixed shotcrete which was carried out by spray of $Ca(OH)_2$ or $Mg(OH)_2$. As a consequence, the temperature of the exhaust gas falls below 453 K at the inlet of the de-NO*x* reactor and heating the catalyst bed is necessary to activate catalysts. Therefore, the development of a de-NO*x* process operated at low temperatures is now a prime task. Recently, there have been many reports about the catalyst activated in the region 300-500 K.[8-12]

The purpose in this paper is to study a de-NO*x* process (SCR of NO with NH_3) that proceeds at room temperature. We have reported that SCR of NO with NH_3 in the presence of O_2 at room temperature proceeded over irradiated Rb-ion-modified silica-supported vanadium oxide catalyst (Rb-VS)[13] and irradiated silica-supported titanium oxide catalyst.[14] These photoassisted SCR of NO with NH_3 proceeded smoothly in the region 300-473 K. Our studies were the first studies for SCR of NO with NH_3 over a photocatalyst.

It is known that photocatalysts can promote the reaction under mild conditions, at ambient temperatures and at low pressures. Above all, TiO_2 is the most well-known photocatalyst and many studies have been done.[15,16] There are some remarkable reports about

NO*x* removal over a TiO_2 photocatalyst. Courbon and Pichat et al.[17] reported that photoadsorption and photoexchange of oxygen species of NO and lattice oxygen species and photodecomposition of NO take place over an irradiated TiO_2 sample at room temperature. $N^{18}O$ was adsorbed on TiO_2 rapidly and $N^{16}O$ was produced by isotopic exchange. In addition, $N^{18}O$ was decomposed, producing N_2, $N_2{}^{16}O$, and $N_2{}^{18}O$. Illumination of TiO_2 with UV light promotes the detachment of surface oxygen atoms. Recently, the direct NO removal over a photocatalyst has attracted attention for a practical use such as SCR.[18-21] However, the controversial point is that the activity to remove NO is too low and NO converts to nitrate ions in the presence of O_2. Accordingly, it is very difficult to use the direct NO removal method practically and commercially.

We carried out photo-SCR of NO with NH_3 over TiO_2 at room temperature and identified adsorbed species and intermediates derived from NO, NH_3, and O_2 on TiO_2 by means of FT-IR. The SCR of NO with NH_3 proceeded over irradiated TiO_2. NO (2000 ppm) was reduced to N_2 completely after 90 min over 20 mg of TiO_2 in the presence of O_2. It has not been reported that a high concentration of NO*x* is removed over photocatalysts efficiently. The aim of this work is to clarify the relationship between photocatalysis and the adsorption of substrates on the surface. Here we show the results clearly, and propose the reaction mechanism that NO in the gas phase attacks NH_3 adsorbed on the Lewis acid site of TiO_2 and the reaction intermediate is the nitrosoamide species.

Experimental

Reaction

TiO_2 is JRC-TIO-4 (equivalent to aerosil P-25) supplied from the Japan Catalysis Society. The reaction was carried out in a conventional closed circulating system (dead space, 255 cm^3). The catalyst sample was spread on the flat bottom of the reactor. Prior to a reaction, each catalyst sample (0.2 g) was evacuated at 673 K for 30 min, followed by treatment with 8 kPa O_2 for 90 min and evacuation for 30 min at 673 K. The reaction gases (20 μmol ^{15}NO, 20 μmol NH_3, 20μmol O_2, and 260 μmol Ar) were mixed for 30 min before contact with the

catalyst and then were admitted into the reactor. The catalyst sample was irradiated from the flat bottom of the reactor through a reflection by a cold mirror with a 500 W ultrahigh-pressure Hg lamp USH-500D supplied by USHIO Co. The gas composition at a given time was determined by a quadrupole-type mass spectrometer calibrated by an Ar^{2+} internal standard. In any condition, the detected nitrogen gas was only $^{15}N^{14}N$.

Fourier transform infrared spectroscopy

The catalyst sample (50 mg) was pressed into a wafer (diameter = 10 mm) at a pressure of 0.5 MPa and introduced in an *in situ* IR cell equipped with NaCl windows. The cell allowed us to perform heating, O_2 treatment, introduction of substrates, photoirradiation, and measurements of spectra *in situ*. Before a measurement, the sample was evacuated at 673 K for 30 min, followed by treatment with 8 kPa O_2 for 90 min and evacuation for 30 min at 673 K. A 500 W ultrahigh-pressure mercury lamp (Ushio Denki USH-500D) was used as the light source for photoirradiation of the wafer. FT-IR spectra of a sample and adsorbed species were recorded with a Perkin-Elmer SPECTRUM ONE Fourier transform infrared spectrometer in a transmission mode at room temperature. For each spectrum, the data from 10 scans were accumulated at a resolution of 4 cm^{-1}. All difference infrared spectra in this study are that the spectrum after pretreatment is subtracted from the spectra treated with various substrates (for example, NO, NH_3, and O_2).

Results and Discussion

SCR of NO with ammonia in the presence of oxygen

Figure 1(a) shows the time course of N_2 ($^{15}N^{14}N$) evolution and NH_3 and NO consumption in the absence of the catalyst sample after 30 min of gas mixing. Because the change in Gibb's free energy of SCR of NO with NH_3 is negative, this homogeneous reaction proceeds spontaneously. Therefore, NO and NH_3 gradually decreased.

Figure 1(b) and (c) shows the time course of N_2 evolution and NH_3 and NO consumption in the dark over (b) 200 mg and (c) 20 mg of TiO_2 samples. The N_2 evolution

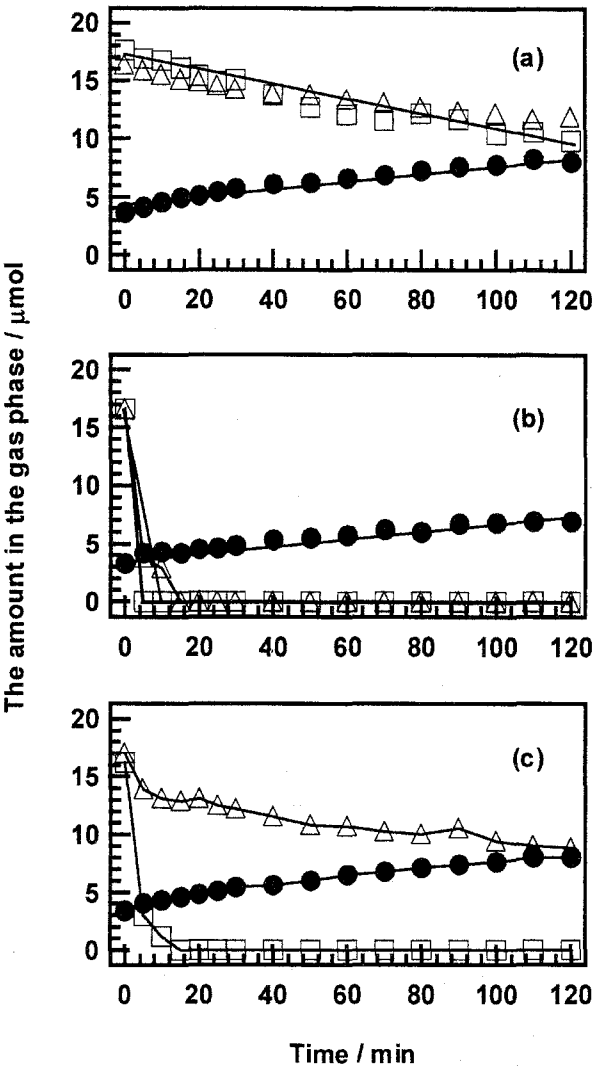

Figure 1 Time course of N_2 (circle), NO (triangle) and NH_3 (square) in the gas phase for SCR of NO with ammonia in the presence of oxygen (a) without catalyst in the dark, (b) over 200 mg JRC-TIO-4 in the dark and (c) over 20 mg JRC-TIO-4 in the dark.

rate was similar to that in the homogeneous reaction as shown in Figure 1(a). However, NH_3 in the gas phase decreased relatively fast. Hattori et al.[22,23] and Tanaka et al.[24] concluded that TiO_2 in the oxidized state exhibits the Lewis acid property. Recently, Martra[25] reported that Ti^{4+} ions exposed on the (0 0 1) and (0 1 0) faces of two types of titania powders (TiO_2 P-25 and TiO_2 Merck) are the Lewis acid centers. In our case, it is very likely that most of the NH_3 was adsorbed on the Lewis acid sites of JRC-TIO-4 in the dark because NH_3 is a strong base.

The NO consumption rate over 200 mg of TiO_2 is higher than that over 20 mg of

TiO_2, although the N_2 evolution rate and the NH_3 consumption rate over 200 mg of TiO_2 were approximately the same with as those over 20 mg of TiO_2. The difference of adsorption behavior of NO can be explained by the assumption that the adsorption site of NO and NH_3 is the same. Ramis et al.[26] investigated coadsorption of NO/NH_3 and NO_2/NH_3 on TiO_2 anatase by means of FT-IR and found that both the molecules are adsorbed on the Lewis acid sites. In addition, they concluded that NH_3 interacts with Lewis acid sites and displaces a degree of nitrate ions from these sites due to its higher basicity and the coordination degree of nitrate ions is lowered in the presence of ammonia. NH_3 is adsorbed on the Lewis acid site preferentially as compared with NO; i.e., adsorption of NH_3 and NO are competing with each other. Therefore, the considerable portions of the Lewis acid sites are poisoned by NH_3 when the numbers of adsorption sites are comparable to those of the gases. In the case of 20 mg of TiO_2, NO could not be adsorbed on the Lewis acid sites of TiO_2 because NH_3 occupied all the sites.

Figure 2 shows the result of SCR with NH_3 in the presence of O_2 over (a) 200 mg and (b) 20 mg TiO_2 samples under photoirradiation. The N_2 evolution rate was accelerated as compared with that in the dark. The detected nitrogen gas was only $^{15}N^{14}N$. This indicates that N atoms of N_2 molecules consist of one N atom derived from NH_3 and one N atom derived from NO. Cant et al. reported that N_2 and N_2O are produced for the NH_3 + NO reaction over TiO_2 under photoirradiation.[27]

In the case of 200 mg of TiO_2 as shown in Figure 2(a), the initial N_2 evolution rate increased under photoirradiation as compared with that in the dark. However, N_2 evolution was saturated at an early stage. Almost half of the NO remained on the surface as an inactive species. In the case of 20 mg of TiO_2 as shown in Figure 2(b), the NO consumption rate and N_2 evolution rate increased dramatically as compared with those in the dark and, interestingly, the NO consumption curve coincides with the N_2 formation curve. The amount of N_2 is equivalent to admitted NH_3 and NO. Therefore, these results strongly indicated that one NO molecule reacts with one NH_3 molecule. It is deduced that, in the first step of the reaction mechanism for photo-SCR, NO in the gas phase attacks the NH_3 species adsorbed on the Lewis acid site of TiO_2. We carried out the following experiment to clarify the assumption.

NO and O_2 gases were introduced to irradiated TiO_2 after TiO_2 was treated with NH_3 in the dark. N_2 could be detected immediately after admission of NO. Whereas in the case that TiO_2 was treated with NO and O_2 followed by NH_3 under photoirradiation, nothing could be detected except the introduced substances. It is concluded that the photo-SCR reaction involves a strongly adsorbed NH_3 species and a gas phase or weakly adsorbed NO species, according to Eley-Rideal mechanism.

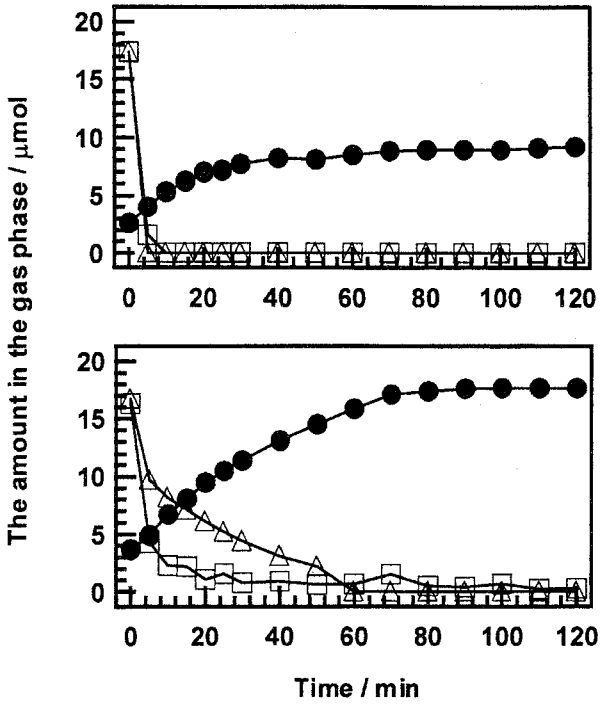

Figure 2 Time course of N_2 (circle), NO (triangle) and NH_3 (square) in the gas phase for SCR of NO in the presence of oxygen (a) over 200 mg JRC-TIO-4 under photoirradiation and (b) over 20 mg JRC-TIO-4 under photoirradiation.

SCR of NO with ammonia in the absence of oxygen

The $^{15}NO + {}^{14}NH_3$ reaction was carried out to examine the role of O_2. Figure 3 shows the profiles of $^{15}N^{14}N$ and $^{15}N_2O$ evolution and $^{14}NH_3$ and ^{15}NO consumption for the NO + NH_3 photocatalytic reaction over 20 mg of TiO_2. $^{15}N_2O$ as well as $^{15}N^{14}N$ was produced in this reaction. Amount of 13.0 μmol of $^{15}N^{14}N$ and 3.9 μmol of $^{15}N_2O$ were formed from 21.3 μmol of ^{15}NO and 20.6 μmol of $^{14}NH_3$, indicating the excellent ^{15}N balance. All of the

introduced ^{15}NO was reduced to $^{15}N^{14}N$ and $^{15}N_2O$. One of the NO + NH_3 reaction stoichiometries when N_2, N_2O, and H_2O are formed is as follows:

$$4NO + 2NH_3 \longrightarrow 2N_2 + N_2O + 3H_2O \qquad (2)$$

Thereby, the N_2/N_2O ratio is two (in the reaction stoichiometry). However, the N_2/N_2O ratio exceeds two when the amount of substrates is comparable with the amount of surface Ti species. The N_2/N_2O ratio eventually approached two when the reaction proceeded catalytically. Therefore, it is expected that N_2O is formed through another route as compared with the generation of N_2. We assumed that N_2O is generated from the reaction (1) because $^{15}N_2O$ was derived form ^{15}NO. Ti^{3+} species have been produced via the formation of N_2 and H_2O by decomposition of intermediates. All of the Ti^{3+} species generated by decomposition of intermediates was not restored to Ti^{4+} species by NO because the number of the NO remaining after formation of intermediates is not sufficient to oxidize all the Ti^{3+}. In the presence of O_2, which is a stronger oxidizing agent than NO, the Ti^{3+} species is restored to Ti^{4+} immediately by O_2 and all the NO molecules are used for the formation of intermediates. Consequently, no N_2O are formed in the presence of O_2. In conclusion, the role of O_2 is the regeneration of the Ti^{4+} species having been reduced when intermediates were decomposed.

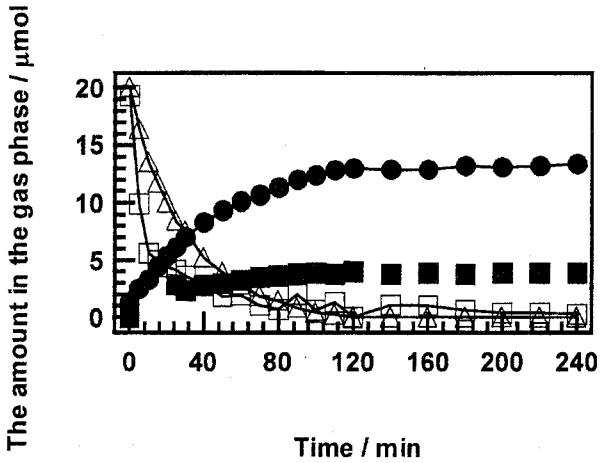

Figure 3 Time course of N_2 (closed circle), N_2O (closed square), NO (open triangle) and NH_3 (open square) in gas phase for SCR of NO in the absence of oxygen over TiO_2 under photoirradiation.

Fourier transform infrared spectroscopy

Figure 4 illustrates the difference infrared spectra from spectra of the adsorbed species on TiO_2 with NO and NH_3 in the ranges 3800-2800 and 1800-1100 cm^{-1}. Introduction of NH_3 led to appearance of eight bands: 3395, 3345, 3298, 3244, 3147, 1599, 1215(shoulder), and 1136 cm^{-1}, as shown in Figure 4(a). Bands at 3395, 3345, 3298, 3244, and 3147 cm^{-1} are assigned to the NH stretching region due to the asymmetric and symmetric νNH as well as to the first overtone of the asymmetric deformation band of the two chemisorbed NH_3 species.[26,28,29] On the other hand, bands at 1599 and at 1215 cm^{-1} can be due to asymmetric and symmetric NH deformation vibration of NH_3 species adsorbed on Lewis acid sites, respectively.[26,28,29] The bands at 1599 and 1215 cm^{-1} originally retained their intensity after evacuation as shown in Figure 4(b). Therefore, the NH_3 species adsorbed on Lewis acid sites of TiO_2 is strongly stable at room temperature and is not desorbed with evacuation. TiO_2 treated with NH_3 was left for 15 min in the dark after introduction of NO as shown in Figure 4(c). A new band was observed at 1678 cm^{-1} after introduction of NO and the intensity of this band did not change for 45 min. This band was assigned to the symmetric NH deformation vibration of the NH_3 species adsorbed on Brønsted acid sites.[28,30] This indicated that the nitrite species is generated on Ti sites. The physisorbed NH_3 species moved to a nitrite site and NH_4NO_2 is formed because the nitrite species expresses a Brønsted acid property. In addition, the intensity of bands derived from NH_3 did not also change in the dark for 45 min. It is concluded that the NO + NH_3 reaction was not accelerated in the dark.

Furthermore, Figure 4(d)-(g) shows that the bands of the NH_3 species adsorbed on the Lewis acid site decreased gradually in intensity with time of irradiation and disappeared almost after 120 min. In addition, the top of the broad band in the region 1100-1300 cm^{-1} shifted gradually from 1215 to 1136 cm^{-1}. It is reported that the bands at around 1136 and 1215 cm^{-1} are assigned to the coordinatively saturated and unsaturated NH_3 species, respectively.[26] It can be seen that the NH_3 species for itself was decomposed or reacted with NO under photoirradiation. In the absence of NO, The bands of adsorbed NH_3 species did not decrease in intensity over irradiated TiO_2. Furthermore, a new band at 1624 cm^{-1} appeared under photoirradiation and grew with time of irradiation. It is well-known that this band is

assigned to the deformation vibration of H_2O.[31] A Broad band in the region 2800-3600 cm^{-1} assigned to molecular water also increased in intensity with time of irradiation. As mentioned above, it is concluded that NO in the gas phase attacks the NH_3 species adsorbed on the Lewis acid site and that N_2 and H_2O would be generated.

The hydroxyl group of titanium oxide appears at 3675 cm^{-1}. The band increased in intensity under photoirradiation. This indicates that the adsorbed NH_3 species is activated under photoirradiation. The hydroxyl groups in the surface of TiO_2 combine with each other

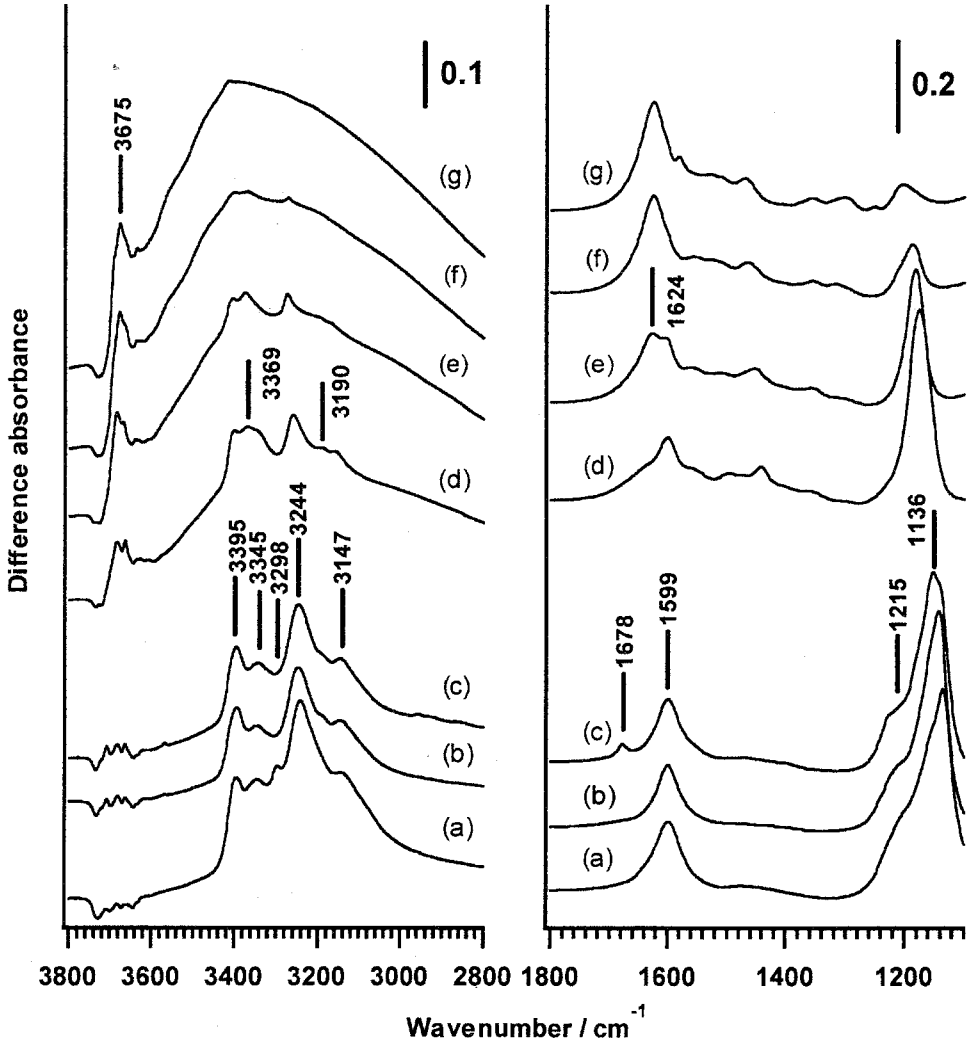

Figure 4 The difference infrared spectra from spectra of the adsorbed species on TiO_2 with NO and NH_3 in the ranges 3800-2800 and 1800-1100 cm^{-1}. (a) after introduction of NH_3, (b) after evacuation, (c) after introduction of NO and left for 15 min in the dark, (d) under photoirradiation for 10 min, (e) for 30 min, (f) for 60 min and (g) for 120 min.

to form Ti-O-Ti sites because TiO_2 is pretreated with O_2 and water is desorbed. When NH_3 is adsorbed on the Lewis acid site of Ti-O-Ti, it is expected that the Ti-O-Ti site is changed to $Ti-NH_2$ (radical amide species) and Ti-OH under photoirradiation. It is assumed that NO in the gas phase attacks $Ti-NH_2$ and an intermediate is formed. Therefore, the increase of intensity derived from Ti-OH indicates that the NO + NH_3 reaction is accelerated smoothly and the amide species as intermediate is formed on the surface of TiO_2.

On the other hand, new bands at 3369 and 3190 cm^{-1} appeared under photoirradiation. These bands are assigned to the NH stretching vibration of amide species. And, many bands in the region 1550-1300 cm^{-1} were observed under photoirradiation. Figure 5 shows the difference infrared spectra of TiO_2 with (a) introduction of ^{14}NO and (b) introduction of ^{15}NO to TiO_2 treated with NH_3 under photoirradiation for 30 min in the ranges 1800-1200 cm^{-1}. The bands at 1550 and 1350 cm^{-1} did not shift, but the bands at 1490, 1470, 1435, and 1400 cm^{-1} shifted to the side of low wavenumbers. Therefore, the bands at 1490, 1470, 1435, and 1400 cm^{-1} are derived from NO. Ramis et al.[26,32] reported that the bands at 1490 and 1550 cm^{-1} are

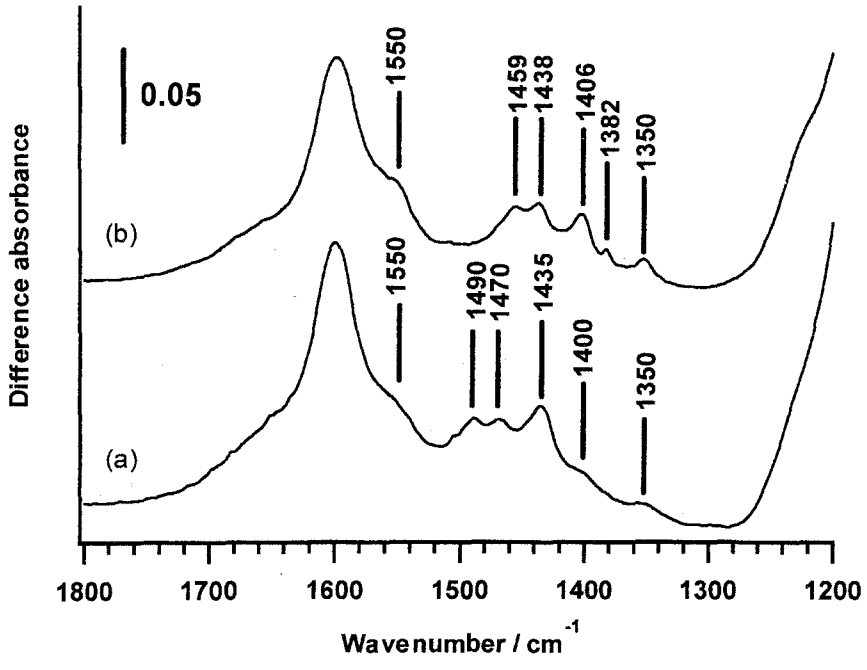

Figure 5 The difference infrared spectra from spectra of the adsorbed species on TiO_2 under photoirradiation for 30 min in the ranges 1800-1200 cm^{-1}. (a) with ^{14}NO and NH_3 and (b) ^{15}NO and NH_3.

assigned to the NO deformation vibration and the NH_2 bending vibration of the nitrosamide species, respectively. The band at 1350 cm^{-1} is also assigned to the amide species.[32] These indicate that the nitrosamide species as an intermediate was generated after NO in the gas phase or adsorbed weakly attacks the radical amide species. It is considered that NO combines with the radical amide species easily because NO is also a radical. On the other hand, it is expected that the bands at 1435 and 1400 cm^{-1} are assigned to the NO stretching vibration of the nitro species[33,34] and the band at 1470 cm^{-1} is derived from the NO stretching vibration of the monodentate nitrite.[34] However, it is unknown whether the nitro species or the monodentate nitrite participates in photo-SCR of NO with NH_3.

Figure 6 illustrates that the difference infrared spectra of TiO_2 treated with NO and O_2 after treatment of NH_3 in the ranges 3800-2800 and 1800-1100 cm^{-1}. Figure 6(a)-(c) are almost same as Figure 4(a)-(c). Bands at 1750, 1623, 1584, 1501, 1450(shoulder), 1400(shoulder), 1298, and 1248 cm^{-1} appeared and the bands assigned to the NH_3 species on Lewis acid sites at 1136 and 1599 cm^{-1} disappeared after introduction of NO and O_2 in the dark as shown in Figure 6(d). It is well-known that NO_3^- species identified in the ranges 1530-1480 and 1290-1250 cm^{-1}, in 1565-1500 and 1300-1260 cm^{-1} and in 1650-1600 and 1225-1170 cm^{-1} are assigned to monodentate, bidentate, and bridging nitrate species; in addition, the band at 1380 cm^{-1} is free NO_3^- ion.[34-36] Furthermore, Ramis et al.[26] reported that the three couples of bands at 1586 and 1291 cm^{-1}, at 1608 and 1250 cm^{-1}, and at 1630 and 1195 cm^{-1} are assigned to monodentate, bidentate, and bridging nitrate species on TiO_2, respectively. On the other hand, bands of nitrite species appear in almost the same region as that of the nitrate species. It is well-known that NO_2^- species identified in 1220-1205 cm^{-1}, in 1440-1335 and 1350-1315 cm^{-1}, in 1520-1390 and 1260-1180, and in 1470-1450 and 1065-1050 cm^{-1} are assigned to the bridging nitrite, nitro compound, monodentate nitrite, and chelating nitro compound, respectively; in addition, the bands at 1260 and 1330 cm^{-1} are free NO_2^- ion.[34-36] It is very difficult to distinguish clearly between nitrate and nitrite. In this study, we ascribe the results reported by Ramis et al. The bands at 1584 and 1298 cm^{-1}, at 1248 cm^{-1}, and at 1623 cm^{-1} are due to monodentate, bidentate, and bridging nitrate species, respectively, and did not change under photoirradiation as shown in Figure 6(e)-(g). Therefore, the nitrate

species is inactive for photo-SCR of NO with NH_3. The broad band at 1501 cm^{-1} is assigned to the NO stretching vibration of the monodentate NO_3^- species, in line with their more labile character.[26] The band did not decrease in intensity continuously under photoirradiation although the intensity under photoirradiation is lower than that in the dark. In this connection, the band at 1750 cm^{-1} and the shoulder band at 1450 cm^{-1} are assigned to symmetric and asymmetric N-H deformation vibrations of ammonium ion adsorbed on the Brønsted acid site.

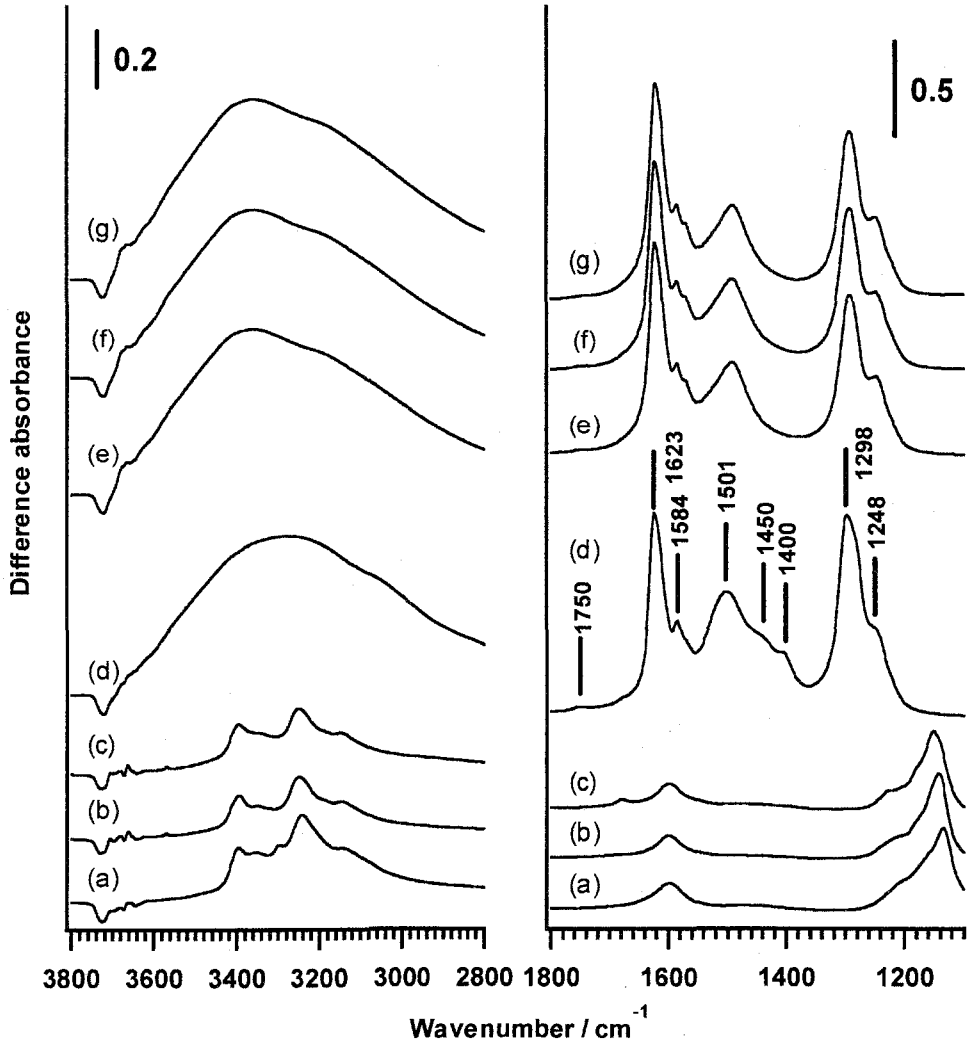

Figure 6 The difference infrared spectra from spectra of the adsorbed species on TiO_2 with NO, NH_3 and O_2 in the ranges 3800-2800 and 1800-1100 cm^{-1}. (a) after introduction of NH_3, (b) after evacuation, (c) after introduction of NO and left for 15 min in the dark, (d) after introduction of O_2 and left for 15 min in the dark, (e) under photoirradiation for 10 min, (f) for 30 min and (g) for 60 min.

Ramis et al.[26] observed the same band after NO_2/NH_3 coadsorption experiments on TiO_2 anatase. Hadjiivanov et al.[37] almost reported that the band assigned to the ammonium ion on the Brønsted acid site appears for NO_2/NH_3 coadsorption on TiO_2. They concluded that the presence of nitrate ions causes the generation of the Brønsted acid sites and contributes to the formation of ammonium ions. Therefore, NO is oxidized to NO_2 on the sites unoccupied by NH_3 in the presence of O_2 and the formed NO_2 is adsorbed as NO_3^- or NO_2^- on irradiated TiO_2. The nitrate ion or nitrite ion causes the formation of Brønsted acid sites and combines with NH_3 to generate $NH_4^+NO_3^-$ or $NH_4^+NO_2^-$. It is seen that these Brønsted acid sites are formed rapidly because the bands assigned to adsorbed NH_3 species disappeared in intensity quickly after NO and O_2 are introduced to the sample as shown in Figure 6(d). And, these Brønsted acid sites have stronger acidity than the Lewis acid site on TiO_2. It is assumed that the photo-SCR reaction proceeded smoothly because the broad band assigned to H_2O in the region 3600-2800 cm^{-1} increased in intensity; however, the bands derived from nitrosamide species could not be confirmed in this case because the bands assigned at nitrate species overlapped. From this result, it is difficult to identify the nature of the intermediate, which is NH_2NO, $NH_4^+NO_2^-$ or $NH_4^+NO_3^-$.

Figure 7 and Figure 8 illustrate that the difference infrared spectra of JRC-TIO-4 with coadsorption of NO/NH_3 and $NO/NH_3/O_2$ in the ranges 3800-2800 and 1800-1100 cm^{-1}, respectively. The result of NO/NH_3 coadsorption as shown in Figure 7 was consistent with that in Figure 4 because the band identified as the adsorbed NH_3 species at 1145 and 1599 cm^{-1} decreased gradually in intensity, and the band assigned to the deformation vibration of H_2O at 1631 cm^{-1} increased gradually in intensity under photoirradiation; in addition, the bands assigned to NH_2NO were generated. On the other hand, the result of $NO/NH_3/O_2$ coadsorption as shown in Figure 8 was inconsistent with that in Figure 6. $NO/NH_3/O_2$ coadsorption led to the appearance of five bands with maxima at 1662, 1597, 1439, and 1184 cm^{-1} as shown in Figure 8(a). The intensities of these bands were changed in the dark. The bands at 1597 and 1184 cm^{-1} are assigned to asymmetric and symmetric NH deformation vibration of NH_3 adsorbed on Lewis acid sites of TiO_2. The bands at 1662 and 1439 cm^{-1} are assigned to symmetric and asymmetric NH deformation vibration of NH_4^+ adsorbed on

Brønsted acid sites of TiO_2. Both bands of NH_3 species adsorbed on the Lewis acid site and on the Brønsted acid site decreased in intensity under photoirradiation. However, the band assigned to the NH_3 species adsorbed on the Lewis acid site was hardly shifted to the high wavenumber side. Therefore, this indicated that the adsorbed NH_3 is almost the coordinatively saturated species. The physisorbed NH_3 species disappears easily after evacuation. However, the NH_3 species adsorbed on Brønsted acid sites is not evacuated at room temperature. It is speculated that these NH_3 species moves to unoccupied Lewis acid sites. On the other hand,

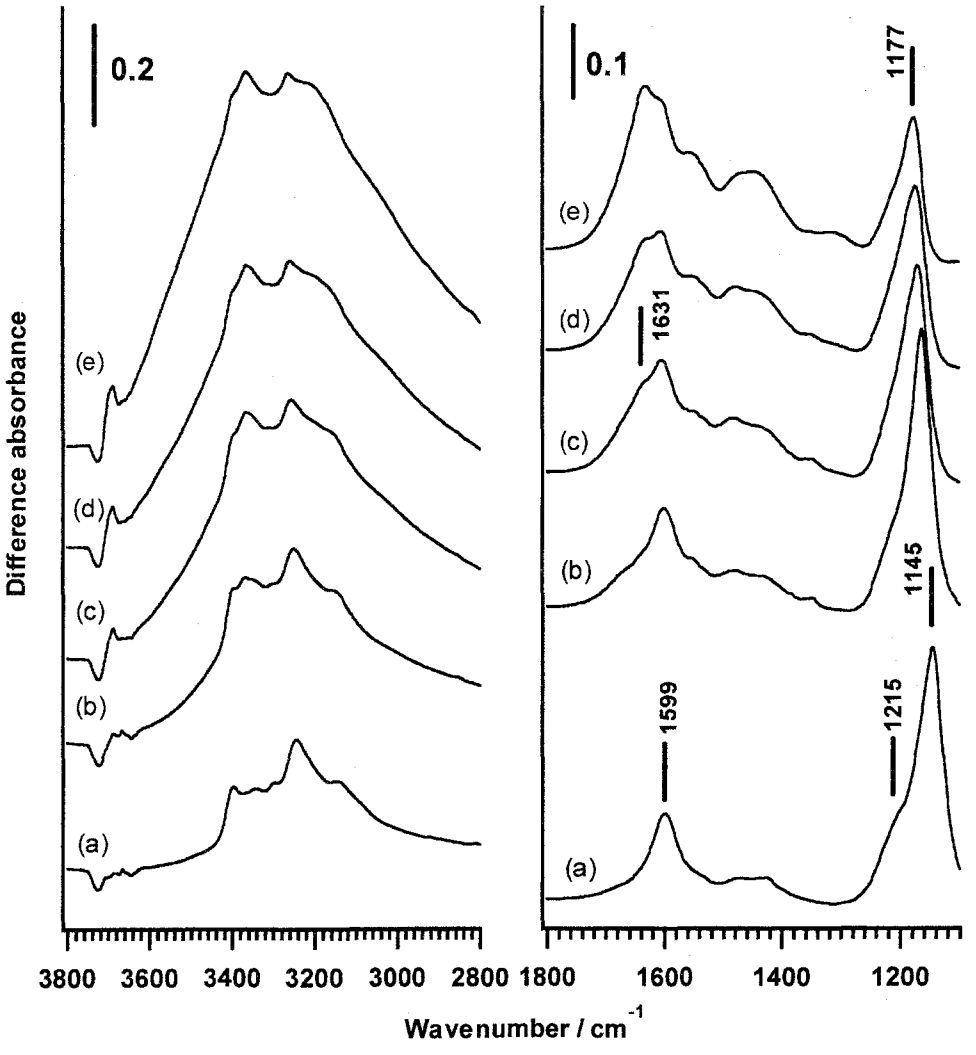

Figure 7 The difference infrared spectra from spectra of the adsorbed species on TiO_2 with NO and NH_3 in the ranges 3800-2800 and 1800-1100 cm^{-1}. (a) after introduction of the gas mixed NO and NH_3 and left for 15 min in the dark, (b) under photoirradiation for 10 min, (c) for 30 min, (d) for 60 min and (e) for 120 min.

the new bands at 1633, 1560, 1475, 1382, and 1352 cm^{-1} appeared under photoirradiation as shown in Figure 8(b). The band at 1633 cm^{-1} is assigned to the deformation vibration of H_2O. The photo-SCR reaction proceeded smoothly because this band increased generally under photoirradiation. As mentioned earlier, the bands at 1560 and 1475 cm^{-1} are assigned to the NH_2 bending vibration and the NO deformation vibration of the nitroamine species. In addition, the band at 1382 and 1352 cm^{-1} are identified as the nitro species or monodentate nitrite. The intensities of these bands were not varied under irradiation and after evacuation.

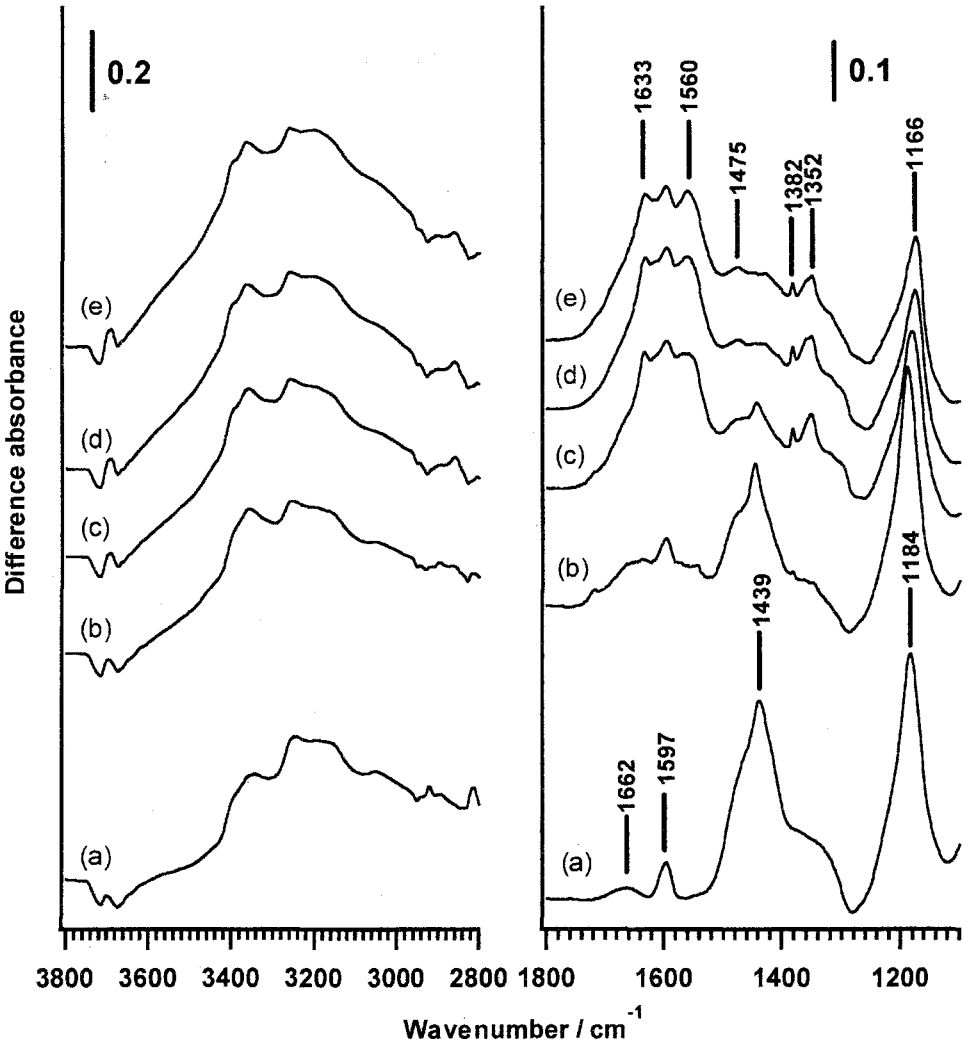

Figure 8 The difference infrared spectra from spectra of the adsorbed species on TiO_2 with NO, NH_3 and O_2 in the ranges 3800-2800 and 1800-1100 cm^{-1}. (a) after introduction of the gas mixed NO, NH_3 and O_2 and left for 15 min in the dark, (b) under photoirradiation for 10 min, (c) for 30 min, (d) for 60 min and (e) for 120 min.

Therefore, it is expected that the NH_4NO_2 species is not intermediate for photo-SCR of NO with NH_3. The band of the nitrate species did not appear with $NO/NH_3/O_2$ coadsorption under photoirradiation because the bands at 1560 and 1597 cm^{-1} did not shift using ^{15}NO gas. The band at 1597cm^{-1} is assigned to asymmetric NH deformation vibration of NH_3 adsorbed on the Lewis acid site. We assumed that NH_3 blocks the sites where nitrate species can be adsorbed. As mentioned earlier, It is known that NO is converted to nitrate species on the Lewis acid site of TiO_2 in the presence of O_2. Therefore, both sites adsorbed NH_3 and NO_3^- are the same. The nitrate species could not be generated from NO and O_2 because NH_3 was adsorbed more rapidly on the Lewis acid site than NO.

The reaction mechanism

The results mentioned above are summarized as follows:

(1) The active site for photo-SCR is the Ti^{4+} Lewis acid site.

(2) The Ti-O-Ti site adsorbing NH_3 is changed to Ti-NH_2 and Ti-OH under photoirradiation.

(3) NO in the gas phase attacks the NH_2 species adsorbed on the Lewis acid site of TiO_2.

(4) The nitrosamide species as intermediate is formed from NO in the gas phase and radical amide species on TiO_2.

(5) The nitrate species is inactive for photo-SCR of NO with NH_3.

(6) The N_2 evolution rate is higher in the presence of O_2 than in the absence of O_2. N_2O derived from NO is generated in the absence of O_2.

(7) Photoexcitation of the catalysts promotes the catalysis.

It is known that the conventional NH_3-SCR process proceeds according to Eley-Rideal mechanism. Therefore, NO in the gas phase attacks the adsorbed NH_3 species. The two research groups proposed a different adsorbed NH_3 species and reaction mechanism for conventional NH_3-SCR of NO over V_2O_5/TiO_2. Ramis et al.[30] proposed that Lewis acid sites of the vanadium center are active sites and that the nitrosoamide species is formed as an intermediate in these sites. On the other hand, Topsøe et al.[38-40] proposed that V^{5+}-OH and V^{5+}=O are acid site and redox site as active sites, respectively, and NH_3 is adsorbed on a Brønsted acid site. In our case, the Lewis acid site of TiO_2 is an active site and the nitrosamide

species was identified by infrared spectroscopy. Therefore, we conclude that the mechanism of photo-SCR over TiO_2 is similar to the former.

Conclusion

Over irradiated TiO_2, most NO could be removed in the presence of NH_3 and O_2. The active site for photo-SCR of NO is the Ti^{4+} species. NH_3 is adsorbed easily on the Lewis acid site of TiO_2 in the dark. The photoformed hole is captured by the amide species evolved from adsorbed NH_3 to form an amide radical, and the photoformed electron reduces a titanium cation. The NO molecule in the gas phase reacts with the amide radical to form the nitrosamide species as an intermediate like the Eley-Ridial mechanism. And, the nitrosamide intermediate is decomposed to N_2 and H_2O leaving reduced titanium cations, Ti^{3+}. NO converts to the nitrate species via NO_2 in the presence of O_2 on Ti sites unoccupied by NH_3. The nitrate species forms a Brønsted acid site and stocks the NH_3 species as an ammonium ion. However, the nitrate species poisons the Ti site and the activity is lower because the nitrate species is very stable. Oxygen plays a role in reoxidizing reduced titanium cations. In the absence of O_2, NO oxidize Ti^{3+} sites and N_2O is generated.

References

(1) Wood, S. C. *Chem. Eng. Prog.* **1994**, *90(I)*, 32.

(2) Pârvulescu, V. I.; Grange, P.; Delmon, B. *Catal. Today* **1998**, *46*, 233.

(3) Bosch, H.; Janssen, F. *Catal. Today* **1988**, *2*, 369.

(4) Busca, G.; Lietti, L.; Ramis, G.; Berti, F. *Appl. Catal. B: Environ.* **1998**, *18*, 1.

(5) Forzatti, P.; Lietti, L. *Heterogeneous Chem. Rev.* **1996**, *3*, 33.

(6) Cho, S. M. *Chem. Eng. Prog.* **1994**, *90(I)*, 39.

(7) Forzatti, P. *Appl. Catal. A-Gen.* **2001**, *222*, 221.

(8) Zhu, Z. P.; Liu, Z. Y.; Liu, S. J.; Niu, H. X. *Appl. Catal. B-Environ.* **1999**, *23*, L229.

(9) Zhu, Z. P.; Liu, Z. Y.; Liu, S. J.; Niu, H. X.; Hu, T. D.; Liu, T.; Xie, Y. N. *Appl. Catal.*

B: Environ. **2000**, *26*, 25.

(10) Zhu, Z. P.; Liu, Z. Y.; Liu, S. J.; Niu, H. X. *Appl. Catal. B-Environ.* **2001**, *30*, 267.

(11) Smirniotis, P. G.; Pena, D. A.; Uphade, B. S. *Angew. Chem.-Int. Edit.* **2001**, *40*, 2479.

(12) Long, R. Q.; Yang, R. T.; Chang, R. *Chem. Commun.* **2002**, 452.

(13) Tanaka, T.; Teramura, K.; Funabiki, T. *Phys. Chem. Chem. Phys.* **2000**, *2*, 2681.

(14) Tanaka, T.; Teramura, K.; Yamamoto, T.; Takenaka, S.; Yoshida, S.; Funabiki, T. *J. Photochem. Photobiol. A-Chem.* **2002**, *148*, 277.

(15) Linsebigler, A. L.; Lu, G.; Yates Jr., J. T. *Chem. Rev.* **1995**, *95*, 735.

(16) Fujishima, A.; Rao, T. N.; Tryk, D. A. *J. Photochem. Photobiol. C-Photochem. Rev.* **2000**, *1*, 1.

(17) Courbon, H.; Pichat, P. *J. Chem. Soc., Faraday Trans. 1* **1984**, *80*, 3175.

(18) Hashimoto, K.; Wasada, K.; Toukai, N.; Kominami, H.; Kera, Y. *J. Photochem. Photobiol. A-Chem.* **2000**, *136*, 103.

(19) Hashimoto, K.; Wasada, K.; Osaki, M.; Shono, E.; Adachi, K.; Toukai, N.; Kominami, H.; Kera, Y. *Appl. Catal. B-Environ.* **2001**, *30*, 429.

(20) Yamashita, H.; Ichihashi, Y.; Anpo, M.; Hashimoto, M.; Louis, C.; Che, M. *J. Phys. Chem.* **1996**, *100*, 16041.

(21) Zhang, J. L.; Ayusawa, T.; Minagawa, M.; Kinugawa, K.; Yamashita, H.; Matsuoka, M.; Anpo, M. *J. Catal.* **2001**, *198*, 1.

(22) Hattori, H.; Itoh, M.; Tanabe, K. *J. Catal.* **1975**, *38*, 172.

(23) Hattori, H.; Itoh, M.; Tanabe, K. *J. Catal.* **1976**, *41*, 46.

(24) Tanaka, T.; Kumagai, H.; Hattori, H.; Kudo, M.; Hasegawa, S. *J. Catal.* **1991**, *127*, 221.

(25) Martra, G. *Appl. Catal. A-Gen.* **2000**, *200*, 275.

(26) Ramis, G. G.; Busca, G.; Lorenzelli, V.; Forzatti, P. *Appl. Catal.* **1990**, *64*, 243.

(27) Cant, N. W.; Cole, J. R. *J. Catal.* **1992**, *134*, 317.

(28) Kung, M. C.; Kung, H. H. *Catal. Rev. -Sci. Eng.* **1985**, *27*, 425.

(29) Chuang, C. C.; Shiu, J. S.; Lin, J. L. *Phys. Chem. Chem. Phys.* **2000**, *2*, 2629.

(30) Ramis, G.; Busca, G.; Bregani, F.; Forzatti, P. *Appl. Catal.* **1990**, *64*, 259.

(31) Ito, E.; Mergler, Y. J.; Nieuwenhuys, B. E.; Calis, H. P. A.; vanBekkum, H.; vandenBleek, C. M. *J. Chem. Soc.-Faraday Trans.* **1996**, *92*, 1799.

(32) Nonella, M.; Muller, R. P.; Huber, J. R. *J. Mol. Spectro.* **1985**, *112*, 142.

(33) Levin, I. W.; Milne, G. W. A.; Axenrod, T. *J. Chem. Phys.* **1970**, *53*, 2505.

(34) Hadjiivanov, K. I. *Catal. Rev.-Sci. Eng.* **2000**, *42*, 71.

(35) Pozdniyakov, D. V.; Filimonov, V. N. *Kinet. Katal.* **1973**, *14*, 760.

(36) Davydov, A. A. *Infrared Spectroscopy of Adsorbed Species on the Surface of Transition Metal Oxides*; John Wiley & Sons: England, 1984.

(37) Hadjiivanov, K.; Bushev, V.; Kantcheva, M.; Klissurski, D. *Langmuir* **1994**, *10*, 464.

(38) Topsøe, N. Y. *Science* **1994**, *265*, 1217.

(39) Topsøe, N. Y.; Topsøe, H.; Dumesic, J. A. *J. Catal.* **1995**, *151*, 226.

(40) Topsøe, N. Y.; Dumesic, J. A.; Topsøe, H. *J. Catal.* **1995**, *151*, 241.

Chapter 4

Photoinduced electron transfer between adsorbent and adsorbed species

Abstract

The formation of stable NH_2 radical over UV-irradiated TiO_2 was confirmed by EPR spectroscopy. The NH_2 radical having generated on TiO_2 adsorbing NH_3 reacts with NO gas to produce a NH_2NO intermediate in the dark. Photoformed holes and electrons on TiO_2 are trapped by NH_2^- species and Ti^{4+} species, birnging about the formation of a NH_2 radical and a Ti^{3+} species. This shows that electron transfer takes place between a Ti^{4+} atom and a N atom of adsorbed NH_3 efficiently, resulting in the formation of the NH_2 radical stable even in the dark. The stability of the NH_2 radical causes the high reaction cross section with NO and it is quenched just after introduction of NO leaving the Ti^{3+} species.

Introduction

In previous works, we have already reported photo-SCR over TiO_2 photocatalyst at room temperature where 83 % of NO conversion and 96 % of N_2 selectivity are achieved in the conventional fixed bed flow system[1] and proposed the reaction mechanism of our photo-SCR system as shown in Scheme 1[2]. NH_3 is adsorbed on Lewis acid site of TiO_2 in the dark (Step1). NH_3 in the gas phase was diminished rapidly on introducing to TiO_2. The NH_3 species adsorbed on Lewis acid site of TiO_2 was confirmed by FT-IR spectroscopy. One hydrogen atom of the adsorbed NH_3 species interacts with a lattice oxygen atom. Electron transfer takes place from N-atom of NH_3 adsorbed on TiO_2 to Ti-atom of TiO_2 bulk under photoirradiation. The photoformed hole is captured by the NH_2^- species evolved from adsorbed NH_3 to form a NH_2 radical (Step 2). An OH stretching vibration band of TiO_2 (3675 cm^{-1}) increased in intensity under photoirradiation after treatment of NH_3. The NH_2 radical reacts with NO in the gas phase readily to generate a NH_2NO species as an intermediate (Step

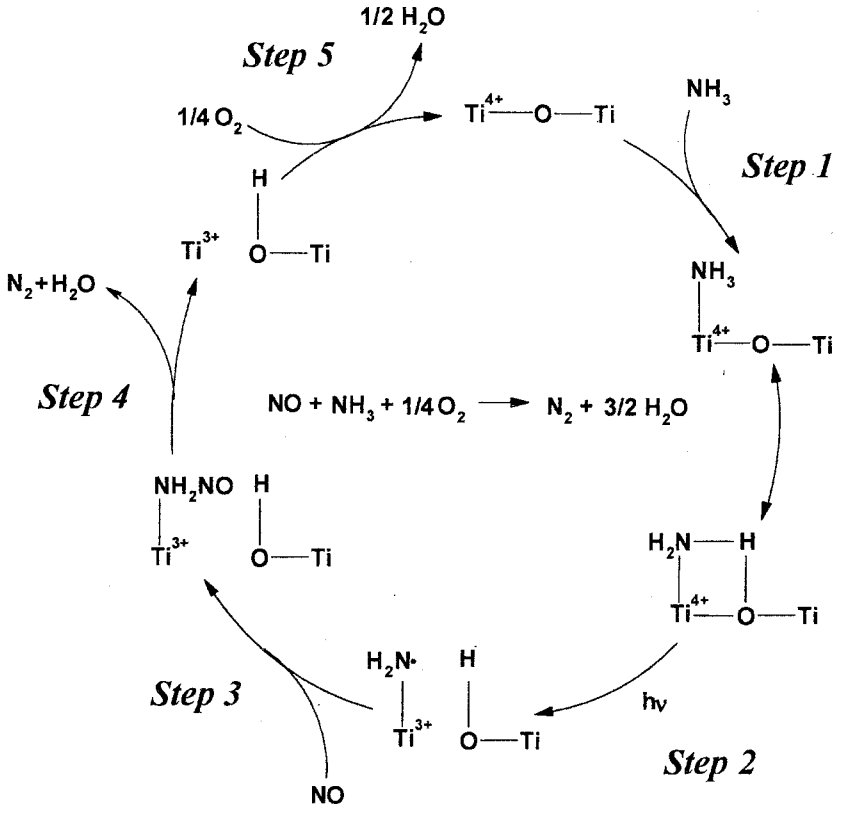

Scheme 1 Reaction mechanism of photo-SCR with NH_3 over TiO_2.

3). The bands derived from the NH_2NO intermediate was monitored by FT-IR spectroscopy when TiO_2 adsorbing NH_3 was irradiated in the presence of NO. This species was not observed in the dark. Thus, the formed NH_2NO intermeidate is decomposed to N_2 and H_2O (Step 4). N_2 was detected by TCD-GC in the photo-SCR reaction. As mentioned above, the high NO conversion and the excellent N_2 selectivity was achieved in the conventional fixed bed flow system. In addition, the detected N_2 gas was only $^{15}N^{14}N$ on using ^{15}NO and $^{14}NH_3$ in the photo-SCR reaction. This indicates that N atoms of N_2 molecule consist of one N atom derived from NH_3 and one N atom derived from NO. On the other hand, a Ti^{3+} species formed by the electron transfer is re-oxidized to a Ti^{4+} species by O_2 (Step 5). It was affirmed by UV-Vis spectroscopy that the Ti^{3+} species of TiO_2 reduced by H_2 was reoxidized to the Ti^{4+} species as shown in Figure 1. In this way, the photo-SCR reaction proceeds catalytically. Accordingly, the reaction stoichiometry in the photo-SCR is same as that in the conventional NH_3-SCR.

We did not confirm yet whether or not the NH_2 radical is generated on TiO_2 and reacts with NO in the gas phase (from Step 2 to Step 3) although a NH_2 radical was observed on various solid materials absorbing NH_3 under photoirradiation by EPR spectroscopy.[3-6] In addition, many EPR studies related to TiO_2 were reported under various condition.[7,8] However, a NH_2 radical has not been assigned on TiO_2 absorbing NH_3 under photoirradiation yet. In the present paper, we proposed the formation of a NH_2 radical which readily reacts with NO in the gas phase deduced by EPR spectroscopy.

Experimental

Catalyst preparation

JRC-TIO-4 (equivalent to Degussa P-25) supplied from the Japan Catalysis Society was hydrated in distilled water for 2 h at 353 K, followed by filteration with suction pump. The sample was kept at 383 K for 24 h in an oven, followed by calcinations in air at 773 K for 3 h. The specific surface area was evaluated to be 48 m^2g^{-1} by the BET method using N_2 adsorption isotherm at 77 K. Powder XRD tells that JRC-TIO-4 consists of anatase and rutile

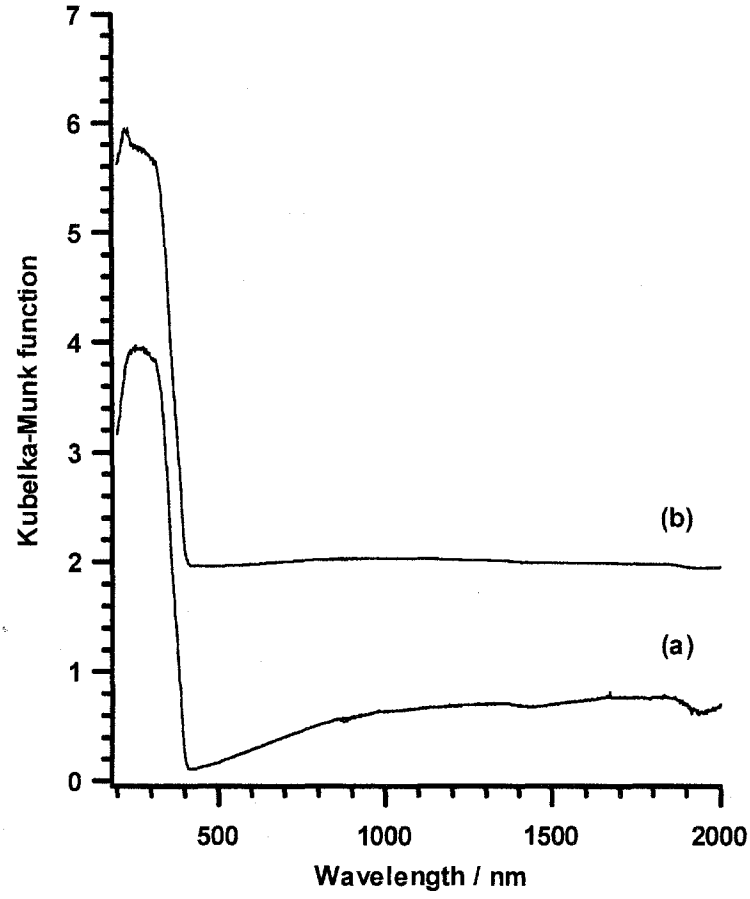

Figure 1 UV-Vis spectra of TiO_2 (a) after H_2 treatment and (b) after O_2 introduction.

phases.

Electron Paramagnetic Resonance (EPR)

EPR spectra were recorded using an in-situ quartz cell with an X-band EPR spectrometer (JOEL JES-SRE2X) with 100 k Hz field modulation at 123 K. Before a measurement, the catalyst sample was heated at 673 K in air and evacuated for 30 min at the same temperature, followed by treatment with 8 kPa O_2 for 90 min and evacuation for 30 min at 673 K. The *g* value and the relative amount of radical species were determined using a Mn marker. The effect of NH_3 adsorption onto TiO_2 upon the EPR spectra was investigated by recording the spectra after the equilibrium adsorption of NH_3 at room temperature followed by evacuation. On the other hand, NO was introduced to TiO_2 adsorbing NH_3 under the measurement condition. Some spectra were recorded under illumination $\lambda > 300$ nm from a

500 W ultrahigh-pressure mercury lamp with UV-33 cut filter (TOSHIBA).

Results and Discussion

Figure 2 and Figure 3(a) shows the EPR spectrum of TiO_2 pretreated in the presence of O_2 at 673 K in the dark. The spectrum corresponded to the typical spectrum of mixture of anatase and rutile. The lines appeared at g = 1.983, 1.980, 1.969, 1.963 and 2.005. The lines at 1.983, 1.980, 1.969 and 1.963 were assigned to the Ti^{3+} species.[9-12] Recently, Hurum et al.[13] investigated the in-situ EPR spectra of TiO_2 (Degussa P-25) under irradiation and assigned four g-values to the Ti^{3+} species derived from anatase and rutile. We also determined that the lines at g = 1.983, 1.969 and those at g = 1.980, 1.963 were derived from anatase and rutile, respectively, although the EPR spectrum of TiO_2 was measured in the dark. On the other hand, the line at g = 2.005 is assignable to an electron trapped in an F centre. It have been determined by XRD that the crystal phase of JRC-TIO-4 is mixture of anatase and rutile

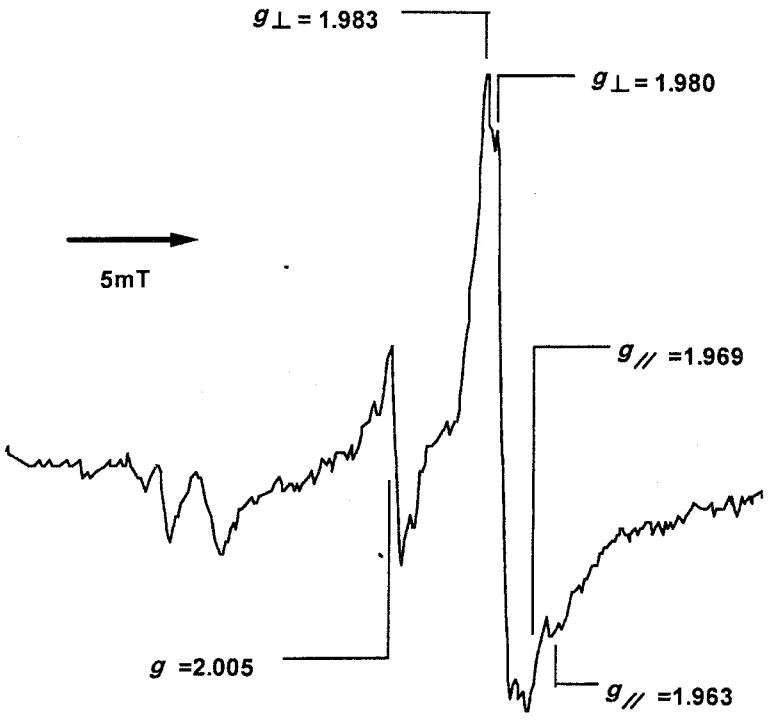

Figure 2 EPR spectrum of TiO_2 pretreated in the presence of O_2 at 673 K.

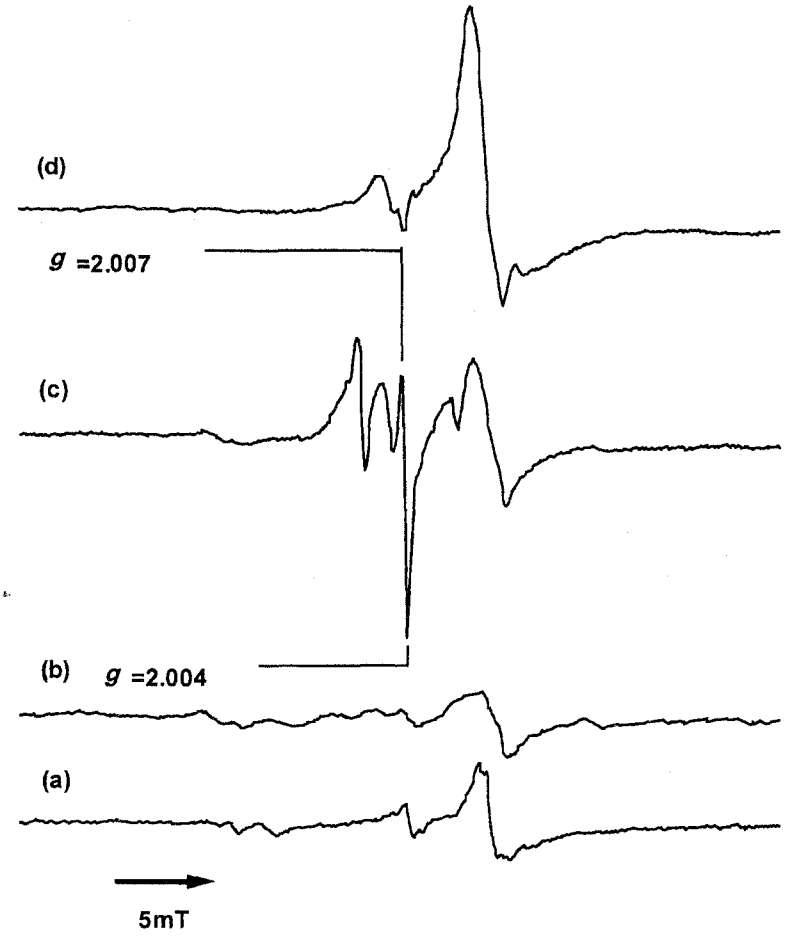

Figure 3 EPR spectra of TiO_2 (a) after pretreatment, (b) after introduction of NH_3 in the dark, (c) under photoirradiation and (d) after introduction of NO in the dark.

although we do not know how to produce JRC-TIO-4 (equivalent to Degussa P-25) in detail. It is well-known that oxygen defect sites, which work as F centre, are formed in TiO_2 treated at high temperature. Calcination at 1173 K causes the formation of rutile phase in TiO_2. Therefore, it is appropriated that the electron trapped in the F centre of TiO_2 is detected at g = 2.005 by EPR spectroscopy.

Introduction of NH_3 to TiO_2 make the EPR spectrum change a little as shown in Figure 3(b). The lines assigned to the Ti^{3+} species and the electron trapped in the F centre decreased in intensity after addition of NH_3. It was reported that NH_3 is adsorbed on a Lewis acid site of TiO_2 rapidly.[2,14,15] In the present study, NH_3 was also adsorbed on TiO_2 quickly.

Consequently, the intensities would be relieved by adsorption of NH_3. Next, NH_3 in the gas phase was evacuated by a vacuum pump, followed by photoirradiation with a 500 W ultrahigh-pressure mercury lamp equipped with UV-33 cut filter. New lines were observed as soon as TiO_2 adsorbing NH_3 was illuminated at 123 K as shown in Figure 3(c). Figure 4 shows the EPR spectrum expanded Figure 3(c) with assignable g values (solid line) and the simulated EPR spectrum (dot line). Many signals appeared at g = 1.972, 1.980, 1.990, 2.004, 2.007, 2.009, 2.019 and 2.021 after photoirradiation. These new signals were quite stably present even after more than one hour at 123 K when the irradiation was ceased. Some research groups clarified the NH_2 radical was generated under photoirradiation to NH_3 matrix by EPR spectroscopy. The first EPR spectrum of the NH_2 radical was obtained by irradiation under UV light of ammonia in a matrix of argon in 1958.[16] In the case of the conventional NH_2 radical, the three ^{14}N lines are further split into three lines by the hyperfine interaction with two equivalent hydrogen atoms. Therefore, nine lines are identified in the EPR spectrum of TiO_2 adsorbing NH_3. On the other hand, the EPR spectra of the NH_2 radical trapped on the surface of Zeolite[3], SiO_2[4,5] and PVG[6] adsorbing NH_3 under photoirradiation are complicated because the signal is not split into nine excellent lines. We referred their hyperfine tensors of nitrogen-14 of the NH_2 radical to simulate the obtained EPR spectrum of TiO_2 adsorbing NH_3 under photoirradiation (dot line in Figure 4) and determined our hyperfine tensor as shown in Table 1. The lines at g > 2.004 of the EPR spectrum simulated $^{14}NH_2$ radical were corresponded with that of the obtained spectrum. Accordingly, we made use of $^{15}NH_3$ instead of $^{14}NH_3$ to assign the obtained signals. Figure 5 shows the EPR spectrum of TiO_2 adsorbing $^{15}NH_3$ under irradiation with assignable g values (solid line) and simulated $^{15}NH_2$ radical (dot line). In this case, the lines at g > 2.005 of the spectrum simulated the $^{15}NH_2$ radical consisted of that of the obtained spectrum. It was concluded that the lines g > 2.004 of the obtained spectrum were assigned to the NH_2 radical. On the other hand, the lines at g < 2.004 remained although $^{15}NH_3$ was admitted instead of $^{14}NH_3$ and were attributed to the other species. The lines at g < 2.004 are not derived from the NH_2 radical but the Ti^{3+} species, since the line at g = 1.980 have been assignable to the Ti^{3+} species in the discussion of Figure 2. The line assigned to the Ti^{3+} species increased in intensity under photoirradiation in comparison with

that of TiO_2 pretreated at 773K. In conclusion, Figure 4 is identified to the EPR spectrum of the NH_2 radical overlapped with that of the Ti^{3+} species. Photoirradiation to TiO_2 adsorbing NH_3 contributes to the formation of the NH_2 radical and the Ti^{3+} species. This suggests that the electron transfer takes place from the N atom of NH_3 adsorbed on TiO_2 to the Ti atom of TiO_2 bulk. An electron reduced a Ti^{4+} species to a Ti^{3+} species and a hole is captured by the $NH_2^{\cdot}$ species evolved from adsorbed NH_3 to form a NH_2 radical. Consequently, Step 2 in Scheme 1 was proved to be the reasonable mechanism in the present work.

As mentioned above, the lines assigned to the NH_2 radical were quite stable even after more than one hour at 123 K when the irradiation was ceased. However, these signals vanished quickly as soon as NO was introduced to the reactor in the dark, whereas the lines of

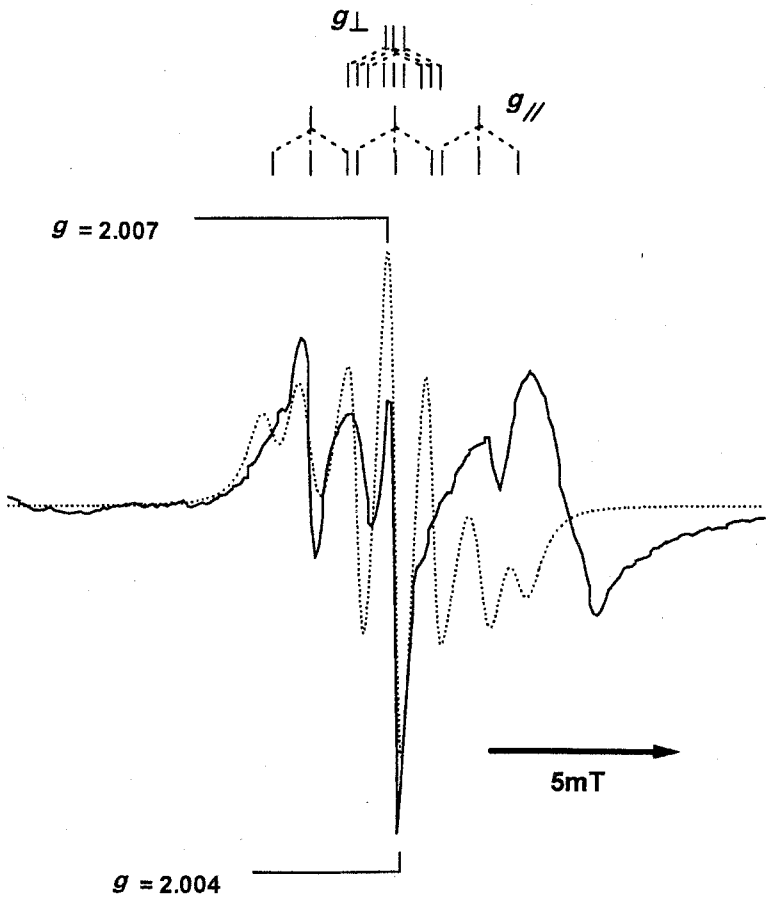

Figure 4 EPR spectra of TiO_2 after introduction of $^{14}NH_3$ under photoirradiation (solid line) and simulated $^{14}NH_2$ radical (dot line).

Table 1 Magnetic parameters for $^{14}NH_2$ and $^{15}NH_2$ radical in TiO_2

Radical	$A^N_{\perp}$ /G	$A^N_{//}$ /G	A^H /G
$^{14}NH_2$	22.5	3	10
$^{15}NH_2$	40	6	15

the Ti^{3+} species increased in intensity more as shown in Figure 3(d). The quick disappearance of the NH_2 radical suggests whether the NH_2 radical itself changed to an EPR silent species or NO in the gas phase attacks to the NH_2 radical on TiO_2 to form the NH_2NO intermediate. We agreed with the latter. In the previous study, it have been already reported that a NH_2NO intermediate was detected by FT-IR spectroscopy after NO was introduced TiO_2 adsorbing NH_3 under photoirradiation.[2] The NH_2NO intermediate is decomposed to N_2 and H_2O. This is

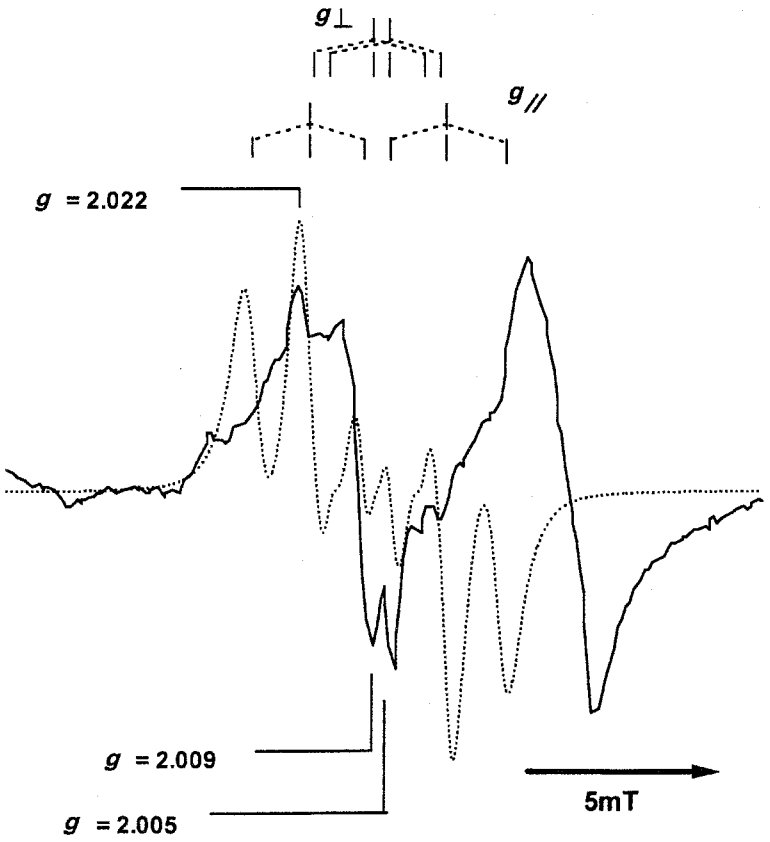

Figure 5 EPR spectra of TiO_2 after introduction of $^{15}NH_3$ under photoirradiation (solid line) and simulated $^{15}NH_2$ radical (dot line).

supported by the fact that the detected nitrogen gas was only $^{15}N^{14}N$ in the $^{15}NO + {}^{14}NH_3 + O_2$ reaction. Taking into account of these results, we can conclude that NO in the gas phase reacts with NH_3 adsorbed on TiO_2. In addition, a spin state of NO, a doublet, coincides with that of a NH_2 radical. In conclusion, it is reasonable that ^{15}NO in the gas phase attacks a $^{14}NH_2$ radical anchored on TiO_2 to form a NH_2NO intermediate. And, the NH_2 radical and the NH_2NO intermediate could be detected by EPR spectroscopy and FT-IR spectroscopy, respectively. On the other hand, the line assigned to the Ti^{3+} species increased in intensity after introduction of NO. In the previous paragraph, we proposed that the electron transfer takes place from the N atom of NH_3 adsorbed on TiO_2 to the Ti atom of TiO_2 bulk. In other words, the electron is trapped on Ti atom and the hole is captured by the NH_2^- species evolved from adsorbed NH_3. The NH_2^- species captured the hole converts to the active NH_2 radical. However, the electron moves about into inside of TiO_2 bulk as a stable free electron. Before introduction of NO, recombination usually takes place between the Ti^{3+} species and the NH_2 radical. On the contrary, after NO admittance, the electron can not recombine to lose an opponent. The line assigned to the Ti^{3+} species increased in intensity because the electron was localized and stabilized in inside of TiO_2.

In the present study, we clarified the electron transfer from the N atom of NH_3 adsorbed on TiO_2 to the Ti atom of TiO_2 (a hole and an electron are localized on a NH_2^- species and the Ti^{3+} species, respectively). As a result, the stable NH_2 radical was generated over TiO_2. This NH_2 radical reacts with NO in the gas phase preferentially as compared with O_2, since a spin state of NO, a doublet, coincides with that of a NH_2 radical. The fact demonstrates Step 2 and 3 as shown in Scheme 1. It is well-known that NO was oxidized to a NO_3^- ion in the presence of O_2 over irradiated TiO_2.[17,18] We have also reported that the NO_3^- ion is accumulated on TiO_2 and the photo-SCR reaction is terminated in the case of using a large quantity of TiO_2.[2] However, in the photo-SCR with NH_3, NO was not oxidized to NO_3^- ion by O_2 but captured by the NH_2 radical anchored on TiO_2 to form the NH_2NO intermediate. In addition, O_2 re-oxidizes the Ti^{3+} species to the Ti^{4+} species. We confirmed by UV-Vis spectroscopy that the Ti^{3+} species are restored to the Ti^{4+} species by gaseous oxygen. Accordingly, it is suggested strongly that Scheme 1 is an appropriate mechanism of the

photo-SCR with NH_3 over TiO_2. Especially, it is interesting that the electron transfer takes place between an adsorbant and an adsorbed species elongates the lifetime of excited states to promote photocatalytic reaction.

Conclusion

A NH_2 radical and a Ti^{3+} species were confirmed on TiO_2 adsorbing NH_3 under photoirradiation by EPR spectroscopy. Introduction of NO make the NH_2 radical vanish. NO in the gas phase attacks the NH_2 radical on TiO_2 to generate a NH_2NO intermediate. This work clarified the electron transfer from the N atom of NH_3 adsorbed on TiO_2 to the Ti atom of TiO_2 and the reaction mechanism of the photo-SCR with NH_3 over TiO_2.

References

(1) Tanaka, T.; Teramura, K.; Arakaki, K.; Funabiki, T. *Chem. Comm.* **2002**, 2742.

(2) Teramura, K.; Tanaka, T.; Funabiki, T. *Langmuir* **2003**, *19*, 1209.

(3) Vansant, E. F.; Lunsford, J. H. *J. Phys. Chem.* **1972**, *76*, 2716.

(4) Brotikovskii, O. I.; Zhidomirov, G. M.; Kazanskii, V. B.; Mashchenko, A. I.; Shelimov, B. N. *Kinet. Katal.* **1971**, *12*, 616.

(5) Nagai, S. *Bull. Chem. Soc. Jpn.* **1973**, *46*, 1144.

(6) Shimamoto, N.; Hatano, K.; Katsu, T.; Fujita, Y. *Bull. Chem. Soc. Jpn.* **1975**, *48*, 18.

(7) Nakaoka, Y.; Nosaka, Y. *J. Photochem. Photobiol. A-Chem.* **1997**, *110*, 299.

(8) Coronado, J. M.; Maira, A. J.; Conesa, J. C.; Yeung, K. L.; Augugliaro, V.; Soria, J. *Langmuir* **2001**, *17*, 5368.

(9) Meriaudeau, P.; Che, M.; Jorgensen, C. K. *Chem. Phys. Lett.* **1970**, *5*, 131.

(10) Hauser, C.; Cornaz, P. *Chem. Phys. Lett.* **1970**, *5*, 226.

(11) Che, M.; Naccache, C. *Chem. Phys. Lett.* **1971**, *8*, 45.

(12) Howe, R. F.; Gratzel, M. *J. Phys. Chem.* **1985**, *89*, 4495.

(13) Hurum, D. C.; Agrios, A. G.; Gray, K. A.; Rajh, T.; Thurnauer, M. C. *J. Phys. Chem.*

B **2003**, *107*, 4545.

(14) Ramis, G. G.; Busca, G.; Lorenzelli, V.; Forzatti, P. *Appl. Catal.* **1990**, *64*, 243.

(15) Martra, G. *Appl. Catal. A-Gen.* **2000**, *200*, 275.

(16) Foner, S. N.; L., C. E.; Bowers, V. A.; Jen, C. K. *Phys. Rev. Lett.* **1958**, *1*, 91.

(17) Hashimoto, K.; Wasada, K.; Toukai, N.; Kominami, H.; Kera, Y. *J. Photochem. Photobiol. A-Chem.* **2000**, *136*, 103.

(18) Hashimoto, K.; Wasada, K.; Osaki, M.; Shono, E.; Adachi, K.; Toukai, N.; Kominami, H.; Kera, Y. *Appl. Catal. B-Environ.* **2001**, *30*, 429.

Part II

Selective photo-oxidation of hydrocarbons in the liquid phase over supported vanadium oxides

Introduction of Part II

It is not too much to say that the selective oxidation process occupies a very important place of chemical processes and takes a leading part of petrochemistry and fine chemistry. Hydrocarbon oxidation systems operated in industrial plants often consists of many steps like the cumene method. Disadvantages of multi-step-process are (1) formation of harmful or needless by-products and (2) waste of energy. Nowadays, much attention is paid to one-step oxygen atom insertion to hydrocarbons from the viewpoint of the Green Sustainable Chemistry.[1,2] One-step oxygen insertion process must proceed under mild condition (at room temperature and atmospheric pressure) with the formation of only harmless by-products (i.e. H_2O and CO_2). Recently, many research groups reported that H_2O_2 is applied to the selective oxidation as an oxidant. However, ultimately, it is an ideal that the selective oxidation proceeds in the presence of molecular oxygen included in air.

From 1970's to 1980's, there were many reports related to the selective oxidation of various hydrocarbons (alkane, olefin, alcohol etc.) over TiO_2 photocatalyst. Pichat[3] and Fox[4] summarized the studies of the selective oxidation of a variety of organic compounds in the liquid phase over TiO_2 and concluded that TiO_2 photocatalyst can selectively oxidize a variety of organic compounds in the liquid phase. However, Pichat also mentioned that oxidation by heterogeneous photocatalysis is limited to a small number of cases at the present state of knowledge. Recently, it is well-known that TiO_2 photocatalyst is applied to the deep oxidation of harmful organic compounds (i.e dioxin compounds, endocrine disrupters and volatile organic compounds (VOCs)).[5,6] A series of reports clarified that it is difficult to inhibit the deep consecutive oxidation of hydrocarbons over TiO_2 photocatalyst. Therefore, since then, the study of the selective photo-oxidation has been scarcely reported.

Very recently, some research groups revive the study of the selective photocatalytic oxidation of hydrocarbons with new concepts.[7] Ohno et al. reported that the epoxidation of olefins[8-10] and the dihydroxylation of napththalene[11,12] proceed over irradiated TiO_2. They clarified the relationship between the crystal phase of TiO_2 and the photocatalytic activity.[13-15] On the other hand, we have reported a series of works on the selective photo-oxidation of

gaseous light alkenes[16-18] and alkanes[19-24] over silica–supported vanadium oxide in the presence of O_2 since 1980's. It has been clarified that the active sites of the selective photo-oxidation are the isolated tetrahedral VO_4 species, which are highly dispersed on a support. Many groups also investigated the photo-activity of highly dispersed vanadium oxide on supports.[25-30] We reported the formation of acrolein and acetaldehyde in the selective photo-oxidation of propene over V_2O_5/SiO_2. In addition, it was found that the propene epoxidation proceeds over Nb_2O_5/SiO_2[31], MgO/SiO_2 and SiO_2[32]. Recently, Yoshida et al.[33,34] carried out the screening of the propene epoxidation in the gas phase over silica-supported various metal oxide and found that TiO_2/SiO_2 and ZnO/SiO_2 are the most active photocatalyst. In the case of TiO_2/SiO_2, they investigated the reaction mechanism by means of UV-Vis spectroscopy, luminescence, EPR spectroscopy etc. and proposed that the active site of the photo-epoxidation is isolated tetrahedral TiO_4 species on silica.[35] We also obtained acetone or methyl ethyl ketone in the selective photo-oxidation of alkane over alkali-ion-modified silica-supported vanadium oxide[20,21,24] and molybdenum oxide[36,37] at fairly high rate with excellent selectivity. The enhancement of conversion and selectivity is caused by expansion of effective wavelength to visible field. The structure of isolated tetrahedral VO_4 species is changed by the addition of alkali ion, and the LUMO level is stabilized and HOMO loses its stability.[38] It was confirmed that the selective photo-oxidation of alkane in the gas phase proceeds efficiently in a conventional fixed bed flow system.[24]

Accordingly, the author also applied various supported vanadium oxide to the desirable selective photo-oxidation of various hydrocarbons in the liquid phase, for example, cyclohexane oxidation. As mentioned above, the selective oxidation of hydrocarbons in the liquid phase attracts a great deal of attention lately. The oxidation of cyclohexane is an essential process to produce 6-nylon and 6,6-nylon.[39-41] ε-Caprolactam or adipic acid which is a key material for 6-nylon or 6,6-nylon synthesis is obtained by the cyclohexanone oximation with hydroxylammonium sulfate or the oxidation of K/A (cyclohexanone/cyclohexanol) oil by means of HNO_3, respectively.[39,40,42] The K/A oil is produced by auto-oxidation process of cyclohexane over cobalt-based homogeneous catalyst above 423 K under about 8 kPa pressure.[41,43] It is very difficult to control the conversion of cyclohexane and the K/A ratio

because of auto-oxidation. The conventional cyclohexane oxidation is operated at not higher than 4 % conversion to inhibit the formation of by-products and the deep oxidation to CO_2. Cyclohexanol produced as a by-product is dehydrogenated to cyclohexanone using Zn or Cu catalyst. It is one of the most important issues to enhance the K/A ratio in the cyclohexane oxidation system. In 1989, Mu et al.[44] reported the selective photo-oxidation of cyclohexane in the liquid phase in the presence of O_2 over TiO_2 for the first time. After that, Lu et al.[45] have confirmed the reproducibility of their report and have found that the conversion of cyclohexane is high over the mixture of TiO_2 and TS-1 in comparison with that over TiO_2 only. Shimizu et al.[46] researched the selective oxidation of benzene and cyclohexane over Ti-mica under irradiation in the liquid phase. These studies have shown that highly dispersed titanium oxide exhibits the appreciable activity in the selective photo-oxidation. Maldotti et al. also reported the selective photo-oxidation of cyclohexane over Fe-prophyrin modified TiO_2[47,48], polyoxotungstate modified SiO_2[49,50] and MCM-41[51].

The above is the background of this part. In chapter 5, the photo-oxidation of cyclohexane over various supported vanadium oxide catalyst is described to find out which supports can be applied to the selective photo-oxidation of cyclohexane. In chapter 6, the author proposes the reaction mechanism of the photo-oxidation of cyclohexane over V_2O_5/Al_2O_3 on the basis of the observation of the selective photo-oxidation of neat cyclohexane. From the viewpoint of the protection of the environment, it is important that the synthesis is carried out without solvent. In addition, the author has investigated the method for controlling the K/A ratio and the selectivity to CO_2 with the formation of by-products suppressed and found that the O_2 concentration and the wavelength of the irradiated light are the key factors. Chapter 7 describes the selective photo-oxidation of various hydrocarbons over V_2O_5/Al_2O_3 to find out which carbon atom is attacked selectively for the design of another photocatalytic system.

References

(1) Centi, G.; Misono, M. *Catal. Today* **1998**, *41*, 287.

(2) Arends, I.; Sheldon, R. A. *Appl. Catal. A-Gen.* **2001**, *212*, 175.

(3) Pichat, P. *Catal. Today* **1994**, *19*, 313.

(4) Fox, M. A.; Dulay, M. T. *Chem. Rev.* **1993**, *93*, 341.

(5) Mills, A.; Davies, R. H.; Worsley, D. *Chem. Soc. Rev.* **1993**, *22*, 417.

(6) Hoffmann, M. R.; Martin, S. T.; Choi, W. Y.; Bahnemann, D. W. *Chem. Rev.* **1995**, *95*, 69.

(7) Maldotti, A.; Molinari, A.; Amadelli, R. *Chem. Rev.* **2002**, *102*, 3811.

(8) Ohno, T.; Kigoshi, T.; Nakabeya, K.; Matsumura, M. *Chem. Lett.* **1998**, 877.

(9) Ohno, T.; Nakabeya, K.; Matsumura, M. *J. Catal.* **1998**, *176*, 76.

(10) Ohno, T.; Masaki, Y.; Hirayama, S.; Matsumura, M. *J. Catal.* **2001**, *204*, 163.

(11) Jia, J. G.; Ohno, T.; Masaki, Y.; Matsumura, M. *Chem. Lett.* **1999**, 963.

(12) Jia, J. G.; Ohno, T.; Matsumura, M. *Chem. Lett.* **2000**, 908.

(13) Ohno, T.; Sarukawa, K.; Tokieda, K.; Matsumura, M. *J. Catal.* **2001**, *203*, 82.

(14) Ohno, T.; Sarukawa, K.; Matsumura, M. *J. Phys. Chem. B* **2001**, *105*, 2417.

(15) Ohno, T.; Sarukawa, K.; Matsumura, M. *New J. Chem.* **2002**, *26*, 1167.

(16) Yoshida, S.; Tanaka, T.; Okada, M.; Funabiki, T. *J. Chem. Soc., Faraday Trans. 1* **1984**, *80*, 119.

(17) Tanaka, T.; Ooe, M.; Funabiki, T.; Yoshida, S. *J. Chem. Soc., Faraday Trans. I* **1986**, *82*, 35.

(18) Tanaka, T.; Nishimura, Y.; Kawasaki, S.; Ooe, M.; Funabiki, T.; Yoshida, S. *J. Catal.* **1989**, *118*, 327.

(19) Tanaka, T.; Takenaka, S.; Funabiki, T.; Yoshida, S. *Chem. Lett.* **1994**, 1585.

(20) Takenaka, S.; Kuriyama, T.; Tanaka, T.; Funabiki, T.; Yoshida, S. *J. Catal.* **1995**, *155*, 196.

(21) Tanaka, T.; Takenaka, S.; Funabiki, T.; Yoshida, S. *J. Chem. Soc., Faraday Trans.* **1996**, *92*, 1975.

(22) Takenaka, S.; Tanaka, T.; Funabiki, T.; Yoshida, S. *J. Chem. Soc., Faraday Trans.* **1997**, *93*, 4151.

(23) Tanaka, T.; Ito, T.; Funabiki, T.; Yoshida, S. *Stud. Surf. Sci. Catal.* **2000**, *130*, 1961.

(24) Tanaka, T.; Ito, T.; Takenaka, S.; Funabiki, T.; Yoshida, S. *Catal. Today* **2000**, *61*, 109.

(25) Gritscov, A. M.; Shvets, V. A.; Kazansky, V. B. *Kinet. Katal.* **1974**, *15*, 1257.

(26) Gritscov, A. M.; Shvets, V. A.; Kazansky, V. B. *Chem. Phy. Lett.* **1975**, *35*, 511.

(27) Anpo, M.; Tanahashi, I.; Kubokawa, Y. *J. Phys. Chem.* **1980**, *84*, 3440.

(28) Tanaka, T.; Yamashita, H.; Tsuchitani, R.; Funabiki, T.; Yoshida, S. *J. Chem. Soc., Faraday Trans. I* **1988**, *84*, 2987.

(29) Yoshida, S.; Tanaka, T.; Hanada, T.; Hiraiwa, T.; Kanai, H.; Funabiki, T. *Catal. Lett.* **1992**, *12*, 277.

(30) Tanaka, T.; Nishimura, Y.; Kawasaki, S. I.; Funabiki, T.; Yoshida, S. *J. Chem. Soc., Chem. Commun.* **1987**, 506.

(31) Tanaka, T.; Nojima, H.; Yoshida, H.; Nakagawa, H.; Funabiki, T.; Yoshida, S. *Catal. Today* **1993**, *16*, 297.

(32) Yoshida, H.; Tanaka, T.; Yamamoto, M.; Yoshida, T.; Funabiki, T.; Yoshida, S. *J. Catal.* **1997**, *171*, 351.

(33) Yoshida, H.; Murata, C.; Hattori, T. *Chem. Commun.* **1999**, 1551.

(34) Yoshida, H.; Murata, C.; Hattori, T. *J. Catal.* **2000**, *194*, 364.

(35) Murata, C.; Yoshida, H.; Kumagai, J.; Hattori, T. *J. Phys. Chem. B* **2003**, *107*, 4364.

(36) Takenaka, S.; Tanaka, T.; Funabiki, T.; Yoshida, S. *J. Phys. Chem. B* **1998**, *102*, 2960.

(37) Takenaka, S.; Tanaka, T.; Funabiki, T.; Yoshida, S. *J. Chem. Soc.-Faraday Trans.* **1998**, *94*, 695.

(38) Takenaka, S.; Tanaka, T.; Yamazaki, T.; Funabiki, T.; Yoshida, S. *J. Phys. Chem. B* **1997**, *101*, 9035.

(39) Castellan, A.; Bart, J. C. J.; Cavallaro, S. *Catal. Today* **1991**, *9*, 237.

(40) Bellussi, G.; Perego, C. *Cattech* **2000**, *4*, 4.

(41) Schuchardt, U.; Cardoso, D.; Sercheli, R.; Pereira, R.; de Cruz, R. S.; Guerreiro, M.

C.; Mandelli, D.; Spinace, E. V.; Pires, E. L. *Appl. Catal. A-Gen.* **2001**, *211*, 1.

(42) Dartt, C. B.; Davis, M. E. *Ind. Eng. Chem. Res.* **1994**, *33*, 2887.

(43) Suresh, A. K.; Sharma, M. M.; Sridhar, T. *Ind. Eng. Chem. Res.* **2000**, *39*, 3958.

(44) Mu, W.; Herrmann, J. M.; Pichat, P. *Catal. Lett.* **1989**, *3*, 73.

(45) Lu, G. X.; Gao, H. X.; Suo, J. H.; Li, S. B. *J. Chem. Soc., Chem. Commun.* **1994**, 2423.

(46) Shimizu, K. I.; Kaneko, T.; Fujishima, T.; Kodama, T.; Yoshida, H.; Kitayama, Y. *Appl. Catal. A-Gen.* **2002**, *225*, 185.

(47) Amadelli, R.; Bregola, M.; Polo, E.; Carassiti, V.; Maldotti, A. *J. Chem. Soc. Chem. Commun.* **1992**, 1355.

(48) Molinari, A.; Amadelli, R.; Antolini, L.; Maldotti, A.; Battioni, P.; Mansuy, D. *J. Mol. Catal. A-Chem.* **2000**, *158*, 521.

(49) Molinari, A.; Amadelli, R.; Andreotti, L.; Maldotti, A. *J. Chem. Soc., Dalton Trans.* **1999**, 1203.

(50) Molinari, A.; Amadelli, R.; Mazzacani, A.; Sartori, G.; Maldotti, A. *Langmuir* **2002**, *18*, 5400.

(51) Maldotti, A.; Molinari, A.; Varani, G.; Lenarda, M.; Storaro, L.; Bigi, F.; Maggi, R.; Mazzacani, A.; Sartori, G. *J. Catal.* **2002**, *209*, 210.

Chapter 5

Selective photo-oxidation of cyclohexane over various supported vanadium oxide catalysts

Abstract

Alumina-supported vanadium oxide exhibited specific photocatalytic performance in the oxidation of cyclohexane to produce cyclohexanol and cyclohexanone. Higher loading of vanadium oxide (above 5 wt.%) on alumina support resulted in reducing activity, suggesting that the active species are stable isolated-VO_4 on alumina.

Introduction

Silica-supported vanadium oxide (VS) is known as a photocatalyst for oxidation of CO[1,2], hydrocarbons[3,4] and alcohols[5], and the photoactive species is accepted to be the isolated vanadates with the specific structure of tetrahedral VO_4 with monooxo species. Although the structure of supported vanadium oxide has been studied extensively[6-8] and highly dispersed vanadate realizes the similar structure over many kinds of metal oxide supports like silica, alumina, ziconia, titania, etc., there has been only a few reports on photoactivity of titania-supported vanadium oxide (VT), zirconia-supported vanadium oxide (VZ) and alumina-supported vanadium oxide (VA). In the present work, we have examined the photoactivity of these supported vanadium oxides with photooxidation of cyclohexane as a probe reaction. The oxidation of cyclohexane to form cyclohexanone is significantly important reaction since cyclohexanone is an intermediate material to ε-caprolactam which is a raw material for nylon synthesis. The oxidation process of cyclohexane to produce cyclohexanone has been industrialized over cobalt-base catalyst with oxygen above 423 K under high pressure.[9] To make the reaction condition milder, new reaction system has been sought out. Hydrogen peroxide is often used as an oxidizing reagent to achieve the mild reaction condition.[10,11] Nevertheless, realization of oxidation by molecular oxygen is strongly desired. From this point of view, we chose this reaction as a test reaction for photooxidation by supported vanadium oxides and eventually, we have found VA an effective photocatalyst. Here, we report the photooxidation of cyclohexane over alumina-supported vanadium oxide photocatalyst.

Experimental

Supported vanadium oxides were prepared by impregnating various supports with aqueous solution of ammonium metavanadate at 353 K for 2 h and evaporation to dryness at 373 K. The supports used in the study were SiO_2[12] (628 m^2/g), γ-Al_2O_3 (177 m^2/g : JRC-ALO-4), TiO_2 (50 m^2/g : JRC-TIO-4) and ZrO_2[13] (64 m^2/g). The sample was kept at 383

Table 1 Specific surface area and surface density of the supported

Sample	Specific surface area / m^2g^{-1}	Surface density (V atom / nm_2)
V_2O_5/SiO_2	567	0.29
V_2O_5/Al_2O_3	170	0.97
V_2O_5/ZrO_2	64	2.6
V_2O_5/TiO_2	44	3.7

K for 12 h, followed by calcination at 773 K for 5 h. Loading amount of V was 2.5 wt.% as V_2O_5. Table 1 shows specific surface area and surface density of vanadium atom about supported vanadium oxide. No crystalline vanadium compounds were detected with XRD analysis. Prior to photooxidation, each catalyst sample (0.2 g) was heated at 673 K for 30 min in air and evacuated at 673 K for 30 min, followed by treatment with 9.3×10^3 Pa O_2 for 90 min and evacuation for 30 min at 673 K. After cooling down to room temperature, cyclohexane (0.5 ml : Wako, 99.5 %) and acetonitrle (1.5 ml : Wako, 99.5 %) were added into a reactor. These substrates were used without further purification. The reaction mixture was stirred by a magnetic stirrer at 298 K for 5 h under oxygen at atmospheric pressure, and irradiated from the side with a 500 W ultrahigh-pressure mercury lamp. During 5 h irradiation, products yield increased linearly with irradiation time. The linearity of the conversion to irradiation time allows to evaluate the catalyst activity. Therefore, we did not prolong the irradiation time more than 5 h. The reactor volume was ca. 150 ml.

Results and Discussion

Figure 1 shows the result of photooxidation of cyclohexane with gaseous oxygen over various supported vanadium oxides. Cyclohexanol and cyclohexanone were obtained as main products under irradiation of the light, and the formation of trace amount of

cyclohexandiol and cyclohexandione was confirmed. Any products were not observed in the dark at all, indicating that all the catalyst samples showed photoactivity. VA exhibited the highest activity in the four samples and the activities of VS, VT and VZ were quite lower than that of VA. To confirm the activity of alumina or V_2O_5 itself, we carried out the photoreaction with these metal oxide samples. No products were formed under photo-irradiation of alumina nor V_2O_5. We conclude that the active species is vanadium species supported on alumina. The 55 μmol vanadium atom exists in each 200 mg of 2.5 wt.% supported vanadium oxide and the apparent turn over number (TON) of the photooxidation of cyclohexane on VA was calculated for the 5 h reaction. The TON is 1.9 and this indicates that VA acts as a photocatalyst.

The four samples showed similar tendency of the selectivities to cyclohexanol and cyclohexanone. The produced amount of cyclohexanone was higher than that of cyclohexanol over each sample and the ratio of cyclohexanol to cyclohexanone was ca. 0.6. The selectivity suggests that oxidation of cyclohexane proceeds in the same way over the four catalyst samples. Since we used an integrated reactor, we guess that consecutive oxidation of

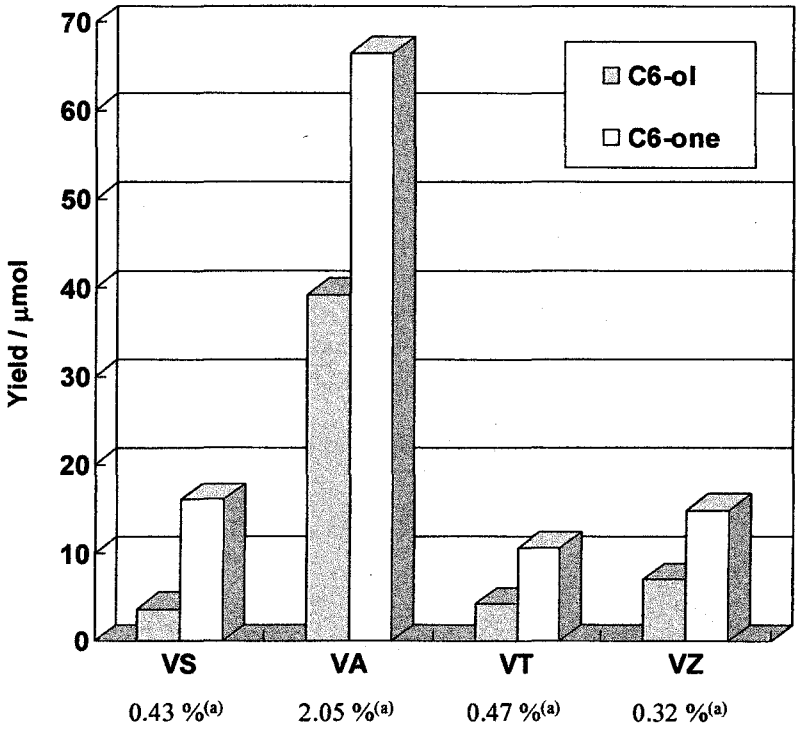

Figure 1 The result of photooxidation of cyclohexane with gaseous oxygen over various supported vanadium oxides. (a) Conversion based on cyclohexane at 5 h photoirradiation.

cyclohexanol to cyclohexanone is not a main path and ketone forms in parallel to alcohol.

Figure 2 shows an effect of loading amount of vanadium oxide on alumina upon products yield for 5 h reaction. The total yield of cyclohexanol and cyclohexanone exhibited the highest between 2.5 and 5.0 wt.%. And, the loading amount for the best yield of cyclohexanol and cyclohexanone was 2.5 wt.% respectively. The total yield was almost proportional to the loading amount up to 2.5 wt.% and decreased over 5.0 wt.%. It is known that vanadium oxide can be highly dispersed on alumina at low loading and stabilized as isolated VO_4 species.[6-8,14-16] Gao and Wachs[6] reported that polymerized VO_4 species appeared at 7.0 wt % loading (2.2 atoms / nm^2) and increased with an increase in V_2O_5 loading. A drop of activity of the sample with higher loadings than 5.0 wt.% would be attributed to the polymerization of VO_4 species. In the present reaction, we conclude that highly dispersed VO_4 species over alumina is the active species. Actually, in cases of VZ and VT, their surface vanadium atom density (2.6 and 3.7 atoms / nm^2) is high so that the polymerized VO_4 and VO_5 would be the main species and VZ and VT exhibited poorer activity than VA.

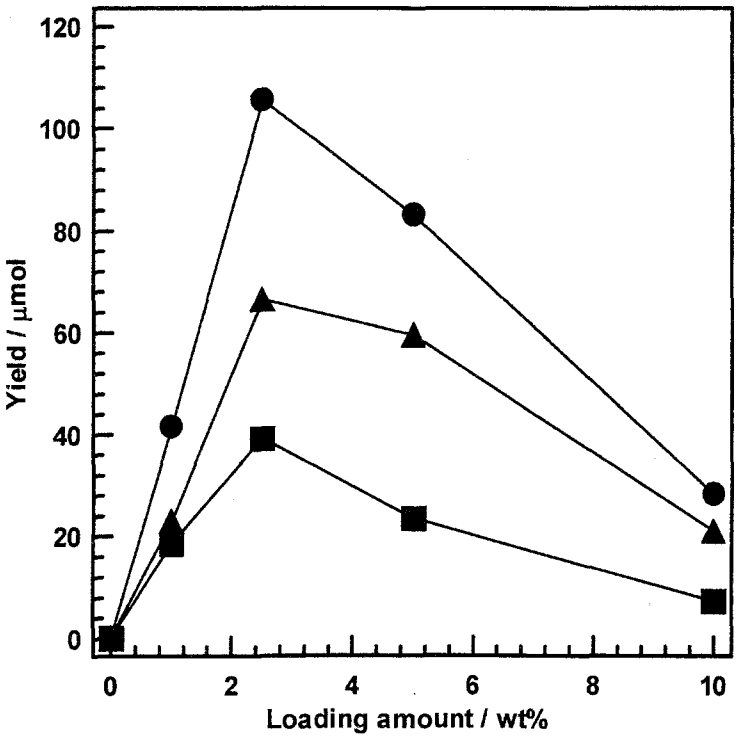

Figure 2 The effect of loading amount of vanadium oxide on alumina upon products yield.

On the other hand, although VS shows much lower vanadium density than VA, the activity is very poor. Surface structure depends on the density as well as on the state of the sample. In cases of VA, VZ[6] and presumably VT, the surface species do not change by hydration. However, surface vanadates over silica change their structure easily by hydration[6,14-17], i.e., isolated VO_4 → polymerized VO_5/VO_6. The oxidation of cyclohexane fatally produces water molecules at the vicinity of vanadium atoms. The adsorption of H_2O changes surface vanadates to polymerized one. Therefore, catalytic reaction is terminated by the formation of polyvanadates.

As a conclusion, the active species for photooxidation of cyclohexane is stable isolated-VO_4 species. In order to improve the activity, the preparation of the catalyst sample of high vanadium content with stable isolated-VO_4 is necessary.

References

(1) Anpo, M.; Tanahashi, I.; Kubokawa, Y. *J. Phys. Chem.* **1980**, *84*, 3440.

(2) Yoshida, S.; Matsumura, Y.; Noda, S.; Funabiki, T. *J. Chem. Soc., Faraday Trans. 1* **1981**, *77*, 2237.

(3) Yoshida, S.; Magatani, Y.; Noda, S.; Funabiki, T. *J. Chem. Soc., Chem. Commum.* **1982**, 601.

(4) Kalliaguin, S.; Shelomov, B. N.; Kazansky, V. B. *J. Catal.* **1978**, *55*, 384.

(5) Tanaka, T.; Nishimura, Y.; Kawasaki, S.; Ooe, M.; Funabiki, T.; Yoshida, S. *J. Catal.* **1989**, *118*, 327.

(6) Gao, X. T.; Wachs, I. E. *J. Phys. Chem. B* **2000**, *104*, 1261.

(7) Khodakov, A.; Olthof, B.; Bell, A. T.; Iglesia, E. *J. Catal.* **1999**, *181*, 205.

(8) Olthof, B.; Khodakov, A.; Bell, A. T.; Iglesia, E. *J. Phys. Chem. B* **2000**, *104*, 1516.

(9) Davis, D. D.; Kemp, D. R. *Kirk-Othmer Encyclopedia of Chemical Techonology*; Wiley: New York, 1991; Vol. 1.

(10) Carvalho, W. A.; Wallau, M.; Schuchardt, U. *J. Mol. Catal. A: Chemcal* **1999**, *144*, 91.

(11) Armengol, E.; Corma, A.; Fornes, V.; Garcia, H.; Primo, J. *Appl. Catal. A: General* **1999**, *181*, 305.

(12) Yoshida, S.; Matsuzaki, T.; Mori, K.; Tarama, K. *Bull. Chem. Soc. Jpn.* **1974**, *47*, 1564.

(13) Kohno, Y.; Tanaka, T.; Funabiki, T.; Yoshida, S. *J. Chem. Soc., Faraday Trans.* **1998**, *94*, 1875.

(14) Yoshida, S.; Tanaka, T.; Nishimura, Y.; Mizutani, H.; Funabiki, T. The local structure of vanadium oxide on silica and ganma-alumina studied by X-ray absorption (XANES/EXAFS) spectroscopy - The effect of hydration. In *the Proc. 9th Int. Congr. Catal.*; Phillips, M. J., Ternan, M., Eds.; The Chemical Institute of Canada: Ottawa, 1988; Vol. 3; pp 1473.

(15) Tanaka, T.; Yamashita, H.; Tsuchitani, R.; Funabiki, T.; Yoshida, S. *J. Chem. Soc., Faraday Trans. I* **1988**, *84*, 2987.

(16) Yoshida, S.; Tanaka, T.; Hanada, T.; Hiraiwa, T.; Kanai, H.; Funabiki, T. *Catal. Lett.* **1992**, *12*, 277.

(17) Gao, X.; Bare, S. R.; Weekhuysen, B. M.; Wachs, I. E. *J. Phy. Chem.* **1998**, *102*, 10842.

Chapter 6

Identification of reaction mechanism of selective photo-oxidation of cyclohexane over V_2O_5/Al_2O_3

Abstract

V_2O_5/Al_2O_3 exhibits the high selectivity to partial oxidation compounds (cyclohexanol and cyclohexanone) as compared with TiO_2 in the photo-oxidation of cyclohexane in the liquid phase. This reaction is an environmentally friendly reaction since it proceeds at ambient temperature and atmospheric pressure without a solvent. The features of the reaction are a high selectivity to partial oxidation products and a reasonable ketone/alcohol ratio (K/A ratio). However, by elongation of the photoirradiation time, cyclohexyl hexanoate as a by-product was generated and the K/A ratio decreased gradually. Retention of the high O_2 concentration in the gas phase and irradiation of light $\lambda > 330$ nm are keys to the selective formation of the partial oxidation compounds with a reasonable K/A ratio in the photo-oxidation of cyclohexane over V_2O_5/Al_2O_3. In the present study, a selectivity of 87 % to the partial oxidation compounds was achieved with the K/A ratio of 3.8.

Introduction

Nowadays, much attention is paid to the one-step oxygen atom insertion to hydrocarbons, what is called "selective or partial oxidation process", in the presence of O_2 as an oxidant in the viewpoint of the Green Sustainable Chemistry.[1,2] In particular, the application of photocatalyst to the selective oxidation in the presence of O_2 has been investigated for a long time since the reaction can be operated under mild conditions (at room temperature and ambient pressure). From 1970's to 1980's, there were many reports related to the selective oxidation over TiO_2 photocatalyst. Pichat[3] summarized the studies of the selective oxidation of a variety of organic compounds in the liquid phase over TiO_2 and concluded that TiO_2 photocatalyst can selectively oxidize a variety of organic compounds in the liquid phase. However, he also mentioned that oxidations by heterogeneous photocatalysis are limited to a small number of cases at the present state of knowledge. It is well-known that TiO_2 photocatalyst is applied to the complete oxidation of harmful organic compounds (i.e dioxin compounds, endocrine disrupters and volatile organic compounds (VOCs)).[4,5] A series of reports clarified that it is difficult to inhibit the complete oxidation of hydrocarbons over TiO_2 photocatalyst. Therefore, since then, the study of the selective photo-oxidation has been scarcely reported.

Recently, some research groups revive the study of the selective photocatalytic oxidation of hydrocarbons with new concepts.[6] Ohno et al. reported that the epoxidation of olefins[7-9] and the dihydroxylation of napththalene[10,11] proceeded over irradiated TiO_2. They clarified the relationship between the crystal phase of TiO_2 and the photocatalytic activity.[12-14] On the other hand, Yoshida et al.[15,16] reported the epoxidation of propene in the gas phase over TiO_2/SiO_2 and Shimizu et al.[17] researched the selective oxidation of benzene and cyclohexane over Ti-mica under irradiation in the liquid phase. These studies have shown that highly dispersed titanium oxide exhibits the appreciable activity in the selective photo-oxidation. Maldotti et al. also reported the selective photo-oxidation of cyclohexane over Fe-prophyrin modified TiO_2[18,19], polyoxotungstate modified SiO_2[20,21] and MCM-41[22]. We have reported a series of works on the selective photo-oxidation of gaseous light

alkenes[23-25] and alkanes[26-31] over silica–supported vanadium oxide in the presence of O_2. It has been clarified that the active sites of the selective photo-oxidation are the isolated tetrahedral VO_4 species, which are highly dispersed on a support. Many groups also investigated the photo-activity of highly dispersed vanadium oxide on supports.[32-37] Recently, we have performed the photo-oxidation of cyclohexane in the liquid phase in the presence of O_2 over various oxide supported vanadium oxide catalysts and have found out that the most active catalyst is alumina-supported vanadium oxide (V_2O_5/Al_2O_3).[38] It is the first report that the highly dispersed vanadium species on alumina exhibits photo-activity although vanadium oxide and alumina are photo-inactive.

The selective photo-oxidation of cyclohexane is an attractive reaction since ε-caprolactam and adipic acid, which are key intermediates for nylon synthesis, are produced from cyclohexanone.[39-41] The main manufacturing process of cyclohexanol and cyclohexanone synthesis is the direct oxidation of cyclohexane in the air although there are alternative routes, the hydrogenation of phenol and the hydration of cyclohexane.[40,41] The reaction in the conventional process is fundamentally auto-oxidation. Accordingly, it is difficult to control the ratio of cyclohexanone to cyclohexanol (K/A ratio). Cyclohexanol produced as a by-product is dehydrogenated to cyclohexanone using Zn or Cu catalyst. It is one of the most important issues to enhance the K/A ratio in the cyclohexane oxidation system. In 1989, Mu et al.[42] reported the selective photo-oxidation of cyclohexane in the liquid phase in the presence of O_2 over TiO_2 for the first time; 0.3 % conversion of cyclohexane and 88 % selectivity to the partial oxidation products were observed and the K/A ratio was 16.6. Lu et al.[43] have confirmed the reproducibility of their report and have found that the conversion of cyclohexane is high over the mixture of TiO_2 and TS-1 in comparison with that over TiO_2 only. In addition, Boarini and co-workers[44] have reported that the selectivity to CO_2 is 5.2 % after 90 min for the photo-oxidation of neat cyclohexane over TiO_2. The feature of their report is that the selectivity to CO_2 is very low. However, Shimizu et al.[17] recently reported that the selectivity to CO_2 is 78.7 % over irradiated TiO_2 for 12 h. They defined the selectivity to CO_2 as (CO_2 / (C_6-ol + C_6-one + CO_2)). We evaluated the selectivity on the basis of cyclohexane conversion (1/6 CO_2 / (C_6-ol + C_6-one + 1/6 CO_2)) and concluded

that the selectivity to CO_2 was 39%. In the case of the cyclohexane oxidation process, it is important to keep the high K/A ratio and inhibit the formation of by-products and CO_2. In the present work, we have carried out the photo-oxidation of neat cyclohexane over V_2O_5/Al_2O_3 and TiO_2 as an archetypal example. We have investigated the method for controlling the K/A ratio and the selectivity to CO_2 with the formation of by-products suppressed and have found that the O_2 concentration and the wavelength of the irradiated light are the key factors.

Experimental

Materials

Alumina-supported vanadium oxide catalyst (V_2O_5/Al_2O_3) was prepared conventionally by impregnating alumina with an aqueous solution of ammonium metavanadate (NH_4VO_3) at 353 K for 2 h. Alumina used as a support in this study is JRC-ALO-8 supplied from the Japan Catalysis Society. After the impregnation, the suspension was evaporated to dryness at 373 K gradually. The sample was kept at 383 K for 24 h in an oven, followed by calcining in air at 773 K for 5 h. The sample was ground to powder under 100 mesh after calcination. The loading amount of vanadium atom is 2.5 wt.% as V_2O_5. Specific surface area is estimated to be 170 m^2g^{-1} by the BET method. No crystalline vanadium compounds were identified by XRD analysis. It has been confirmed by XAFS spectroscopy that vanadium species are highly dispersed on alumina.

Reaction

The reaction was carried out in a closed batch system or a quasi-flowing system at atmospheric pressure. The reactor used in this study is similar to a Schrenck flask and is made of Pylex glass with a flat glass in the bottom. V_2O_5/Al_2O_3 as a catalyst sample (0.1 g) and cyclohexane as a substrate (30 ml : Wako GR, 99.5 %) were introduced to the reactor. In this study, no solvents were used. The catalyst was neither evacuated nor pretreated in the presence of O_2. Cyclohexane was used without further purification. The suspension stirred by a magnetic stirrer at 323 K was irradiated from the flat bottom of the reactor through

reflection by a cold mirror with a 500 W ultrahigh-pressure Hg lamp supplied by USHIO Denki Co. Oxygen was kept at 1 atm with a rubber balloon in the case of the closed batch system. On the other hand, oxygen was flowed to the reactor at 2 cm^3/min through cyclohexane saturators in the case of the quasi-flowing system. Organic products were analyzed by FID GC and GC mass spectrometry. The O_2 concentration was monitored by TCD GC and was determined with regard to the N_2 concentration and the vapor pressure of cyclohexane. Further, at the downstream of the flow reactor, a trap with barium hydroxide solution ($Ba(OH)_2$) was equipped to determine the quantity of carbon dioxide (CO_2) as barium carbonate ($BaCO_3$).

Results and Discussion

The products were cyclohexanol, cyclohexanone and CO_2 over V_2O_5/Al_2O_3. Other possible products like diols and diones were not detected during the whole reaction time. This is very likely judging from the product distribution dealing in the gas phase photocatalytic oxidation of light alkanes.[30,31] Fundamentally, the oxygenation is initiated with the interaction between hydrogen atom of the hydrocarbon and oxygen atom of the surface vanadate species and therefore ketone is formed primarily.[29] If the diol or dione was formed, they would be produced by consecutive oxidation of the ketone. But when the photooxidation was carried

Table 1 The selected results of the photo-oxidation of cyclohexane over V_2O_5/Al_2O_3 and TiO_2.

Entry	Catalyst	C_6H_{12}	Solvent	Time	Conv. (%)	Selec. (%)			K/A	Ref.
						$C_6H_{11}OH$	$C_6H_{10}O$	CO_2		
1	TiO_2 / 70 mg	10 ml	---	3 h	0.3	5	83	12	17	42
2	TiO_2 / 30 mg	10 ml	---	3 h	0.055	5.0	82.5	12.5	17	43
3	TiO_2 + TS-1	10 ml	CH_2Cl_2 / 10 ml	3 h	0.27	30.9	67.6	1.5	2.2	43
4	TiO_2 / 20 mg	10 ml	H_2O / 10 ml	12 h	0.25	0	61	39	---	17
5	Ti-mica	10 ml	H_2O / 10 ml	12 h	0.084	26	68	6	2.6	17
6	TiO_2 / 100mg	30 ml	---	24 h	0.76	1	66	33	66	This study
7	V_2O_5 / Al_2O_3 / 100mg	30 ml	---	5 h	0.11	24	64	12	2.7	This study
8	V_2O_5 / Al_2O_3 / 100mg	30 ml	---	24 h	0.35	34	57	9	1.7	This study

out with cyclohexanone as a reactant, only carbon dioxide was obtained. When the sole reactant was changed to cyclohexanol, cyclohexanone and carbon dioxide were produced. These results show that the dione and diol are formed as neither a primary product nor a consecutive product in the present system. No hydroperoxides (for example, hydrogen peroxide and cyclohexanehydroperoxide) was detected by iodometry. In addition, dicyclohexyl was not found out in the liquid suspension. Some groups confirmed that dicyclohexyl was produced for the photo-oxidation of cyclohexane over TiO_2 and proposed that the formation of the cyclohexyl radical, namely, the photon abstraction, is a primary reaction.[44,45] However, it is expected that a free radical is not concerned with the oxidation of cyclohexane over V_2O_5/Al_2O_3 because neither the hydroperoxides nor the dicyclohexyl was detected in the present reaction. It is known that V_2O_5 itself is photo-inert.[46,47] We confirmed that neither of V_2O_5 nor Al_2O_3 was photo-active for this reaction. No product was observed at 353 K in the dark at all. The increase in the products stopped when the light-irradiation was turned off, and the amount of cyclohexanol and cyclohexanone increased when the light-irradiation was turned on again. This indicates the good response to photoirradiation. In addition, the reaction did not proceed under irradiation without a catalyst at all. Evidently, it is not a photochemical reaction but a photocatalytic reaction. The catalyst was not deactivated after 600 h. Table 1 shows the conversion of cyclohexane, the selectivities to cyclohexanol, cyclohexanone and CO_2, and the K/A ratio for the oxidation of cyclohexane over irradiated V_2O_5/Al_2O_3 or TiO_2 and the relevant reported results[17,42,43] are shown for comparison. The conversion and the selectivity were estimated with the following formulae:

Conversion (%) = (C_6-ol + C_6-one + 1/6 CO_2) / C_6H_{12} * 100

Selecitivity (%) = C_6-ol or C_6-one or 1/6 CO_2 / (C_6-ol + C_6-one + 1/6 CO_2) * 100

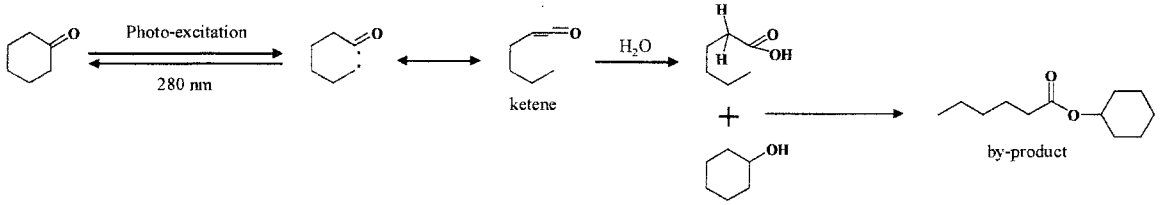

Scheme 1 The formation process of the by-product in the photo-oxidation of cyclohexane over V_2O_5/Al_2O_3.

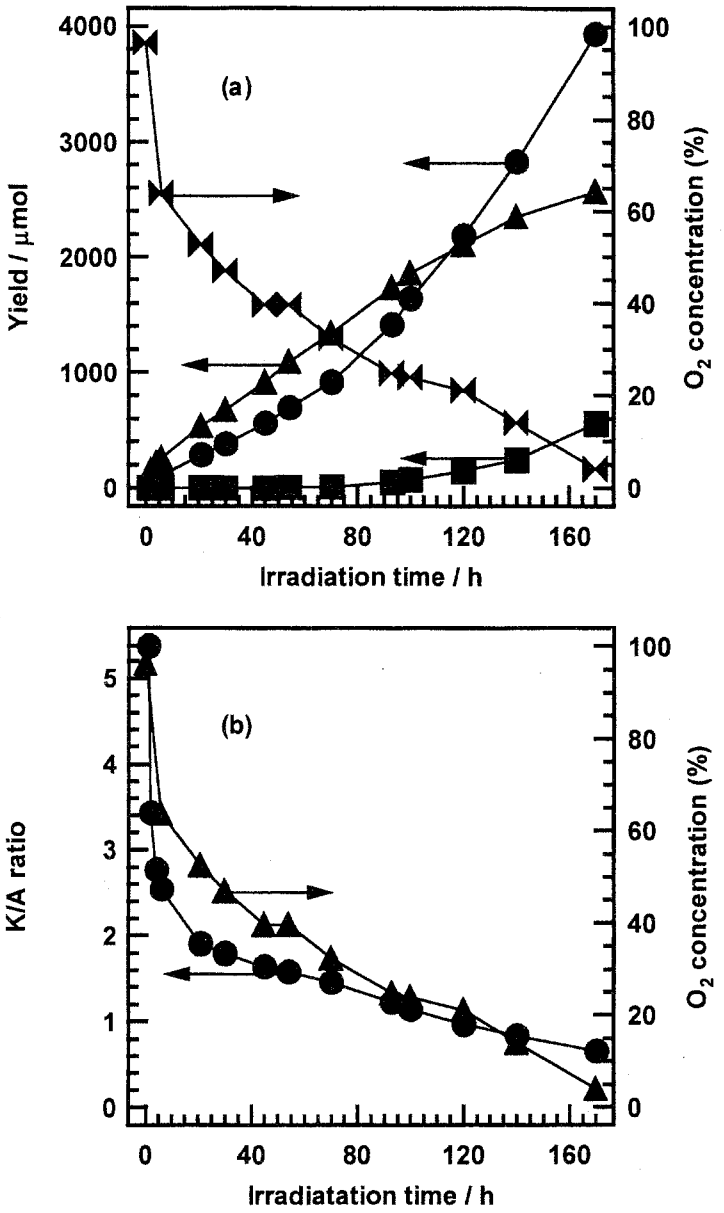

Figure 1 (a) The evolutions of cyclohexanol (circle), cyclohexanone (triangle) and by-product (square), and the consumption of the O_2 concentration (butterfly) (b) The time course of the K/A ratio (circle) and the O_2 concentration (triangle) in the gas phase over 2.5 wt.% V_2O_5/Al_2O_3 (0.1 g).

In our case, the conversion of cyclohexane and the K/A ratio on TiO_2 were very high; however, the selectivity to CO_2 was also extremely high (33 %) though the selectivity to CO_2 was very low (12 %) in Mu's[42] and Lu's[43] reports listed in entries 1-3. In addition, Boarini et al.[44] also reported very low CO_2 selectivity (5.2 %) after 90 min for the photo-oxidation of

neat cyclohexane over TiO_2, although we could not estimate the precise amount of cyclohexane and TiO_2 because the unit of concentration (mol/dm^3) was used. On the other hand, Shimizu et al.[17] reported that the selectivity to CO_2 was 39 % (entry 4-5) and these results were reproduced by us as shown in entry 6. It is very crucial to inhibit the consecutive oxidation over irradiated TiO_2 because the evolution of CO_2 increased with the irradiation time. In the case of V_2O_5/Al_2O_3, the selectivity to the partial oxidation compounds (cyclohexanol and cyclohexanone) was 91 % and the K/A ratio was 1.7 after photoirradiation for 24 h. In the present study, the high selectivity and the reasonable K/A ratio are attained for the first time except for Ti modified catalysts.[17,42-44]

However, when we used a closed batch reactor, by elongation of the photoirradiation time, a by-product was generated and the evolution rate of cyclohexanol increased gradually in contrast to that of cyclohexanone as shown in Figure 1(a). The by-product was assigned to an ester compound, cyclohexyl hexanoate, by GC-Mass spectrometry. We confirmed that this compound was formed by the reaction of ketene and cyclohexanol as shown in Scheme 1.[48]

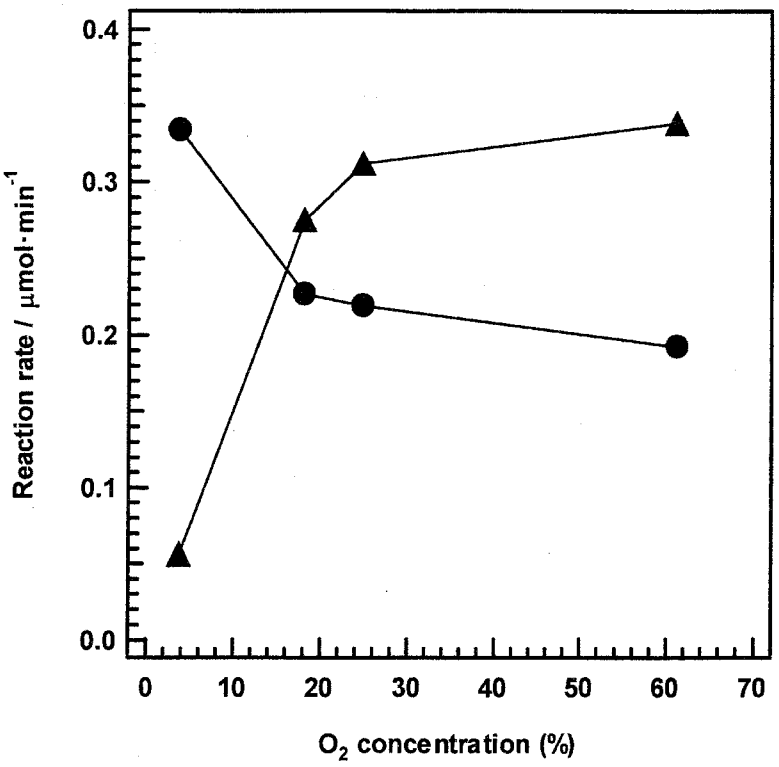

Figure 2 The steady-state rates of cyclohexanol (circle) and cyclohexanone evolution (triangle) under different O_2 concentrations over 2.5 wt.% V_2O_5/Al_2O_3 (0.1 g).

The former compound is formed by photoexcitation of cyclohexanone irradiated by UV-ray, $\lambda < 300$ nm. The produced ketene reacts with H_2O to convert to n-hexanoic acid readily because ketene is very unstable. Finally, cyclohexyl hexanoate is generated from n-hexanoic acid and cyclohexanol. The evolution rate of cyclohexanol increased gradually, and conversely, that of cyclohexanone decreased. The yield of cyclohexanol reached the same level as that of cyclohexanone at 120 h irradiation time. Then, the evolution rate of

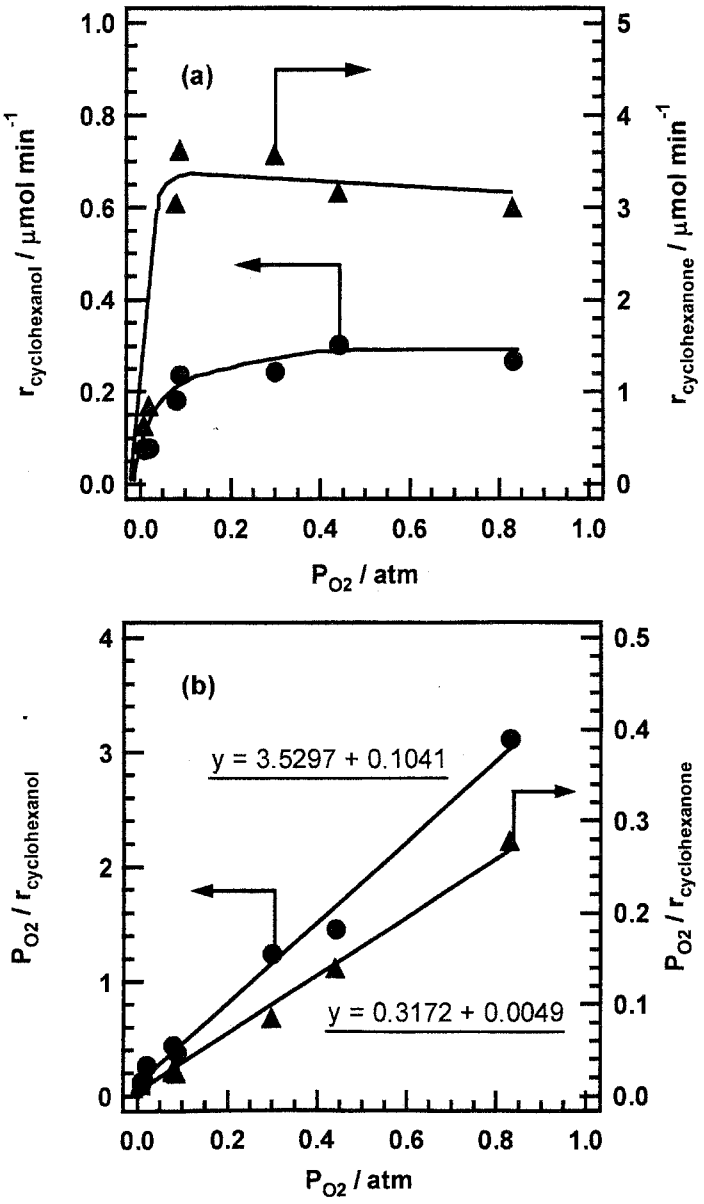

Figure 3 (a) The initial rates of cyclohexanol (circle) and cyclohexanone (triangle) evolution under different O_2 concentrations over 2.5 wt.% V_2O_5/Al_2O_3 (0.1 g). (b) The Langmuir-plot of (a).

cyclohexanol increased. Then, the O_2 concentration in the gas phase remarkably decreased. The K/A ratio decreased, corresponding to lowering of the O_2 concentration as shown in Figure 1(b). This suggests that the evolution rates of cyclohexanol and cyclohexanone are related to the O_2 concentration.

Figure 2 shows the evolution rates of cyclohexanol and cyclohexanone under different O_2 concentrations. The O_2 concentration was kept constant by using the quasi-flowing batch system. The reaction rate was monitored 5 h after photoirradiation started where the products yield increased linearly with the irradiation time. The production rates of cyclohexanol and cyclohexanone show different dependency upon the O_2 concentration, respectively. The evolution rate of cyclohexanol is reduced and that of cyclohexanone enhanced with an increase in the O_2 concentration. Above 30 % O_2 concentration, both rates leveled off. This result shows that high K/A ratio can be achieved at the O_2 concentration higher than 30 %.

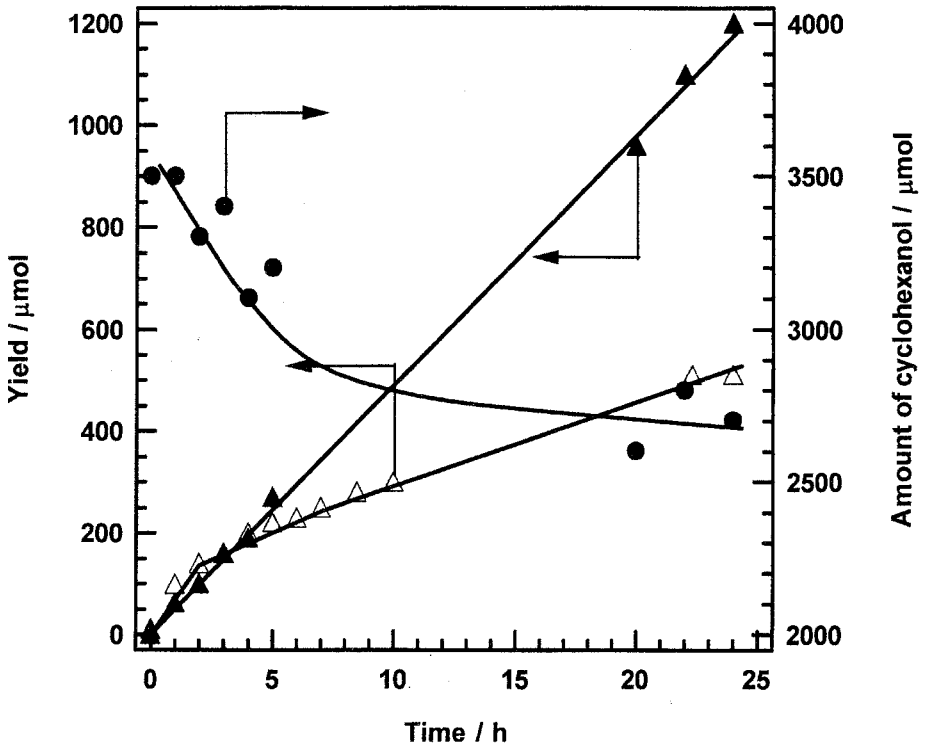

Figure 4 The time course of cyclohexanone (closed triangle) and cyclohexanol (closed circle) for the photo-oxidation of cyclohexane in the presence of 3100 μmol cyclohexanol over 2.5 wt.% V_2O_5/Al_2O_3 (0.1 g) as compared with that of cyclohexanone (opened triangle) in the absence of additives.

It is important to investigate initial evolution rates of cyclohexanol and cyclohexanone in order to elucidate the role of the O_2 concentration for the photo-oxidation of cyclohexane. Figure 3(a) shows the initial evolution rates of the selective oxidation compounds under different O_2 concentrations. The initial evolution rate of cyclohexanone is always kept high as compared with that of cyclohexanol and both rates were constant above 10 % O_2 concentration. Figure 3(b) shows the Langmuir-plot converted from Figure 3(a). It was determined that the initial evolution rate of cyclohexanol is first order against the O_2 pressure, while that of cyclohexanone is zeroth order. Boarini and co-workers[44] investigated the effect of the O_2 partial pressure on the formation of cyclohexanol and cyclohexanone in suspensions of TiO_2 in a 1:1 C_6H_{12}/CH_2Cl_2 medium. They proposed that cyclohexanol and cyclohexanone are formed by the different radical reaction mechanisms. From the Langmuir-plot of their data, we confirmed that both the evolution rates of cyclohexanol and cyclohexanone over TiO_2 were first order against the O_2 pressure. Then, we agree with the mechanism they proposed for the photo-oxidation of cyclohexane over TiO_2. On the other hand, in our case, the evolution rate of cyclohexanol is first order against the O_2 pressure, while that of cyclohexanone was zeroth order. In addition, the initial rate of cyclohexanone was 12 times as fast as that of cyclohexanol. Therefore, the evolution processes of cyclohexanol and cyclohexanone over V_2O_5/Al_2O_3 are also independent; however, the O_2 radical species in the liquid phase would not be concerned with the evolution of cyclohexanone.

We performed the photo-oxidation of cyclohexane in the presence of cyclohexanol or cyclohexanone in the liquid phase to investigate the reaction mechanism. Figure 4 shows the time course of the photo-oxidation of cyclohexane substrate in the presence of 3100 μmol cyclohexanol over V_2O_5/Al_2O_3. The amount of cyclohexanol decreased gradually and the evolution of cyclohexanone and CO_2 increased over the case without additives. This indicates that cyclohexanol is oxidized to cyclohexanone over irradiated V_2O_5/Al_2O_3. 2-Pentanone was generated and the initial evolution rates of cyclohexanol and cyclohexanone were suppressed when 2-pentanol as an additive was used instead of cyclohexanol. Accordingly, alcohol is preferentially adsorbed on V_2O_5/Al_2O_3 as compared with cyclohexane and oxidized to ketone

Table 2 The photo-oxidation of cyclohexane in the presence of the additives over V_2O_5/Al_2O_3 under irradiation for 24 h

Additive Compound	Additive amount / μmol	Cyclohexanol / μmol	Cyclohexanone / μmol	CO_2 / μmol
None	---	340	560	510
Cyclohexanone	3600	700	---	990
Cyclopentanone	3400	620	540	920
2-Pentanone	3600	640	940	880

Reaction time : 24 h
Catalyst (2.5 wt.% V_2O_5/Al_2O_3) : 0.1 g
Substrate (Cyclohexane) : 30 ml

or CO_2. Actually, the higher the concentration of cyclohexanol was, the slower the evolution rate of cyclohexanone was. The evolution of 2-propanone and the consumption of 2-propanol were not compatible in the presence of 2-propanol. Most produced alcohols would be adsorbed on alumina support of V_2O_5/Al_2O_3. The oxidation process of cyclohexanol should be also conceivable as one of the evolution process of cyclohexanone but this contribution would be small.

The steady-state rate of cyclohexanone was significantly low compared with the initial rate although that of cyclohexanol was almost constant. This indicates that cyclohexanone is decomposed to other compounds. The photo-oxidation of cyclohexane in the presence of small amount of various ketones was carried out to clarify the effect of decomposition of cyclohexanone. Table 2 shows enhancement of amount of cyclohexanol, cyclohexanone and CO_2 when cyclohexanone, cyclopentanone or 2-pentanone was added into the cyclohexane substrate. It is surprising that the amount of cyclohexanol increased by a large margin by addition of these ketones. It was found that cyclopentanone and 2-pentanone decreased under irradiation. Table 3 shows the evolution of cyclohexanol for the photo-oxidation of cyclohexane in the presence of small amount of cyclohexanone. The evolution of cyclohexanol became negligible when the UV-33 cut filter was used. The formation of cyclohexanol and CO_2 were also confirmed under irradiation without a catalyst,

Table 3 The evolution of cyclohexanol and CO_2 in the photo-oxidation of cyclohexane in the presence of small amount of cyclohexanone

Entry	Catalyst	Cut filter	Cyclohexanol / μmol	CO_2 / μmol
1	None	None	460	250
2	None	UV-35	30	110
3	2.5 wt.% V_2O_5/Al_2O_3, 0.1g	UV-35	130	260

Reaction time : 24 h
Substrate (Cyclohexane) : 30 ml
Additive (Cyclohexanone) : 3000 μmol

but were inhibited under irradiation $\lambda > 300$ nm. The absorption band of the ketones lies at around 300 nm. It is speculated that photo-decomposition of ketone (Norrish Type I reaction) as shown in Scheme 1 contributes to the evolution of cyclohexanol. However, the evolution of cyclohexanol could not be suppressed in the presence of V_2O_5/Al_2O_3 despite of using the cut filter. Therefore, the ketone molecules adsorbed on V_2O_5/Al_2O_3 can be activated under irradiation $\lambda > 300$ nm. It was confirmed by Raman spectroscopy that ketone molecules interact with V=O species of V_2O_5/Al_2O_3.

Figure 5 shows the evolutions of cyclohexanol, cyclohexanone and CO_2 under irradiation of the different wavelength light for 24 h. The wavelength was selected with cut filters (TOSHIBA Co.). UV-*x* and Y-*x* denote the filter which cuts off half light intensity with the wavelengths $\lambda = 10x$ nm and light intensity with the wavelength $\lambda = (10x\text{-}30)$ nm absolutely, respectively. All compounds yield decreased according to cutting wavelength with each cut filter. However, it is worthy of special mention that the oxidation can proceed under irradiation with the Y-43 or 45 filter, namely between visible light area. It is well-known that a fluorescent lamp emits light with 417 nm wavelength strongly. We carried out the oxidation of cyclohexane over irradiated V_2O_5/Al_2O_3 with a fluorescent lamp (Panasonic, 27 W). The reaction proceeded gradually, and 50 μmol cyclohexanone and 4 μmol cyclohexanol were produced for 100 h. In the present case, CO_2 was not detected. From the practical standpoint, it is highly important that the photo-oxidation of cyclohexane proceeds under fluorescent

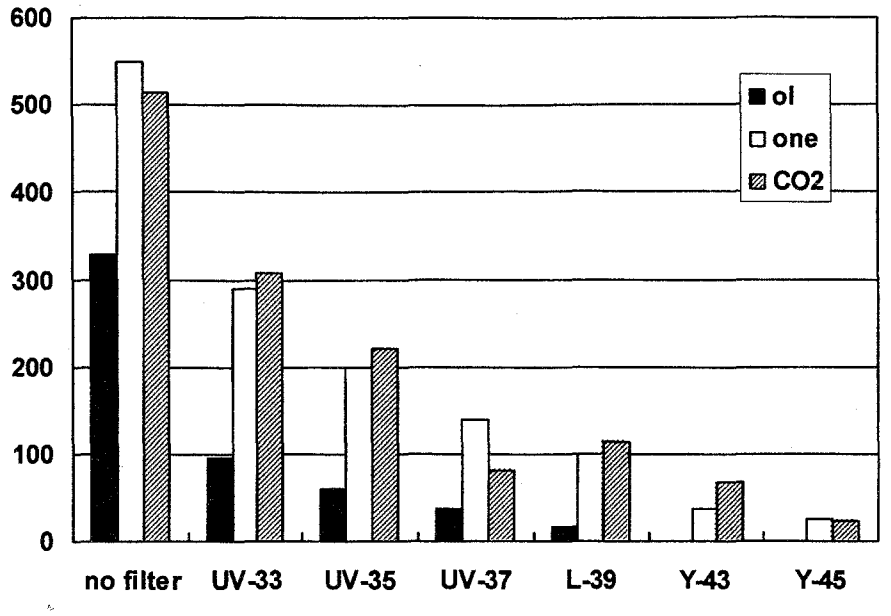

Figure 5 The amounts of cyclohexanol, cyclohexanone and CO_2 under irradiation with cut filter for 24 h over 2.5 wt.% V_2O_5/Al_2O_3 (0.1 g). UV-*x* or Y-*x* denotes the filter which cuts off half light intensity with the wavelengths $\lambda = 10x$ nm and light intensity with the wavelength $\lambda = (10x\text{-}30)$ nm absolutely, respectively.

lamp irradiation. To investigate the effect of the irradiated wavelength upon product selectivity, the amounts of three products (cyclohexanol, cyclohexanone and CO_2) at 0.1 % conversion of cyclohexane were compared under photoirradiation of various wavelengths, as shown in Figure 6. The generation of CO_2 was remarkably suppressed under photoirradiation $\lambda > 330$ nm. However, the K/A ratio scarcely depends on the wavelength of irradiation. (It is important to irradiate the light $\lambda > 330$ nm in order to accomplish the high selectivity to the partial oxidation compounds.) Therefore, the effective wavelength for the selective oxidation is different from that for the complete oxidation.

In the present study, we investigated the superiority of V_2O_5/Al_2O_3 for the selective oxidation as compared with TiO_2. It is clarified that the K/A ratio and the selectivity to the partial oxidation compounds can be controlled by the O_2 concentration and the irradiated wavelength, respectively. The most important factors are

(1) The O_2 concentration should be kept above 30 % to achieve the high K/A ratio.

(2) The irradiated wavelength $\lambda < 300$ nm should be cut off to inhibit the formation of CO_2 and the ester compound as a by-product.

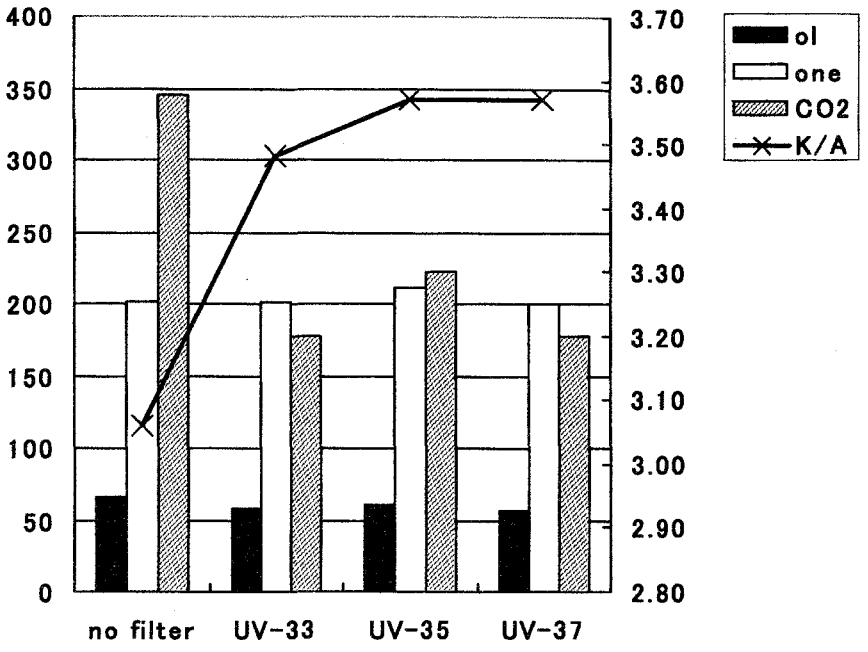

Figure 6 The amounts of cyclohexanol, cyclohexanone and CO_2, and the K/A ratio under photoirradiation of various wavelengths at 0.1 % conversion of cyclohexane over 2.5 wt.% V_2O_5/Al_2O_3 (0.1 g).

We performed optimization for the selective photo-oxidation of cyclohexane over V_2O_5/Al_2O_3. To maintain the high K/A ratio, we carried out the photo-oxidation of cyclohexane over V_2O_5/Al_2O_3 with keeping the O_2 concentration at 80 %, and to avoid the formation of ketene and CO_2, we cut off light with the wavelengths $\lambda < 330$ nm as shown in Figure 7. The wavelength below 300 nm can be cut off absolutely with the UV-33 cut filter. No ester by-product was produced under this condition. Further, the evolution of cyclohexanone became dominant and the high K/A ratio was achieved. The evolution rates of cyclohexanol and cyclohexanone became constant after 5 h. 640 μmol cyclohexanone, 170 μmol cyclohexanol and 704 μmol CO_2 were produced efficiently for 100 h irradiation. As a consequence, a conversion of 0.33 % and a selectivity of 87 % were achieved with the K/A ratio of 3.8.

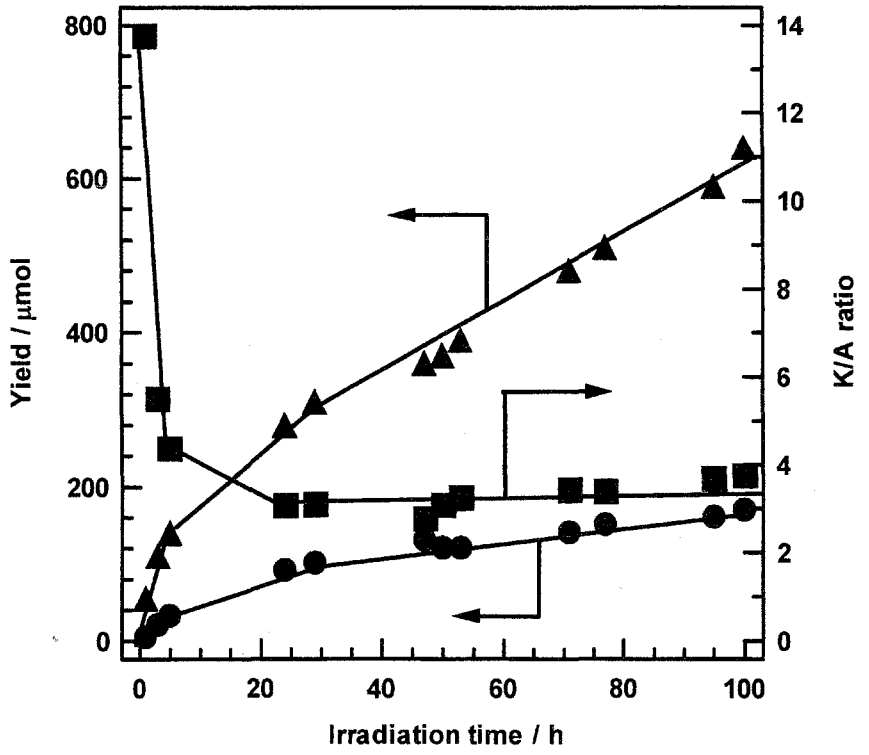

Figure 7 The evolutions of cyclohexanol (circle) and cyclohexanone (triangle), and the K/A ratio (square) at 80 % O_2 concentration under irradiation of the wavelength $\lambda > 300$ nm over 2.5 wt.% V_2O_5/Al_2O_3 (0.1 g).

Conclusion

V_2O_5/Al_2O_3 catalyst is active for the selective oxidation of cyclohexane in the presence of molecular oxygen under photoirradiation. The important factors are (1) the O_2 concentration should be kept above 30 % to achieve the high K/A ratio and (2) the irradiated wavelength $\lambda < 300$ nm should be cut off to inhibit the formation of CO_2 and by-product. This reaction proceeds at ambient temperature and atmospheric pressure without a solvent. Because of photocatalytic reaction, the reaction exhibits high response to the light irradiation. The features of the reaction are the high selectivity to the partial oxidation compounds and the reasonable K/A ratio. In addition, for V_2O_5/Al_2O_3, the effective wavelength for the photo-decomposition of cyclohexanone shifts to longer wavelengths. Mechanistic study and development of more active catalysts are now in progress.

References

(1) Centi, G.; Misono, M. *Catal. Today* **1998**, *41*, 287.

(2) Arends, I.; Sheldon, R. A. *Appl. Catal. A-Gen.* **2001**, *212*, 175.

(3) Pichat, P. *Catal. Today* **1994**, *19*, 313.

(4) Mills, A.; Davies, R. H.; Worsley, D. *Chem. Soc. Rev.* **1993**, *22*, 417.

(5) Hoffmann, M. R.; Martin, S. T.; Choi, W. Y.; Bahnemann, D. W. *Chem. Rev.* **1995**, *95*, 69.

(6) Maldotti, A.; Molinari, A.; Amadelli, R. *Chem. Rev.* **2002**, *102*, 3811.

(7) Ohno, T.; Kigoshi, T.; Nakabeya, K.; Matsumura, M. *Chem. Lett.* **1998**, 877.

(8) Ohno, T.; Nakabeya, K.; Matsumura, M. *J. Catal.* **1998**, *176*, 76.

(9) Ohno, T.; Masaki, Y.; Hirayama, S.; Matsumura, M. *J. Catal.* **2001**, *204*, 163.

(10) Jia, J. G.; Ohno, T.; Masaki, Y.; Matsumura, M. *Chem. Lett.* **1999**, 963.

(11) Jia, J. G.; Ohno, T.; Matsumura, M. *Chem. Lett.* **2000**, 908.

(12) Ohno, T.; Sarukawa, K.; Tokieda, K.; Matsumura, M. *J. Catal.* **2001**, *203*, 82.

(13) Ohno, T.; Sarukawa, K.; Matsumura, M. *J. Phys. Chem. B* **2001**, *105*, 2417.

(14) Ohno, T.; Sarukawa, K.; Matsumura, M. *New J. Chem.* **2002**, *26*, 1167.

(15) Yoshida, H.; Murata, C.; Hattori, T. *Chem. Commun.* **1999**, 1551.

(16) Yoshida, H.; Murata, C.; Hattori, T. *J. Catal.* **2000**, *194*, 364.

(17) Shimizu, K. I.; Kaneko, T.; Fujishima, T.; Kodama, T.; Yoshida, H.; Kitayama, Y. *Appl. Catal. A-Gen.* **2002**, *225*, 185.

(18) Amadelli, R.; Bregola, M.; Polo, E.; Carassiti, V.; Maldotti, A. *J. Chem. Soc. Chem. Commun.* **1992**, 1355.

(19) Molinari, A.; Amadelli, R.; Antolini, L.; Maldotti, A.; Battioni, P.; Mansuy, D. *J. Mol. Catal. A-Chem.* **2000**, *158*, 521.

(20) Molinari, A.; Amadelli, R.; Andreotti, L.; Maldotti, A. *J. Chem. Soc., Dalton Trans.* **1999**, 1203.

(21) Molinari, A.; Amadelli, R.; Mazzacani, A.; Sartori, G.; Maldotti, A. *Langmuir* **2002**, *18*, 5400.

(22) Maldotti, A.; Molinari, A.; Varani, G.; Lenarda, M.; Storaro, L.; Bigi, F.; Maggi, R.; Mazzacani, A.; Sartori, G. *J. Catal.* **2002**, *209*, 210.

(23) Yoshida, S.; Tanaka, T.; Okada, M.; Funabiki, T. *J. Chem. Soc., Faraday Trans. 1* **1984**, *80*, 119.

(24) Tanaka, T.; Ooe, M.; Funabiki, T.; Yoshida, S. *J. Chem. Soc., Faraday Trans. I* **1986**, *82*, 35.

(25) Tanaka, T.; Nishimura, Y.; Kawasaki, S.; Ooe, M.; Funabiki, T.; Yoshida, S. *J. Catal.* **1989**, *118*, 327.

(26) Tanaka, T.; Takenaka, S.; Funabiki, T.; Yoshida, S. *Chem. Lett.* **1994**, 1585.

(27) Takenaka, S.; Kuriyama, T.; Tanaka, T.; Funabiki, T.; Yoshida, S. *J. Catal.* **1995**, *155*, 196.

(28) Tanaka, T.; Takenaka, S.; Funabiki, T.; Yoshida, S. *J. Chem. Soc., Faraday Trans.* **1996**, *92*, 1975.

(29) Takenaka, S.; Tanaka, T.; Funabiki, T.; Yoshida, S. *J. Chem. Soc., Faraday Trans.* **1997**, *93*, 4151.

(30) Tanaka, T.; Ito, T.; Funabiki, T.; Yoshida, S. *Stud. Surf. Sci. Catal.* **2000**, *130*, 1961.

(31) Tanaka, T.; Ito, T.; Takenaka, S.; Funabiki, T.; Yoshida, S. *Catal. Today* **2000**, *61*, 109.

(32) Gritscov, A. M.; Shvets, V. A.; Kazansky, V. B. *Kinet. Katal.* **1974**, *15*, 1257.

(33) Gritscov, A. M.; Shvets, V. A.; Kazansky, V. B. *Chem. Phy. Lett.* **1975**, *35*, 511.

(34) Anpo, M.; Tanahashi, I.; Kubokawa, Y. *J. Phys. Chem.* **1980**, *84*, 3440.

(35) Tanaka, T.; Yamashita, H.; Tsuchitani, R.; Funabiki, T.; Yoshida, S. *J. Chem. Soc., Faraday Trans. I* **1988**, *84*, 2987.

(36) Yoshida, S.; Tanaka, T.; Hanada, T.; Hiraiwa, T.; Kanai, H.; Funabiki, T. *Catal. Lett.* **1992**, *12*, 277.

(37) Tanaka, T.; Nishimura, Y.; Kawasaki, S. I.; Funabiki, T.; Yoshida, S. *J. Chem. Soc., Chem. Commun.* **1987**, 506.

(38) Teramura, K.; Tanaka, T.; Yamamoto, T.; Funabiki, T. *J. Mol. Catal. A-Chem.* **2001**, *165*, 299.

(39) Castellan, A.; Bart, J. C. J.; Cavallaro, S. *Catal. Today* **1991**, *9*, 237.

(40) Bellussi, G.; Perego, C. *Cattech* **2000**, *4*, 4.

(41) Schuchardt, U.; Cardoso, D.; Sercheli, R.; Pereira, R.; de Cruz, R. S.; Guerreiro, M. C.; Mandelli, D.; Spinace, E. V.; Pires, E. L. *Appl. Catal. A-Gen.* **2001**, *211*, 1.

(42) Mu, W.; Herrmann, J. M.; Pichat, P. *Catal. Lett.* **1989**, *3*, 73.

(43) Lu, G. X.; Gao, H. X.; Suo, J. H.; Li, S. B. *J. Chem. Soc., Chem. Commun.* **1994**, 2423.

(44) Boarini, P.; Carassiti, V.; Maldotti, A.; Amadelli, R. *Langmuir* **1998**, *14*, 2080.

(45) Gonzalez, M. A.; Howell, S. G.; Sikdar, S. K. *J. Catal.* **1999**, *183*, 159.

(46) Pichat, P.; Herrmann, J. M.; Disdler, J.; Mozzanega, M. N. *J. Phy. Chem.* **1979**, *83*, 3122.

(47) Yoshida, S.; Matsumura, Y.; Noda, S.; Funabiki, T. *J. Chem. Soc., Faraday Trans. 1* **1981**, *77*, 2237.

(48) Schenck, G. O.; Frank, S. *Chem. Ber.* **1965**, *98*, 2056.

Chapter 7

Selective photo-oxidation of hydrocarbons over V_2O_5/Al_2O_3

Abstract

More than 0.22 mmol of isolated VO_4 species of V_2O_5/Al_2O_3 exhibited the highest evolution of the partial oxidation products (alcohol and ketone) in the oxidation of cyclohexane and cyclopentane. The conversion of cyclohexane and the selectivity of the partial oxidation products were achieved to be 0.49 % and 85 %, respectively, over 0.8 g of 3.5 wt.% V_2O_5/Al_2O_3 where the K/A ratio was 6.2. In addition, V_2O_5/Al_2O_3 can selectively oxidize various hydrocarbons in the liquid phase by the one-step oxygen atom insertion to C-H bond. The order of priority was tertiary carbon > secondary carbon > primary carbon > benzene ring.

Introduction

The oxidation of cyclohexane is an essential process to produce 6-nylon and 6,6-nylon. ε-caprolactam or adipic acid which is a raw material for 6-nylon or 6,6-nylon synthesis is obtained by the cyclohexanone oximation with hydroxylammonium sulfate or the oxidation of the K/A (cyclohexanone/cyclohexanol) oil by means of HNO_3, respectively.[1-3] The K/A oil is produced by auto-oxidation process of cyclohexane over cobalt-base homogeneous catalyst above 423 K under about 8 kPa pressure.[4,5] It is very difficult to control the conversion of cyclohexane and the K/A ratio because of auto-oxidation. The conventional cyclohexane oxidation is operated at 4 % conversion to inhibit the formation of by-product and the complete oxidation to CO_2. Recently, some authors found new catalysts which make the oxidation of cyclohexane proceed under mild condition (at room temperature and atmosphere pressure).[6-20] We investigated the oxidation of cyclohexane over photocatalysts to achieve high conversion and K/A ratio under mild condition. In our laboratory, it has been reported that the selective oxidations of light alkanes[21-26] and alkenes[27-29] in the gas phase proceed over highly dispersed silica-supported vanadium oxide catalyst (V_2O_5/SiO_2). It has been concluded that active sites are the isolated VO_4 species on silica. Many groups also investigated the photo-activity of highly dispersed vanadium oxide on supports.[30-35] On the other hand, in the liquid phase, it was found that 2.5 wt.% V_2O_5/Al_2O_3 exhibits the highest conversion and selectivity in the oxidation of cyclohexane under photoirradiation in four supports (SiO_2, Al_2O_3, TiO_2, ZrO_2).[36] It was first reported that the highly dispersed vanadium species on alumina shows high photoactivity as compared with that on silica. In addition, we clarified two important factors in the photo-oxidation of cyclohexane over V_2O_5/Al_2O_3 photocatalyst in the quasi-flowing system.[37] The factors are described as follows

(1) The O_2 concentration should be kept above 30 % to achieve the high K/A ratio.

(2) The irradiated wavelength should be cut off $\lambda < 300$ nm to inhibit the formation of CO_2 and the ester compound as a by-product.

The K/A ratio depended on the O_2 concentration. In the closed system, the lower the O_2 concentration in the reactor was, the smaller the K/A ratio was. We obtained the factor (1) in

carrying out the photo-oxidation of cyclohexane under various O_2 concentrations in the quasi-flowing system. Moreover, cyclohexyl hexanoate as a by-product was formed by elongation of the photoirradiation time. It is well-known that ketene is generated by photoexcitation of ketone irradiated by UV-ray, $\lambda < 300$ nm (Norrish Type I reaction).[38] Unstable ketene reacts with alcohol to ester readily. Therefore, cyclohexyl hexanoate is generated from photoexcited cyclohexane (ketene) and cyclohexanol which are formed in the photo-oxidation of cyclohexane over V_2O_5/Al_2O_3. The formation of by-product was remarkably suppressed under photoirradiation $\lambda > 330$ nm because Norrish Type I reaction occurs by UV-ray, $\lambda < 300$ nm. In addition, the formation of CO_2 was likewise inhibited under photoirradiation $\lambda > 330$ nm. We acquired the factor (2) in carrying out the photo-oxidation of cyclohexane with various cut-filters. When various ketones were added to cyclohexane substrate, the evolutions of cyclohexane and CO_2 increased in the photo-oxidation of cyclohexane over V_2O_5/Al_2O_3. It has been clarified that the formations of cyclohexane and CO_2 relate to the photodecomposition of ketone (Norrish Type I reaction) closely. In this study, we performed the photo-oxidation of cyclohexane over V_2O_5/Al_2O_3 with various amounts of catalyst and V_2O_5 loading to optimize the reaction in the quasi-flowing system. Moreover, V_2O_5/Al_2O_3 was applied to selective photo-oxidations of various hydrocarbons.

Experimental

Alumina-supported vanadium oxide catalyst (V_2O_5/Al_2O_3) was prepared by impregnation of alumina powder with an aqueous solution of ammonium metavanadate (NH_4VO_3) at 353 K, followed by evaporation, drying and calcination at 773 K in a stream of dry air for 5 h.[36,37] Alumina used as a support in the study is JRC-ALO-8 supplied from the Japan Catalysis Society.

The photocatalytic reaction was carried out in a quasi-flowing batch system at atmospheric pressure. The reactor is similar to a Schrenck flask and is made of Pyrex glass with a flat glass in the bottom. V_2O_5/Al_2O_3 as a catalyst sample (0.1 g) and cyclohexane as a substance (30 ml : Wako GR, 99.5 %) were introduced to the reactor. In this study, no solvent

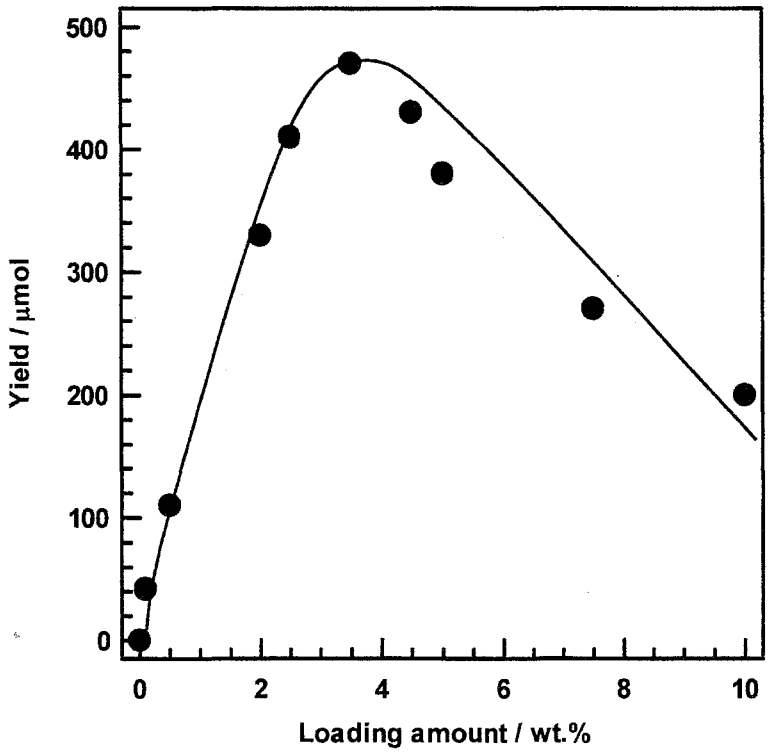

Figure 1 The evolution of cyclohexanone in the photo-oxidation of cyclohexane over V_2O_5/Al_2O_3 (0.1 g) with various amounts of V_2O_5 loading after 24 h photoirradiation.

was used. The catalyst was not evacuated nor pretreated in the presence of O_2. In addition, cyclohexane was used without further purification. The suspension stirred by a magnetic stirrer at 323 K was irradiated from the flat bottom of the reactor through a reflection by a cold mirror with a 500 W ultrahigh-pressure Hg lamp supplied by USHIO Denki Co. Oxygen was flowed to the reactor at 2 cm^3mim^{-1} through cyclohexane saturators. Organic products were analyzed by FID GC and GC mass spectrometry. The O_2 concentration was monitored by TCD GC and was determined with regard to the N_2 concentration and vapor pressure of cyclohexane. Further, at the down stream of the flow reactor, a trap with barium hydroxide solution ($Ba(OH)_2$) was equipped to determine the quantity of carbon dioxide (CO_2) as barium carbonate ($BaCO_3$).

Results and Discussion

Cyclohexanol, cyclohexanone and CO_2 were produced in the photo-oxidation of cyclohexane over V_2O_5/Al_2O_3. Other probable compounds were not detected during the whole reaction time. Cyclohexanediol and cyclohexanedione were not generated in this reaction. The production of cyclohexanehydroperoxide was not identified by iodometry although some authors proposed this product as an intermediate of the cyclohexane oxidation. In addition, dicyclohexyl was not obtained in the liquid suspension. Therefore, the radical species do not relate to the formation of cyclohexanol and cyclohexanone in the photo-oxidation of cyclohexane. No product was detected in the dark at all. The evolution of cyclohexanol and cyclohexanone responded to illumination dominantly. The reaction did not proceed under photoirradiation without a catalyst. Photo-oxidation of cyclohexane over V_2O_5/Al_2O_3 is not a photochemical reaction but a photocatalytic reaction.

We investigated the effect of loading amount of V_2O_5 on the reaction activity and selectivity. Figure 1 shows the evolution of cyclohexanone in the photo-oxidation of cyclohexane over V_2O_5/Al_2O_3 with various amounts of V_2O_5 loading after 24 h

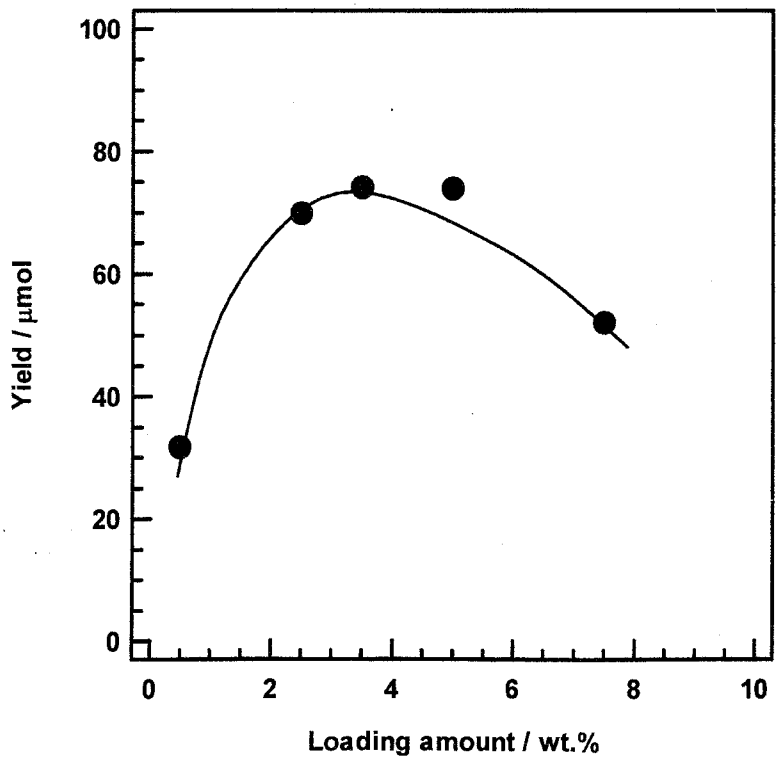

Figure 2 The evolution of cyclopentanone in the photo-oxidation of cyclopentane over V_2O_5/Al_2O_3 (0.1 g) with various amounts of V_2O_5 loading after 24 h photoirradiation.

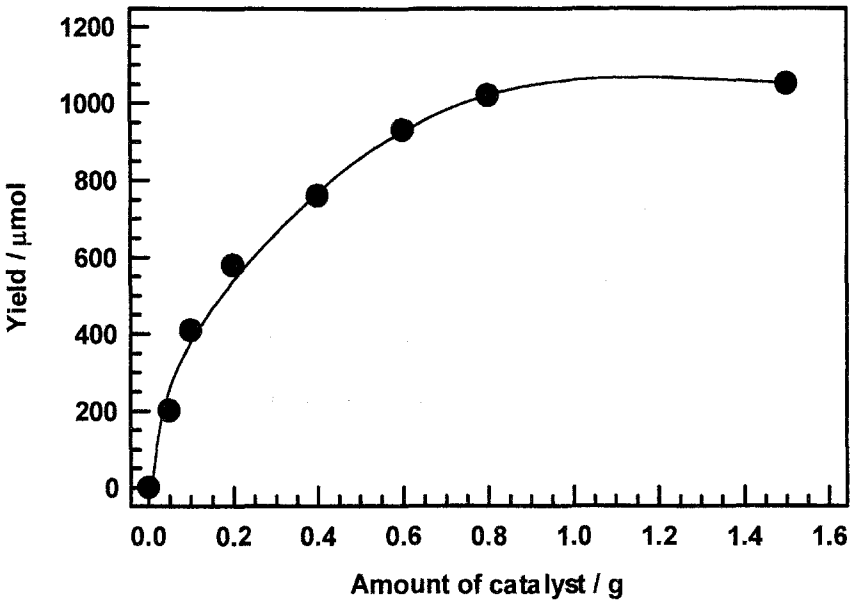

Figure 3 The evolution of cyclohexanone in the photo-oxidation of cyclohexane in increasing in quantity of 3.5 wt.% V_2O_5/Al_2O_3 after 24 h photoirradiation.

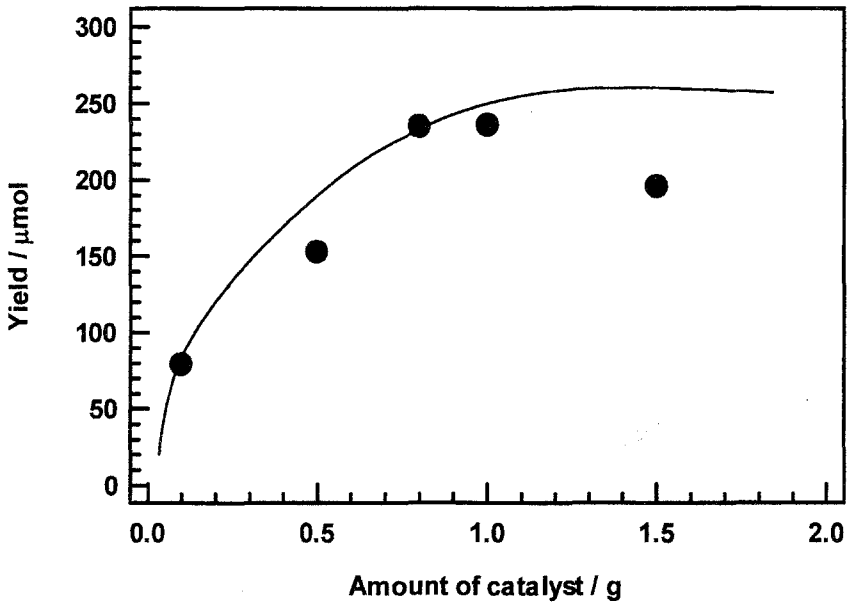

Figure 4 The evolution of cyclopentanone in the photo-oxidation of cyclopentane in increasing in quantity of 3.5 wt.% V_2O_5/Al_2O_3 after 24 h photoirradiation.

photoirradiation. The increase in V_2O_5 loading caused the enhancement of cyclohexanone evolution until 3.5 wt.% loading. After that, the activity fell down in increasing in loading amount more. In addition, V_2O_5 itself was inactive in the photo-oxidation of cyclohexane. It is

well-known that vanadium oxide aggregates as V_2O_5 in increasing loading amount although vanadium species are almost highly dispersed on alumina at low loading and stabilized as an isolated VO_4 species.[39-41] Accordingly, the highly-dispersed species is an isolated VO_4 species and the aggregated species is like V_2O_5. Gao and Wachs[41] confirmed by UV-Vis-NIR diffuse reflectance spectroscopy that the polymerized VO_4 species appeared at 6.92 wt.% loading on alumina (2.2 V atom/nm^2). It was proposed that the vanadium species changes from the isolated VO_4 species to the polymerized VO_5/VO_6 species via the polymerized VO_4 species. Therefore, the isolated VO_4 species build the 2D-network each other and change to the polymerized VO_4 species in increasing in loading amount. The polymerized VO_5/VO_6 species like V_2O_5 (3D-network) are generated at higher loading over monolayer coverage. In our case, it is inferred that the isolated VO_4 species is active and the polymerized VO_4 and VO_5/VO_6 species are inactive. The specific surface area of alumina used in this study was 140 m^2g^{-1}. The surface density of 3.5 wt.% V_2O_5/Al_2O_3 was 1.71 V atom/nm^2. In conclusion, the vanadium species aggregates over 1.71 V atom/nm^2 and the polymerized VO_4 species were

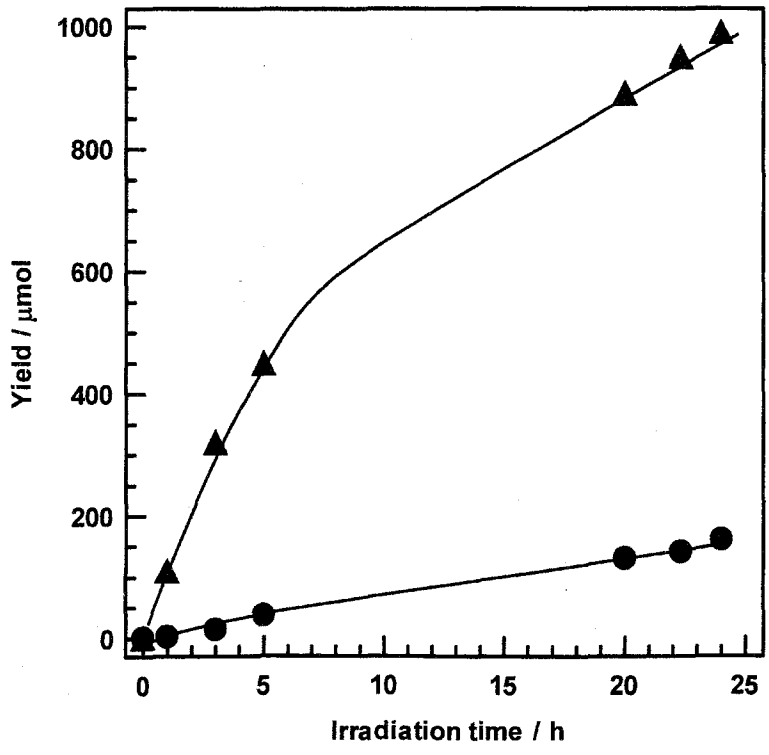

Figure 5 Time course of the cyclohexanone (circle) and cyclohexanol (triangle) evolutions in the selective photo-oxidation of cyclohexane over 0.8 g of 3.5 wt.% V_2O_5/Al_2O_3.

formed on alumina although Gao and Wachs[41] observed the polymerized VO_4 species at 2.2 V atom/nm^2. This result was reconfirmed by the photo-oxidation of cyclopentane over V_2O_5/Al_2O_3. Cyclopentanol, cyclopentanone and CO_2 were produced in this reaction. Figure 2 shows that the evolution of cyclopentanone in photo-oxidation of cyclopentane over V_2O_5/Al_2O_3 with various amounts of V_2O_5 loading after 5 h photoirradiation. In the case of the photo-oxidation of cyclopentane, 3.5 wt.% V_2O_5/Al_2O_3 also exhibited the highest activity.

Figure 3 or Figure 4 shows the evolution of cyclohexanone or cyclopentanone in the photo-oxidation of cyclohexane or cyclopentane in increasing in quantity of 2.5 wt.% V_2O_5/Al_2O_3 after 24 h photoirradiation, respectively. The increase in the quantity of catalyst caused the enhancement of cyclohexanone until 0.8 g. After that, the activity was constant. Because of the photoirradiation to the steady dimension, the amount of vanadium species which are activated under photoirradiation was saturated above 0.8 g. If all vanadium species in 2.5 wt.% V_2O_5/Al_2O_3 are isolated on Al_2O_3, more than 0.22 mmol of V atoms do not make activity high in our system. We have uncovered two important factors for the photo-oxidation of cyclohexane to obtain cyclohexanone preferentially as follows. (1) The O_2 concentration should be kept above 30 % to achieve the high K/A ratio. (2) The irradiated wavelength should be cut off $\lambda < 300$ nm to inhibit the formation of CO_2 and the ester compound as a by-product. We performed optimization in the selective photo-oxidation of cyclohexane over 0.8 g of 3.5 wt.% V_2O_5/Al_2O_3 (0.31 mmol of V atom) keeping the O_2 concentration at 80 % and cutting off the wavelength below 300 nm as shown in Figure 5. 990 μmol cyclohexanone, 160 μmol cyclohexanol and 1260 μmol CO_2 were evolved efficiently for 24 h photoirradiation. Accordingly, the conversion of cyclohexane and the selectivity of the partial oxidation products were achieved to be 0.49 % and 85 %, respectively, where the K/A ratio was 6.2. In addition, 1000 μmol cyclohexanone, 210 μmol cyclohexanol and 1190 μmol CO_2 were evolved efficiently over 0.8 g of 2.5 wt.% V_2O_5/Al_2O_3 (0.22 mmol of V atom). The activity in using 0.8 g of 2.5 wt.% V_2O_5/Al_2O_3 was similar to that in using 0.8 g of 3.5 wt.% V_2O_5/Al_2O_3. This implies the following. The surface vanadium species of 3.5 wt.% V_2O_5/Al_2O_3 are highly dispersed on alumina. When more than 0.22 mmol of isolated VO_4 species are admitted, the charge transfer from O atom to V atom is the time-determine step in

the photo-oxidation of hydrocarbons in the liquid phase. Some isolated VO_4 species can not be activated because the irradiated facet area is limited. Therefore, it is possible to enhance the evolution of cyclohexanone more if the irradiated facet area increased simply.

We performed the photo-oxidation of various hydrocarbons to apply V_2O_5/Al_2O_3 in

Table 1 The evolutions of selective oxidation products in the photo-oxidation of various hydrocarbons over V_2O_5/Al_2O_3 under photoirradiation

Substrate	Time	Yield / μmol		
	24 h	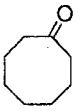 51.2		
	5 h	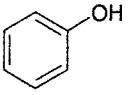 7.0		
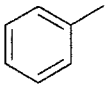	24 h	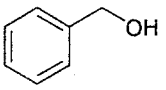 3.6	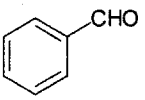 77.8	
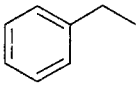	24 h	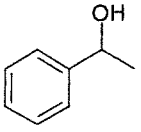 12.2	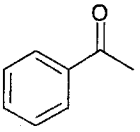 51.7	
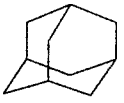	24 h	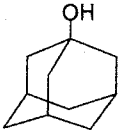 5.7	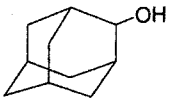 0.3	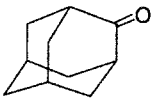 1.6
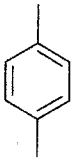	24 h	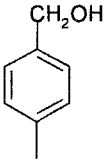 18.6	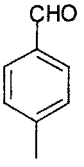 245.2	

Catalyst : 2.5 wt.% V_2O_5/Al_2O_3, 0.1 g
Substrate : 1 ml
Solvent : acetonitrile, 3 ml
* adamantane : 150 μmol, acetonitrile : 4 ml

other selective oxidation systems as shown in Table 1. V_2O_5/Al_2O_3 could oxidize various hydrocarbons selectivity. Only cyclooctanone was formed in the photo-oxidation of cyclooctane. It was confirmed that the formation scheme of ketone do not correspond to that of alcohol because ketone was generated preferentially as compared with alcohol in the photo-oxidation of cyclopentane, cyclohexane and cyclooctane. Therefore, the isolated VO_4 species play an important role in the formation of ketones from hydrocarbons. In addition, benzene and benzene derivatives were also oxidized selectivity over V_2O_5/Al_2O_3 under photoirradiation. It is considerable to produce phenol from benzene by one-step oxidation. In the case of the photo-oxidation of toluene, ethyl benzene or adamantane the major product is benzaldehyde, acetophenone or 1-adamantanol, respectively. Especially, benzoic acid was not generated from toluene. We also performed the photo-oxidation of o-xylene and obtained 4-methy-benzaldehyde as a major product and 4-methy-benzylalcohol as a minor product. In conclusion, the oxidation ability of V_2O_5/Al_2O_3 is the insertion of one oxygen atom to C-H bond and the order of priority was tertiary carbon > secondary carbon > primary carbon > benzene ring. This result was similar to the photo-oxidation of various hydrocarbons over V_2O_5/SiO_2 in the gas phase.[21-26] Therefore, the isolated VO_4 species on supports achieves the selective photo-oxidation of hydrocarbons (one oxygen atom insertion to C-H bond).

Conclusion

In our cyclohexane photo-oxidation system, the evolutions of cyclohexanone and cyclohexanol indicated maximum when 0.22 mmol of isolated VO_4 species were included on the surface of V_2O_5/Al_2O_3 photocatalyst. The conversion of cyclohexane and the selectivity of the partial oxidation products were achieved to be 0.49 % and 85 % over 0.8 g of 3.5 wt.% V_2O_5/Al_2O_3, respectively, where the K/A ratio was 6.2. In addition, V_2O_5/Al_2O_3 exhibited the ability of selective oxidation of various hydrocarbons in the liquid phase. Especially, it is attracted attention that benzene was oxidized to phenol by one-step oxidation. The oxidation ability of V_2O_5/Al_2O_3 is the insertion of one oxygen atom to C-H bond and the order of priority was tertiary carbon > secondary carbon > primary carbon > benzene ring.

References

(1) Castellan, A.; Bart, J. C. J.; Cavallaro, S. *Catal. Today* **1991**, *9*, 237.

(2) Dartt, C. B.; Davis, M. E. *Ind. Eng. Chem. Res.* **1994**, *33*, 2887.

(3) Bellussi, G.; Perego, C. *Cattech* **2000**, *4*, 4.

(4) Suresh, A. K.; Sharma, M. M.; Sridhar, T. *Ind. Eng. Chem. Res.* **2000**, *39*, 3958.

(5) Schuchardt, U.; Cardoso, D.; Sercheli, R.; Pereira, R.; de Cruz, R. S.; Guerreiro, M. C.; Mandelli, D.; Spinace, E. V.; Pires, E. L. *Appl. Catal. A-Gen.* **2001**, *211*, 1.

(6) da Cruz, R. S.; Silva, J.; Arnold, U.; Schuchardt, U. *J. Mol. Catal. A-Chem.* **2001**, *171*, 251.

(7) Larsen, R. G.; Saladino, A. C.; Hunt, T. A.; Mann, J. E.; Xu, M.; Grassian, V. H.; Larsen, S. C. *J. Catal.* **2001**, *204*, 440.

(8) Masters, A. F.; Beattie, J. K.; Roa, A. L. *Catal. Lett.* **2001**, *75*, 159.

(9) Perkas, N.; Wang, Y. Q.; Koltypin, Y.; Gedanken, A.; Chandrasekaran, S. *Chem. Commun.* **2001**, 988.

(10) Perkas, N.; Koltypin, Y.; Palchik, O.; Gedanken, A.; Chandrasekaran, S. *Appl. Catal. A-Gen.* **2001**, *209*, 125.

(11) Pires, E. L.; Arnold, U.; Schuchardt, U. *J. Mol. Catal. A-Chem.* **2001**, *169*, 157.

(12) Kirillova, N. V.; Kuznetsova, N. I.; Kuznetsova, L. I.; Zaikovskii, V. I.; Koscheev, S. V.; Likholobov, V. A. *Catal. Lett.* **2002**, *84*, 163.

(13) Pillai, U. R.; Sahle-Demessie, E. *Chem. Commun.* **2002**, 2142.

(14) Sakthivel, A.; Selvam, P. *J. Catal.* **2002**, *211*, 134.

(15) Dapurkar, S. E.; Sakthivel, A.; Selvam, P. *New J. Chem.* **2003**, *27*, 1184.

(16) Guo, C. C.; Huang, G.; Zhang, X. B.; Guo, D. C. *Appl. Catal. A-Gen.* **2003**, *247*, 261.

(17) Guo, C. C.; Chu, M. F.; Liu, Q.; Liu, Y.; Guo, D. C.; Liu, X. Q. *Appl. Catal. A-Gen.* **2003**, *246*, 303.

(18) Sokmen, K.; Sevin, F. *J. Colloid Interface Sci.* **2003**, *264*, 208.

(19) Iwahama, T.; Syojyo, K.; Sakaguchi, S.; Ishii, Y. *Org. Process Res. Dev.* **1998**, *2*, 255.

(20) Sawatari, N.; Yokota, T.; Sakaguchi, S.; Ishii, Y. *J. Org. Chem.* **2001**, *66*, 7889.

(21) Tanaka, T.; Takenaka, S.; Funabiki, T.; Yoshida, S. *Chem. Lett.* **1994**, 1585.

(22) Takenaka, S.; Kuriyama, T.; Tanaka, T.; Funabiki, T.; Yoshida, S. *J. Catal.* **1995**, *155*, 196.

(23) Tanaka, T.; Takenaka, S.; Funabiki, T.; Yoshida, S. *J. Chem. Soc., Faraday Trans.* **1996**, *92*, 1975.

(24) Takenaka, S.; Tanaka, T.; Funabiki, T.; Yoshida, S. *J. Chem. Soc., Faraday Trans.* **1997**, *93*, 4151.

(25) Tanaka, T.; Ito, T.; Funabiki, T.; Yoshida, S. *Stud. Surf. Sci. Catal.* **2000**, *130*, 1961.

(26) Tanaka, T.; Ito, T.; Takenaka, S.; Funabiki, T.; Yoshida, S. *Catal. Today* **2000**, *61*, 109.

(27) Yoshida, S.; Tanaka, T.; Okada, M.; Funabiki, T. *J. Chem. Soc., Faraday Trans. 1* **1984**, *80*, 119.

(28) Tanaka, T.; Ooe, M.; Funabiki, T.; Yoshida, S. *J. Chem. Soc., Faraday Trans. I* **1986**, *82*, 35.

(29) Tanaka, T.; Nishimura, Y.; Kawasaki, S.; Ooe, M.; Funabiki, T.; Yoshida, S. *J. Catal.* **1989**, *118*, 327.

(30) Gritscov, A. M.; Shvets, V. A.; Kazansky, V. B. *Kinet. Katal.* **1974**, *15*, 1257.

(31) Gritscov, A. M.; Shvets, V. A.; Kazansky, V. B. *Chem. Phy. Lett.* **1975**, *35*, 511.

(32) Anpo, M.; Tanahashi, I.; Kubokawa, Y. *J. Phys. Chem.* **1980**, *84*, 3440.

(33) Tanaka, T.; Yamashita, H.; Tsuchitani, R.; Funabiki, T.; Yoshida, S. *J. Chem. Soc., Faraday Trans. I* **1988**, *84*, 2987.

(34) Yoshida, S.; Tanaka, T.; Hanada, T.; Hiraiwa, T.; Kanai, H.; Funabiki, T. *Catal. Lett.* **1992**, *12*, 277.

(35) Tanaka, T.; Nishimura, Y.; Kawasaki, S. I.; Funabiki, T.; Yoshida, S. *J. Chem. Soc., Chem. Commun.* **1987**, 506.

(36) Teramura, K.; Tanaka, T.; Yamamoto, T.; Funabiki, T. *J. Mol. Catal. A-Chem.* **2001**, *165*, 299.

(37) Teramura, K.; Tanaka, T.; Kani, M.; Hosokawa, H.; Funabiki, T. *J. Mol. Catal.*

A-Chem. in press.

(38) Schenck, G. O.; Frank, S. *Chem. Ber.* **1965**, *98*, 2056.

(39) Khodakov, A.; Olthof, B.; Bell, A. T.; Iglesia, E. *J. Catal.* **1999**, *181*, 205.

(40) Olthof, B.; Khodakov, A.; Bell, A. T.; Iglesia, E. *J. Phys. Chem. B* **2000**, *104*, 1516.

(41) Gao, X. T.; Wachs, I. E. *J. Phys. Chem. B* **2000**, *104*, 1261.

Part III

Photocatalytic reduction of CO_2 to CO in the presence of H_2 or CH_4 as a reductant over MgO

Abstract

MgO exhibits the activity for the reduction of CO_2 to CO under photoirradiation in the presence of H_2 or CH_4 as a reductant, although MgO is an insulating material. The present study clarified the mechanism of the CO_2 photocatalytic reduction in the presence of H_2 or CH_4 over MgO. The electron paramagnetic resonance (EPR) spectra show that a CO_2 molecule adsorbed on MgO was activated to a CO_2^-. radical under photoirradiation. In addition, it was confirmed by photoluminescence that new acceptor level built up between the valence band and the conduction band of MgO on CO_2-adsorbed MgO. The CO_2^-. radical was reduced to a surface bidentate formate or a surface bidentate acetate by H_2 or CH_4 in the dark, respectively. The surface bidentate formate anchors on MgO as a photoactive species and reduces CO_2 in the gas phase to CO since the CO_2 photocatalytic reduction proceeded over MgO absorbing HCHO or CH_3CHO and only ^{12}CO was formed in the presence of $^{12}CO_2$ over MgO modified by a ^{13}C-labeled formate under irradiation. The active species was generated from the side-on adsorption-type bidentate carbonate selectively although the two types of bidentate carbonates were detected by Fourier transform infrared (FT-IR) spectroscopy. On the other hand, the role of the surface bidentate acetate is under discussion. It is the first report that the substrate-modified insulating material exhibits activity in the CO_2 photocatalytic reduction.

Introduction

Carbon dioxide is well-known as a greenhouse effect gas. However, it is common knowledge that CO_2 is a very stable and inert compound. CO_2 cannot be easily reduced under mild conditions of room temperature and atmospheric pressure. For example, a CO_2 reforming system is recognized widely as a method to produce synthesis gas (i.e., $CO + H_2$), which can be used in chemical energy transformation systems or utilized in the Fischer-Tropsch reaction to produce liquid. The reaction formulas in the cases with H_2 or CH_4 as a reductant are as follows:

$$CO_2 + H_2 = CO + H_2O \qquad \Delta H^\circ = 9.8 \text{ kcal/mol} \qquad (1)$$

$$CO_2 + CH_4 = 2CO + 2H_2 \qquad \Delta H^\circ = 59.1 \text{ kcal/mol} \qquad (2)$$

It is well-known that these reactions are achieved at 1000 K and in 2-4 MPa over Ni catalyst. In addition, the methanation between CO_2 and H_2 ($CO_2 + 4H_2 = CH_4 + 2H_2O$), which is an important industrial process, is also carried out under high temperature and pressure. Therefore, development of a CO_2 reduction system that can proceed under mild condition is absolutely required.

Recently, the application of photocatalysts have received much attention since the photocatalytic reactions can be operated under mild conditions. Photocatalytic reduction of CO_2 is also one of the most attractive reactions in addition to photocatalytic decomposition of H_2O and photocatalytic reduction of N_2 to NH_3 because high temperature and pressure are necessary for the transformation of CO_2. In particular, from the viewpoint of natural green plant photosynthesis, there are many reports about the photocatalytic reduction of CO_2 in the presence of H_2O as a reductant over various semiconductor photocatalysts. Inoue et al.[1] have first reported that CO_2 bubbled in water is reduced to HCHO, HCOOH, and CH_3OH over various semiconductor photocatalysts such as TiO_2, ZnO, CdS, GaP, and SiC under photoirradiation of the aqueous suspension. Above all, SiC semiconductor photocatalyst exhibited the highest activity in the suspension photocatalysis system. Contemporaneously, Hemminger et al.[2] investigated the photosynthetic reaction of CO_2 and H_2O in the gas phase to form CH_4 over Pt-$SrTiO_3$. On the other hand, Fruge et al.[3] described the formation of

organic molecules from CO_2 + H_2O over Pt that included chlorophyll under visible light irradiation. These reports on the CO_2 photocatalytic reduction with H_2O having appeared from 1978 through 1980 stimulated many research groups, resulting in the active production of many following reports. The semiconductor materials applied to this reaction brought about various topics. The reported products were HCHO, HCOOH, CH_3OH, C_2H_5OH, CH_3CHO, CH_4, and C_2H_6. Halmann and co-workers[4-7] published many papers on the CO_2 photocatalytic reduction over various semiconductor materials, inspired by their photoelectrochemical results. Tennakone[8] carried out screening of the CO_2 photocatalytic reduction over various metal-supported titanium oxides (Pt, Au, Ag, Co, Pb, and Hg) and demonstrated that Hg-coated TiO_2 shows the highest activity to obtain HCHO. Tennakone et al.[9] also examined the CO_2 photocatalytic reduction with hydrous cuprous oxide ($Cu_2O \cdot xH_2O$). In the case of the suspension system, CO_2 dissolves in water and is transformed into CO_3^- or HCO_3^-. Photocatalytic reduction of carbonate and bicarbonate had been carried out in order to investigate the reaction mechanism since Chandrasekaran et al.[10] reported the photocatalytic reduction of carbonate to formaldehyde on TiO_2 powder.

On the other hand, some groups have reported the photocatalytic reduction of CO_2 with H_2O in the gas phase. Anpo and co-workers[11-15] described that highly dispersed titanium oxide on SiO_2, Vycor glass, Y-zeolite, and β-zeolite indicates activity to produce CH_4 and CH_3OH for the photoreduction of CO_2 in the presence of H_2O in the gas phase. The evolution rates of CH_4 and CH_3OH in all their reports were several nmol/g-cat·h or μmol/g-Ti·h. The activity would be very low. In addition, they investigated that $TiO_2(100)$ has a higher activity than $TiO_2(110)$ for the CO_2 photoreduction with H_2O in the gas phase.[16] Saladin et al.[17,18] reported the photosynthesis of CH_4 over irradiated TiO_2 from gaseous H_2O and CO_2. The formation of O_2 for the photoreduction of CO_2 with H_2O was first investigated by Ogura et al.[19] The maximum yield of H_2 was exhibited with highly dispersed 0.5 wt.% CeO_2-TiO_2.

There are seldom reports of the CO_2 photocatalytic reduction in the presence of reductant except H_2O. Thampi et al.[20] have already investigated the methanation of CO_2 with H_2 under mild conditions with Ru/TiO_2 catalyst, which was developed by Kohno et al.[21,22] who used Rh/TiO_2 catalyst. The photocatalytic reduction of CO_2 in the presence of H_2S as a

reductant was reported by Aliwi and Aljubori.[23] We also reported that the reduction of CO_2 takes place in the presence of H_2 or CH_4 as a reactant over irradiated ZrO_2, and then, CO and H_2 were formed in the gas phase.[24-28] The mechanism for the photocatalytic reduction of CO_2 over ZrO_2 cannot be explained by a simple band theory although ZrO_2 is also a semiconductor. According to phosphorescence excitation spectra, the emission intensity increased at above 300 nm after introduction of CO_2 although the maximum emission intensity of ZrO_2 was obtained at 270 nm.[26] It was confirmed that the band-gap excitation of zirconium oxide is unnecessary for the photocatalytic reduction of CO_2. We proposed the mechanism of the CO_2 photocatalytic reduction in the presence of H_2 or CH_4 over ZrO_2 as follows. CO_2 adsorbed on the surface of ZrO_2 is photoexcited under photoirradiation to the CO_2^-. anion radical. The CO_2^-. radical reacts with H_2 to form the surface formate. In the presence of CH_4 as a reactant, the surface acetate as well as the surface formate is generated. The surface acetate cannot react further but remains on the surfaces. The surface formate acts as a reactant of another CO_2 to CO under photoirradiation. During the reduction of CO_2 by the surface formate, the formate itself is oxidized to the adsorbed CO_2 species again. The production of CO proceeds via the two-step reaction. This suggests that the reaction can be catalyzed by materials that are not semiconductors.

In searching for many reports relevant to the CO_2 photocatalytic reduction, we found that titanium oxide and metal-loaded titanium oxide have been usually used as photocatalysts. It is noted that titanium oxide is a semiconductor photocatalyst and metals are often loaded in order to promote the charge separation. It is thought that semiconductors are well suited to the photocatalysts because photocatalytic system is based on the excitation of electrons from the valence band to the conduction band. We have reported the photocatalytic reduction of CO_2 in the presence of H_2 as a reductant over MgO.[29] It was confirmed that the photocatalytic reduction of CO_2 proceeds over MgO although MgO is an insulating material. CO and H_2 were produced in this reaction. Therefore, the mechanism of the CO_2 photocatalytic reduction cannot be explained by the simple band-gap irradiation. In the present study, we carried out the photocatalytic reduction of CO_2 over MgO in the presence of CH_4 as well as H_2. In addition, the photoactivated species on MgO was identified by electron paramagnetic

resonance spectroscopy (EPR) and luminescence.

Experimental

Materials

The magnesium oxide supplied from the Merck was hydrated in distilled water for 2 h at 353 K and filtered with a pump. After that, the sample was kept at 383 K for 24 h in an oven, followed by calcinations in air at 873 K for 3 h. The sample was ground to a powder under 100 mesh after calcination. The specific surface area is evaluated to be 110 m^2g^{-1} by the BET method using N_2 adsorption isotherm at 77 K.

Estimation of amount of chemisobed CO_2

Amount of chemisorbed CO_2 on MgO was determined by the adsorption equilibrium method as follows. MgO (0.3 g) was evacuated at 673 K as a beforehand treatment. CO_2 was introduced to MgO and an adsorption isotherm was measured at room temperature. Subsequently, CO_2 was evacuated through a N_2 liquid trap for 30 min at room temperature. After that, CO_2 was introduced to MgO and the adsorption isotherm was measured again. We subtracted the second adsorbed amount from the first one at the same equilibrium pressure to account for the physisorbed CO_2. The value obtained by the subtraction represents the amount of chemisorbed CO_2.

Reactions

Reactants were purified prior to use for reactions in the following manner. Hydrogen was purified by passing it through a liquefied nitrogen trap. Carbon dioxide, methane, and acetaldehyde were purified by vacuum distillation at the temperature of liquid nitrogen. ^{13}C-Labeled carbon dioxide and methane were commercially supplied from ICON and used without further purification. Formaldehyde was obtained by heating paraformaldehyde in a vacuum. Acetaldehyde was purified by vacuum distillation with a liquefied nitrogen trap.

The reaction was carried out in a closed static system connected to a vacuum line. A

0.3 g amount of magnesium oxide was spread on the flat bottom of a quartz reactor (dead space : 18.9 mL). Prior to photocatalytic reduction, the catalyst sample was heated at 673 K in air and evacuated for 30 min at the same temperature, followed by treatment with 8 kPa of O_2 for 90 min and evacuation for 30 min at 673 K. The mixture of substrate (CO_2, 150 μmol) and reductant (H_2 or CH_4, 50 μmol) was admitted into the reactor. The catalyst sample was irradiated from the flat bottom of the reactor through a reflection by a cold mirror with a 500 W ultrahigh-pressure mercury lamp USH-500D supplied by USHIO Co. The area subjected to illumination was 12.6 cm^2. After each reaction, the gaseous products were analyzed, and after 5 min of evacuation at room temperature the sample was heated at 673 K for 30 min and the desorbed gases were also analyzed. The analysis of the products was performed with and on-line TCD gas chromatograph (Shimadzu GC-8A) equipped with a column packed with molecular sieve 5A and with Ar as a carrier gas. When formaldehyde or acetaldehyde was used as a reaction substrate, 5 μmol of these substrates was introduced onto 0.3 g of MgO with 150 μmol of CO_2 or 50 μmol of H_2 or CH_4 in the reactor.

Fourier Transform Infrared Spectroscopy (FT-IR)

Infrared spectra of a sample and adsorbed species were recorded with a Perkin-Elmer Spectrum One Fourier transform infrared spectrometer in a transmission mode at room temperature. A magnesium oxide sample (ca. 50 mg) was pressed into a wafer (diameter = 10 mm) at a pressure of 2.0 MPa and introduced in a conventional in-situ IR cell equipped with NaCl windows. The cell allowed us to perform heating, O_2 treatment, introduction of substrates, photoirradiation, and measurements of spectra in situ. Before a measurement, the sample was evacuated at 673 K for 30 min, followed by treatment with 8 kPa of O_2 for 90 min and evacuation for 30 min at 673 K. A 250 W ultrahigh-pressure mercury lamp USH-250D supplied by USHIO Co. was used as a light source for photoirradiation of the wafer. For each spectrum, the data from 10 scans were accumulated at a resolution of $4cm^{-1}$.

Photoluminescence

Photoluminescence spectra were recorded at room temperature with a Hitachi F-3010

fluorescence spectrometer equipped with a phosphoresence unit, which enables to record 1ms-delayed spectra, and an in-situ cell. Before a measurement, the sample was pretreated under the same conditions as for FT-IR spectroscopy measurements. The effect of CO_2 adsorption on the photoluminescence was investigated by recording the spectra under the equilibrium adsorption of CO_2 at room temperature.

Electron Paramagnetic Resonance (EPR)

Electron paramagnetic resonance (EPR) spectra were recorded with an in-situ quartz cell on an X-band EPR spectrometer (JOEL JES-SRE2X) with 100 k Hz field modulation. Before a measurement, the sample was pretreated under the same condition as that of the IR spectra. The *g* values and the amount of radical species were determined by use of a Mn marker and TEMPOL (2,2,6,6-tetramethylpiperidine-1-oxyl), respectively. The effect of CO_2 adsorption onto MgO on the EPR spectra was investigated by recording the spectra after the equilibrium adsorption of CO_2 at room temperature followed by evacuation. Some spectra

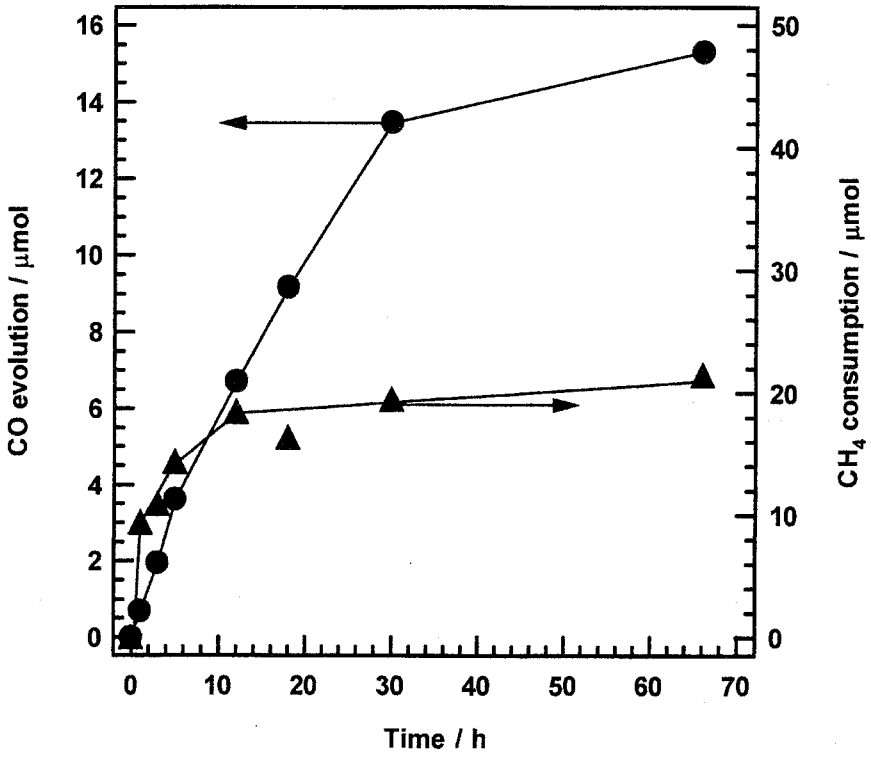

Figure 1 Time dependence of the amount of CO evolution (circle) and CH_4 consumption (triangle) over MgO under photoirradiation.

were recorded under illumination from a 500 W ultrahigh-pressure mercury lamp USH-500D supplied by USHIO Co. Particular attention was paid to the removal of oxygen contamination to prevent the interference of the superoxide anion with the spectra. Prior to introduction into the cell, methane was passed through a Pt catalyst bed maintained at 473 K, and then through a liquid nitrogen trap. CO_2 was purified by a freeze-pump-thaw process with a liquid nitrogen trap for several cycles.

Results and Discussion

Reactions

The products were CO and H_2 in the photocatalytic reduction of CO_2 with CH_4. CO (3.6 μmol) and H_2 (0.05 μmol) were formed over MgO in the presence of CO_2 and CH_4 under photoirradiation for 5 h at room temperature. In a previous study, we reported the photocatalytic reduction of CO_2 in the presence of H_2 as a reductant.[29] In this case, the CO

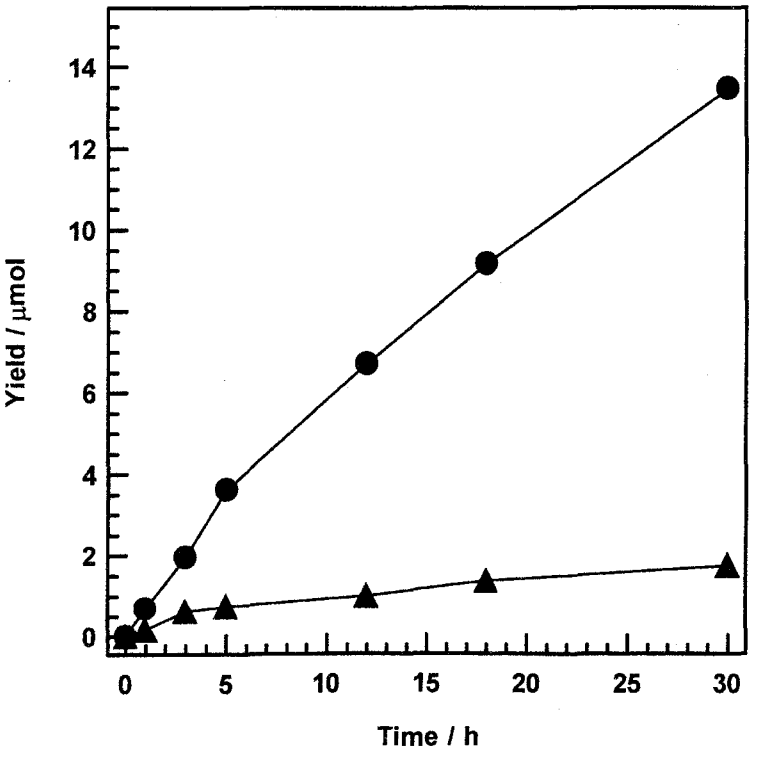

Figure 2 Time course of the CO products by the photocatalytic reaction (circle) and by the heat treatment after photoirradiation (triangle).

evolution exhibited 2.9 μmol after 6 h of photoirradiation. It was found that CH_4 as well as H_2 operates as a reductant for the photocatalytic reduction of CO_2 over MgO. In addition, we have investigated the photocatalytic reduction of CO_2 over ZrO_2.[25,28] The CO evolution over MgO was 5 times higher than that over ZrO_2. When the reaction was carried out in the dark, without a catalyst or without a reactant (H_2 or CH_4), no CO or H_2 was detected in the gas phase. Figure 1 shows the time dependence of the amount of CO evolution and CH_4 consumption over MgO under photoirradiation. The rate of the CO evolution decreased gradually and was stopping after 30 h of photoirradiation. The evolution of CO and H_2 was 13.5 and 0.68 μmol after 30 h, respectively. The conversion of CO_2 was 9.0%. CH_4 was consumed exponentially until 12 h and the rate of the CH_4 consumption was constant after that. The amount of consumed CH_4 was considerably larger than that of evolved CO. The CH_4 consumption was not compatible with the CO evolution stoichiometrically. This suggests that intermediates anchor on the surface of MgO during the photocatalytic reduction of CO_2. We have confirmed that CO_2 was adsorbed on MgO readily. The origin of the carbon atom contained in the products and the surface species was determined by use of carbon isotopes (^{13}C-labeled CO_2 or CH_4). The carbon atom of either CO_2 or CH_4 was labeled by ^{13}C and the photocatalytic reduction of CO_2 with CH_4 was carried out over MgO. ^{13}CO or ^{12}CO was formed in the gas phase in the case of the $^{13}CO_2 + {}^{12}CH_4$ reaction or the $^{12}CO_2 + {}^{13}CH_4$ reaction, respectively. Therefore, all CO generated in the gas phase is derived from CO_2, and CH_4 does not merely reduce CO_2 to two CO molecules on the basis of the formula (2). In the present reaction, the role of CH_4 is the reduction of CO_2 adsorbed on MgO because only 20 μmol of CH_4 was consumed only. It is speculated that CO_2 species reduced by CH_4 anchors as an intermediate on MgO.

CO and H_2 were detected in the gas phase by heating the catalyst sample at 673 K for 30 min after the reaction. It is expected that the intermediate consists of hydrogen, carbon, and oxygen. It has been determined that formate is generated as an intermediate for the $CO_2 + H_2$ photocatalytic reaction over MgO or ZrO_2, and the amount of CO collected by heating the catalyst is equal to that of the formate formed on the surface.[24,26,27] On the other hand, it was reported that acetate is generated expect the formate for the $CO_2 + CH_4$ photocatalytic

reaction over ZrO_2.[28] Figure 2 shows the time course of the CO evolutions by the photocatalytic reaction and by the heat treatment after irradiation, respectively. The CO amount after the catalyst was heated was constant against the irradiation time after 5 h, although the CO amount after irradiation increased gradually. The behavior of the CO evolution upon heating of the catalyst sample is similar to that of the CH_4 consumption. This also indicates that the amount of the intermediates which can be formed on MgO is limited. Figure 3 shows the dependence of the amount of CO evolved by the photocatalytic reaction and by the heat treatment after photocatalytic reaction on the initial amount of introduced CO_2. There was none of the CO evolution by the photocatalytic reaction until the amount of introduced CO_2 reached 20 μmol. The CO evolution increased gradually and was constant after CO_2 reached 40 μmol. On the other hand, the CO evolution by the heat treatment after photocatalytic reaction was maximal when the amount of introduced CO_2 was 20 μmol. As mentioned previously, more than 20 μmol of CH_4 was not also consumed although light

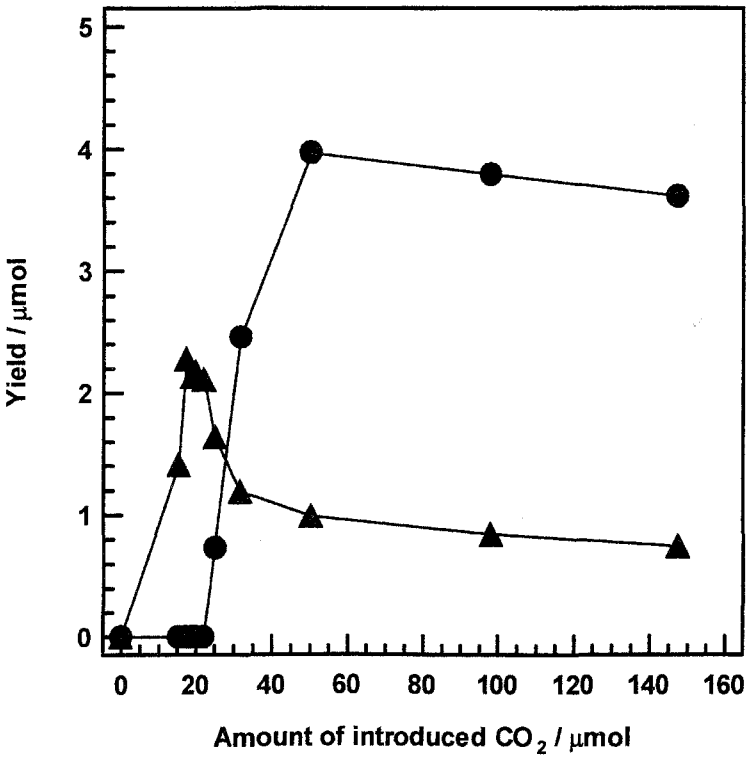

Figure 3 Dependence of the amount of CO evolved by the photocatalytic reaction (circle) and by the heat treatment after photocatalytic reaction (triangle) on the initial amount of introduced CO_2.

irradiation was elongated. Therefore, it is inferred that one CO_2 molecule was reduced by one CH_4 molecule to the intermediate species. The introduction of more than 40 μmol of CO_2 did not have a marked influence on the amount of either mode of CO evolutions.

Estimation of amount of chemisobed CO_2

In previous study, we have confirmed that about 40 μmol of CO_2 is chemisorbed on 0.3 g of MgO (133 μmol·g-MgO^{-1}).[29] The amount of chemisorbed CO_2 was determined as follows. CO_2 was trapped with a liquid N_2 after 150 μmol of CO_2 was introduced to MgO. The amount of trapped CO_2 was subtracted from that of introduced CO_2 which left the amount of chemisorbed CO_2. The amount of chemisorbed CO_2 (133 μmol·g-MgO^{-1}) was compatible with the minimum amount of introduced CO_2 in the maximum CO evolution by the photocatalytic reaction. In the present study, we obtained the adsorption isotherms of CO_2 on MgO as shown in Figure 4(a). After that, CO_2 was adsorbed on MgO again as shown in Figure 4(b). The subtraction between panels (a) and (b) was 130 μmol·g-MgO^{-1}. Thus, the

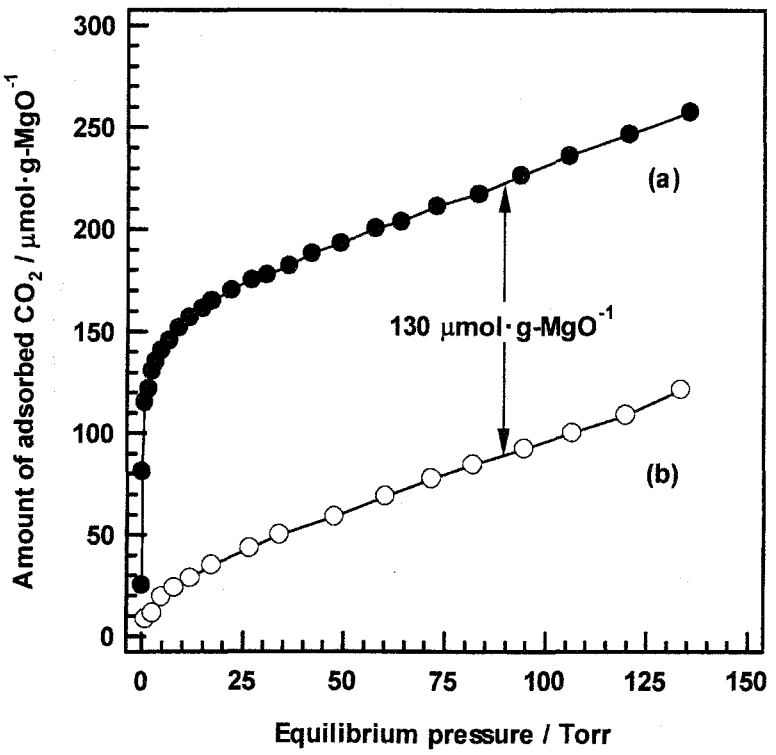

Figure 4 Adsorption isotherms of CO_2 on MgO (a) after pretreatment (closed circle) and (b) after adsorption of CO_2 and evacuation (opened circle).

amount of CO_2 chemisorbed on 0.3 g of MgO corresponds to 39 μmol. This value was almost compatible with that in previous study as mentioned above. Introduction of 66 μmol·g-MgO^{-1} of CO_2 caused the most CO evolution by the heat treatment. In addition, the CO evolution by the photocatalytic reaction could be detected in the gas phase after the amount of introduced CO_2 reached 66 μmol·g-MgO^{-1}. On the other hand, both CO evolutions by the photocatalytic reaction and by the heat treatment were constant after the amount of introduced CO_2 reached 133 μmol · g-MgO^{-1}. It is interesting that there are two different thresholds in the photocatalytic reduction of CO_2 over MgO. These results suggest that the species produced before the introduced CO_2 reached 66 μmol·g-MgO^{-1} is different from that produced after more than 66 μmol·g-MgO^{-1} of CO_2 was introduced.

Fourier Transform Infrared Spectroscopy (FT-IR)

Figure 5 represents the IR spectra of MgO after pretreatment. A peak assigned to an OH stretching vibration band [ν(OH)] of a surface hydroxyl group is observed at 3760 cm^{-1}. In addition, five bands appeared at 1507, 1422, 978, 862 (shoulder), and 844 cm^{-1}. Raman[30,31] described the 985 and 845 cm^{-1} bands as overtones of fundamental frequencies at 490 and 425

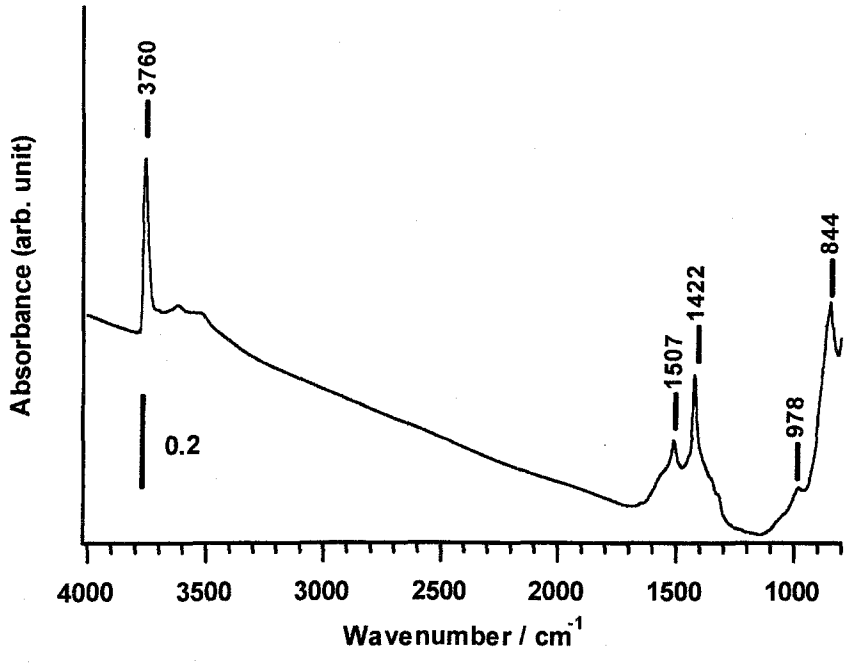

Figure 5 IR spectrum of MgO after pretreatment.

cm^{-1}, respectively. Hanna[32] and Evans and Ehateley[33] agreed with these identifications. Accordingly, the bands at 978, 862, and 844 cm^{-1} in the present study are derived from an overtone of a fundamental lattice vibration (Mg-O stretching). It is known that the bands at 1400-1500 cm^{-1} are a C-O stretching vibration band [ν(C-O)] of carbonate ions.[33,34] Davydov et al.[35] reported that the bands at 1415 and 845 cm^{-1} are assigned to an asymmetric C-O stretching vibration band [ν_{as}(C-O)] and a deformation vibration band [$\delta(CO_3^{2-})$] of carbonate ion on MgO. The bands at 1507, 1422, and 844 cm^{-1} were assigned to carbonate ions. This carbonate ion would be derived from $MgCO_3$.[33] Considering this, the band at 844 cm^{-1} would be formed by overlapping the overtone of a fundamental lattice vibration and a deformation vibration of carbonate ion. Even evacuation at 673 K cannot remove $MgCO_3$ completely, since the decomposition temperature of $MgCO_3$ is higher than 673 K. CO_2 remaining as $MgCO_3$ after pretreatment is not involved in the reaction because CO was not generated under photoirradiation without the introduction of CO_2.

Figures 6 and 7 illustrate the difference IR spectra of the adsorbed species on MgO (a) after introduction of 4.1 kPa of CO_2 and evacuation, (b) after introduction of 5.1 kPa of H_2 or 5.2 kPa of CH_4 and under photoirradiation for 18 h, and (c) after evacuation (H_2 and CH_4 were used as a reductant in Figures 6 and 7, respectively). The spectrum of pretreated MgO was used as a background of all difference IR spectra. When CO_2 was introduced to MgO, many bands appeared in the region of 1800-1250 cm^{-1} (Figures 6(a) and 7(a)). Davydov et

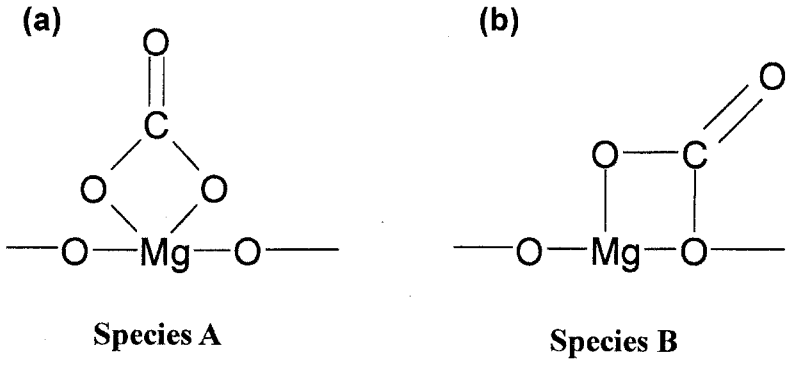

Species A **Species B**

Chart 1 Nature of two speculated species. Species A : one bidentate carbonate (stronger) and Species B : the other bidentate carbonate (weaker).

al.[35] determined that the unidentate carbonate bands at 1520, 1320, and 1020-960 cm^{-1} are an asymmetric OCO stretching vibration band [ν_{as}(OCO)], a symmetric OCO stretching vibration band [ν_{s}(OCO)] and a C-O stretching vibration band [ν(C-O)], respectively. In addition, they reported that the bicarbonate bands at 1700, 1455, and 1220 cm^{-1} are an asymmetric OCO stretching vibration band [ν_{as}(OCO)], a symmetric a OCO stretching vibration band [ν_{s}(OCO)], and a C-O stretching vibration band [ν(C-O)], respectively.[35] In our case, the unidentate carbonate and the surface bicarbonate appeared at 1526 and 1337 cm^{-1} and at 1685 and 1383 cm^{-1}, respectively. On the other hand, bands at 1661, 1631, 1346, and 1313 cm^{-1} (1666, 1631, 1340 and 1316 cm^{-1}, in Figure 7) are assigned to surface bidentate carbonates.[33,36-38] Fukuda and Tanabe[36] reported that two type of bidentate carbonate are generated at room temperature. In addition, Tsuji et al.[37] and Yanagisawa et al.[38] confirmed that the bands at 1668, 1320, 1005, and 849 cm^{-1} (species A as shown in Chart 1(a)) increase in intensity at 373 K by FT-IR spectroscopy and temperature-programmed desorption (TPD) methods, although the bands at 1630, 1277, 955, and 833 cm^{-1} (species B as shown in Chart 1(b)) disappear. It was concluded that species A is adsorbed more strongly on MgO than species B. However, the assignment of these two bidentate carbonate is under discussion. In a previous study, we also monitored the behavior of the absorbance of two bidentate bands by FT-IR spectroscopy when introduced CO_2 was increased gradually. Both species were detected in introducing a small amount of CO_2.[29] The increase in the absorbance of the bidentate bands at 1660 and 1310 cm^{-1} (species A) stopped after introduction of CO_2 exceeded 66 $\mu mol \cdot g\text{-}MgO^{-1}$. On the other hand, the bidentate band at 1624 cm^{-1} (species B) increased in absorbance when more than 66 $\mu mol \cdot g\text{-}MgO^{-1}$ of CO_2 was introduced. Therefore, in this study, it was also classified that the bands at 1661 and 1346 cm^{-1} are stronger than those at 1631 and 1313 cm^{-1}. As mentioned above, the maximum amount of the chemisorbed CO_2 was 130 $\mu mol \cdot g\text{-}MgO^{-1}$. The most CO evolution by the heat treatment was achieved upon introducing 66 $\mu mol \cdot g\text{-}MgO^{-1}$ of CO_2. The CO evolution by the photocatalytic reaction was confirmed in the gas phase when more than 66 $\mu mol \cdot g\text{-}MgO^{-1}$ of CO_2 was introduced to MgO. And, CO evolutions by both the photocatalytic reaction and by the heat treatment became constant after the amount of the introduced CO_2 reached 133 $\mu mol \cdot g\text{-}MgO^{-1}$. The

behavior obtained from the reaction is in agreement with that observed by IR spectra. In conclusion, the stronger bidentate carbonate (species A) is reduced to the mere intermediate, which is inactive for the CO evolution. In introducing more than 66 μmol·g-MgO^{-1} of CO_2, the weaker bidentate carbonate (species B) is generated except species A. The species B is reduced to a surface-active intermediate that can produce CO in the gas phase from CO_2 by H_2 or CH_4 as a reductant because the amount of the CH_4 consumption which was compatible with that of the species B evolution [66 μmol·g-MgO^{-1}].

Figures 6(b) and 7(b) show the IR spectra of MgO irradiated for 15 h in the presence of H_2 or CH_4 as a reactant after evacuation of CO_2. Increase or decrease in intensity and

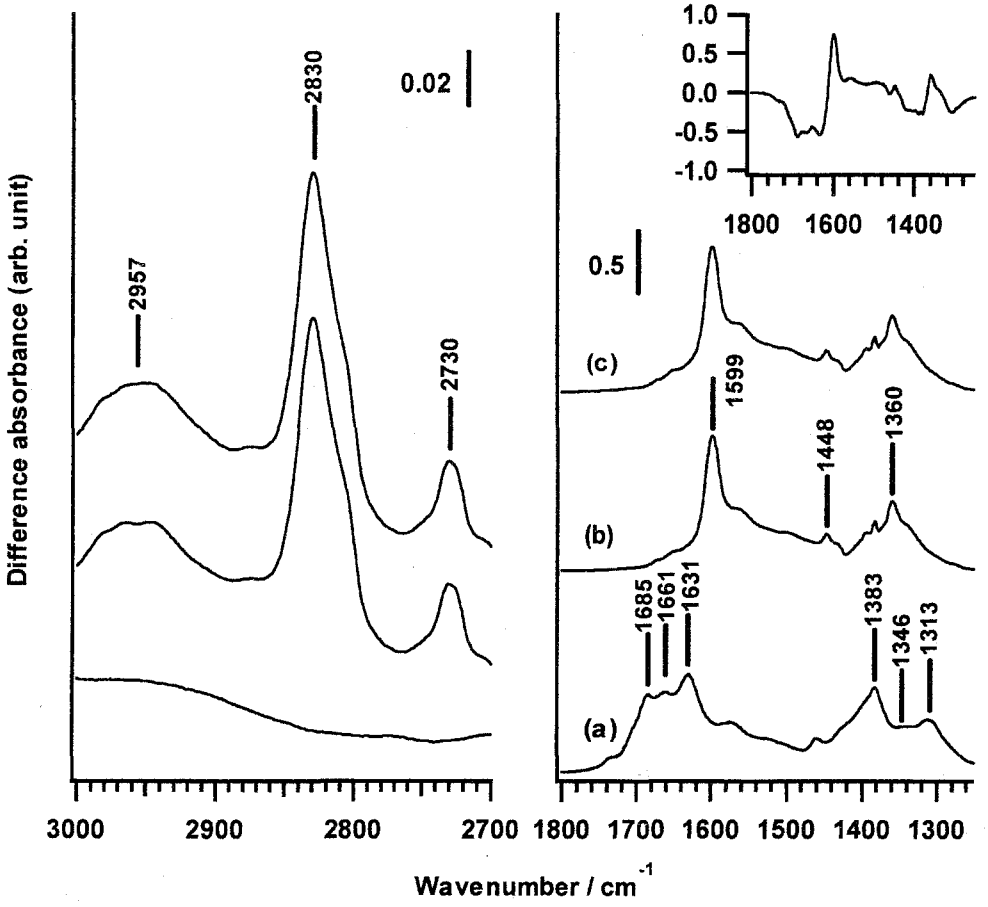

Figure 6 Difference IR spectra of the adsorbed species on MgO (a) after introduction of 3.9 kPa CO_2 and evacuation, (b) after introduction of 5.1 kPa H_2 and under photoirradiation for 18 h and (c) after evacuation. The inset illustrates the difference spectrum between (a) and (b) in the region of 1800-1250 cm^{-1}, indicating the spectrum of adsorbate.

appearance of new bands were observed in the IR spectra in the region of 2900-2700 and 1800-1250 cm^{-1}. These spectra were not changed when MgO was left for 15 h in the presence of H_2 or CH_4 in the dark. The inset picture in Figure 6 shows the subtraction of the IR spectrum of adsorbed species on MgO in the presence of H_2 before photoirradiation (Figure 6(a)) from that after photoirradiation (Figure 6(b)). New bands at 2957, 2830, and 2730 cm^{-1} appeared in the region of 2900-2700 cm^{-1} under photoirradiation. These bands are assigned to a C-H stretching vibration band [ν(CH)].[39-42] Since surface carbonates have no C-H stretching vibration mode [ν(CH)], the appearance of these bands exhibits the formation of a surface species containing a C-H bond, which we expected to be a reaction intermediate.[29] In the

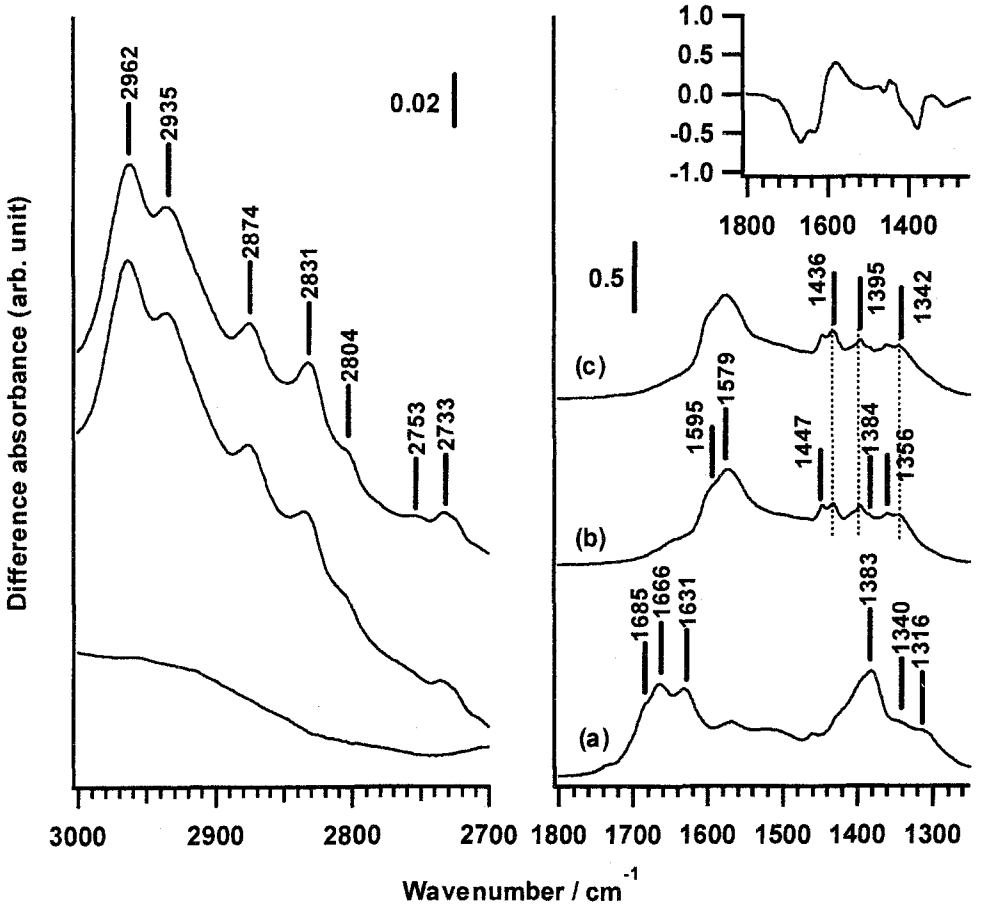

Figure 7 Difference IR spectra of the adsorbed species on MgO (a) after introduction of 3.9 kPa CO_2 and evacuation, (b) after introduction of 5.2 kPa CH_4 and under photoirradiation for 18 h and (c) after evacuation. The inset illustrates the difference spectrum between (a) and (b) in the region of 1800-1250 cm^{-1}, indicating the spectrum of adsorbate.

region of 1800-1250 cm^{-1}, new bands at 1599(ν_{as}(OCO)), 1448(δ(CH)) and 1360 cm^{-1}(ν_s(OCO)) appeared under photoirradiation[41-43], whereas the bands at 1668, 1634, and 1313cm^{-1} assigned to a bidentate carbonate and the bands at 1686, 1459, and 1383 cm^{-1} assigned to a bicarbonate decreased in intensity. Accordingly, it is anticipated that the surface bidentate carbonate and the surface bicarbonate reacted with H_2 as a reductant under photoirradiation to the surface species containing a C-H bond. We have already confirmed that the new bands at 2957, 2830, 2730, 1599, and 1360 cm^{-1} were not formed in the dark or in the absence of H_2.[29] The new bands are derived from an intermediate species formed only in the presence of H_2 under photoirradiation because the CO evolution by the heat treatment after the photoreaction is not observed without irradiation. In our previous paper[26,27,29], we identified that the intermediate for the CO_2 + H_2 reaction over ZrO_2 and MgO is a surface formate species; in addition, we found that a similar spectrum to that of the surface species was obtained when formic acid or formaldehyde was adsorbed on the surface of ZrO_2 or MgO, respectively. The difference IR spectrum of MgO irradiated for 15 h in the presence of H_2 after evacuation of CO_2 (same as Figure 6(b)) is similar to that of formaldehyde species adsorbed on pretreated MgO as shown in Figure 8. Wang and Hattori[44] reported that the bands at 2840 [ν(CH)], 1604 [ν_{as}(OCO)] and 1370 cm^{-1} [ν_s(OCO)] are assigned to a surface bidentate formate when formaldehyde is adsorbed on pretreated MgO. We have already proposed the molecular structure of the adsorbed species followed by Peng and Barteau.[45] Formaldehyde loses one hydrogen atom to connect with one lattice oxygen atom of MgO and forms a surface bidentate formate. Therefore, it was concluded that the surface species arising during the photoreaction between CO_2 and H_2 is a surface bidentate formate.

On the other hand, the inset picture in Figure 7 shows the subtraction of the IR spectrum of adsorbed species on MgO in the presence of CH_4 before photoirradiation (Figure 7(a)) from that after photoirradiation (Figure 7(b)). In the case of using CH_4 as a reductant, new bands in the region of 2900-2700 and 1800-1250 cm^{-1} were observed in addition to the bands in the case of using H_2 as a reductant and the bands at 1666, 1631, and 1316 cm^{-1} were assigned to a bidentate carbonate and the bands at 1684, 1460, and 1382 cm^{-1} were assigned to a bicarbonate decreased in intensity. In the range of 2900-2700 cm^{-1}, seven bands at 2962,

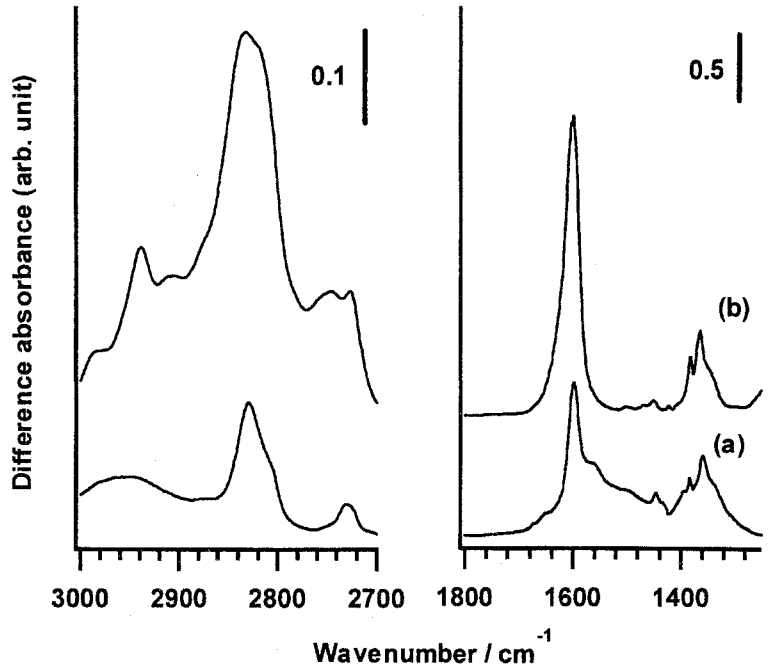

Figure 8 Difference IR spectra of the adsorbed species (a) on MgO after introduction of 5.1 kPa H_2 and under photoirradiation for 18 h (same as Figure 6(b)) and (b) on pretreated MgO after introduction of formaldehyde.

2935, 2874, 2831 2804, 2753 and 2733 cm^{-1} were observed and assigned to $\nu_{as}(CH_3)$ (2962 cm^{-1}), $\nu_s(CH_3)$ (2935 cm^{-1}) and $\nu(CH)$ (2874, 2831, 2804, 2753, and 2733 cm^{-1}).[39-42] In the range of 1800-1250 cm^{-1}, new bands appeared at 1595(s), 1579, 1447, 1436, 1395, 1384, 1356, and 1342 cm^{-1}. The bands at 1595, 1447, 1384, and 1356 cm^{-1} are assigned to $\nu_{as}(OCO)$, $\delta(CH)$, $\delta(CH)$, and $\nu_s(OCO)$, respectively, and derived from a format e because these bands were the same as that in the case of H_2 as a reductant.[41-43] In contrast, it was anticipated that the other bands were derived from an acetate. The band at 1579 cm^{-1} can be correlated to a C-O symmetric vibration mode.[46] The bands at 1436, 1395, and 1342 cm^{-1} are assigned to a C-H deformation vibration mode: $\delta_{as}(CH_3)$, $\delta(CH)$ and $\delta_s(CH_3)$, respectively.[47,48] As mentioned above, the spectrum of MgO irradiated in the presence of H_2 after evacuation of CO_2 was similar to that of pretreated MgO adsorbing formaldehyde (Figure 8). The surface species was a bidentate formate. Therefore, in the case of CH_4 as a reductant, it is expected that not only a bidentate formate but also a bidentate acetate are generated on MgO and the spectrum of MgO irradiated in the presence of CH_4 after CO_2 evacuation is similar to that of

MgO adsorbing acetaldehyde. Khaleel et al.[49] reported that the adsorbed acetaldehyde interacts with lattice oxygen and transforms to a surface bidentate acetate when acetaldehyde is introduced to MgO. Figure 9 exhibits the difference IR spectra of acetaldehyde species adsorbed on pretreated MgO as compared with Figure 7(b). The bands in the region of 3000-2700 cm and 1800-1250 cm^{-1} could be confirmed to be similar to those in Figure 7(b). Consequently, the species adsorbed on MgO converts to the surface bidentate acetate as well as the surface bidentate formate as an intermediate in the presence of CH_4 under photoirradiation after CO_2 evacuation.

We carried out the CO_2 photocatalytic reduction over MgO pretreated with HCHO or CH_3CHO to investigate the role of the surface bidentate formate and the surface bidentate acetate as an intermediate. CO was not generated in the gas phase in the presence of only HCHO or CH_3CHO as a substrate under photoirradiation. In addition, we have no CO over MgO pretreated with HCHO or CH_3CHO in the presence of CH_4 as a reductant under

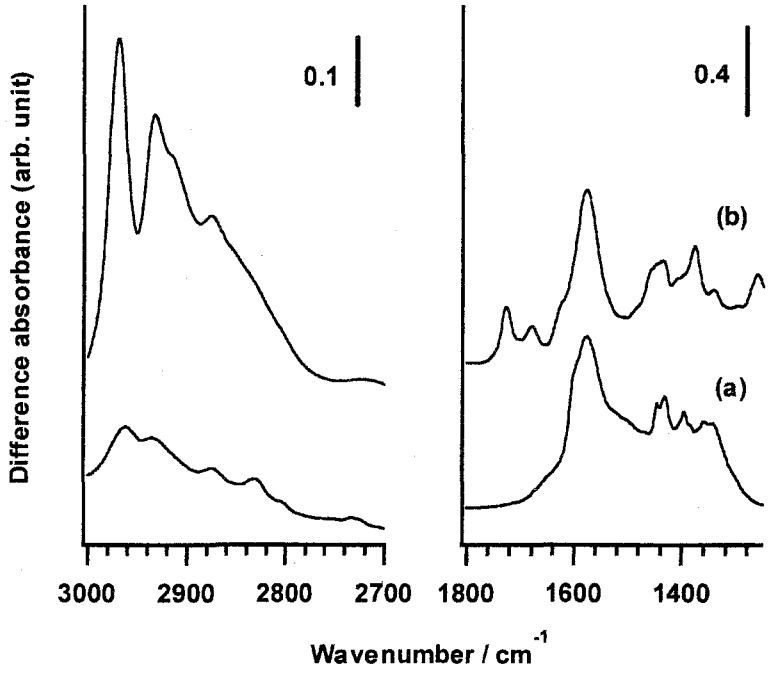

Figure 9 Difference IR spectra of the adsorbed species (a) on MgO after introduction of 5.2 kPa CH_4 and under photoirradiation for 18 h (same as Figure 7(b)) and (b) on pretreated MgO after introduction of acetaldehyde.

photoirradiation. However, CO was detected in the gas phase when CO_2 was introduced to MgO in the presence of HCHO or CH_3CHO under photoirradiation. This reaction did not proceed in the dark. The origin of the carbon atom contained in the products and the surface species was determined by use of carbon isotopes (^{13}C-labeled CO_2). The carbon atom of CO_2 was labeled by ^{13}C and the photoreaction between $^{13}CO_2$ and $H^{12}CHO$ was carried out over MgO. Only ^{13}CO was formed in the gas phase. Therefore, CO generated in the gas phase is derived from CO_2.

These results are summarized as follows. Both the stronger bidentate carbonate (species A) and the weaker bidentate carbonate (species B) are generated when CO_2 is admitted to MgO. Species A increased by priority as compared with species B until the amount of introduced CO_2 reached 66 μmol·g-MgO^{-1}. In introducing more than 66 μmol·g-MgO^{-1} of CO_2, species B increased and CO was produced in the gas phase. The CO evolution by the photocatalytic reaction and the heat treatment became constant after more than 133 μmol·g-MgO^{-1} of CO_2 is introduced to MgO. This value is compatible with the amount of CO_2 chemisorbed on MgO [130 μmol·g-MgO^{-1}]. Therefore, the same amount of Species A and Species B [66 μmol·g-MgO^{-1}] are formed on MgO, respectively. In conclusion, Species A would be connected with only magnesium atom and remain on MgO as an inactive species because there are excessive base sites of MgO. On the other hand, species B, which was adsorbed by the side-on adsorption-type form, is reduced to a surface bidentate formate or a surface bidentate acetate by H_2 or CH_4. These species are not intermediates but a photoactive species on MgO because they are very stable and reduce CO_2 in the gas phase to CO.

Photoluminescence

From the FT-IR spectroscopy, it was investigated that the photoactive species for the CO_2 photocatalytic reduction is produced from a side-on adsorption-type carbonate (species B) and reduces CO_2 to CO. The adsorption of CO_2 on MgO is related to the mechanism of formate and acetate formations. The CO_2 species adsorbed on MgO is reduced to a surface bidentate formate or acetate in the presence of H_2 or CH_4 under photoirradiation, respectively.

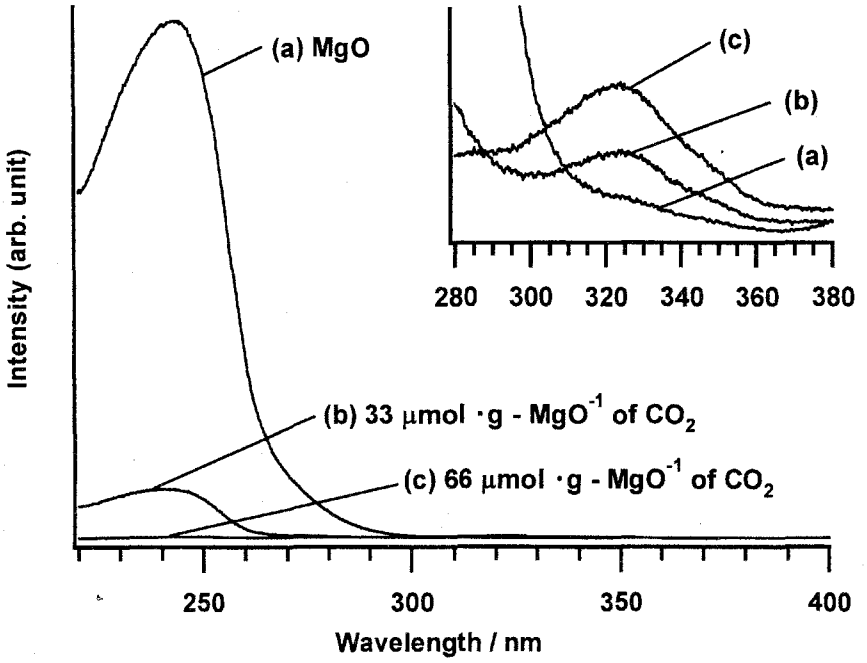

Figure 10 Phosphorescence excitation spectra of MgO (a) after pretreatment, (b) after introduction of 33 μmol·g-MgO^{-1} of CO_2 and (c) after introduction of 66 μmol·g-MgO^{-1} of CO_2.

And, the formate and the acetate contribute to the evolution of CO under photoirradiation. Therefore, it is anticipated that CO_2 adsorbed on MgO are photoactivated under photoirradiation. We have already reported the study of CO_2 adsorbed on ZrO_2 by the UV-vis spectroscopy and photoluminescence.[26] In the case of ZrO_2, we have no spectral changes in the diffuse reflectance UV-vis spectra; however, there were some peaks caused by the formation of new photoactive species in photoluminescence. In this study, we also carried out to identify a photoactive species in photoluminescence. Figure 10 shows phosphorescent excitation spectra of MgO (a) after pretreatment, (b) absorbing 33 μmol·g-MgO^{-1} of CO_2 and (c) absorbing 66 μmol·g-MgO^{-1} of CO_2, and the inset is expanded at 280-380 nm. The emission light was monitored at 450 nm, because the maximum emission intensity was obtained at around that wavelength. The maximum excitation intensity, which was observed at 240 nm (5.2 eV), was assigned to excitation of bulk MgO. This result is reasonable as compared with the absorption band in the diffuse reflectance UV-vis spectrum, although Zecchina et al.[50] described that the absorption bands of lowest energy in undamaged crystal of

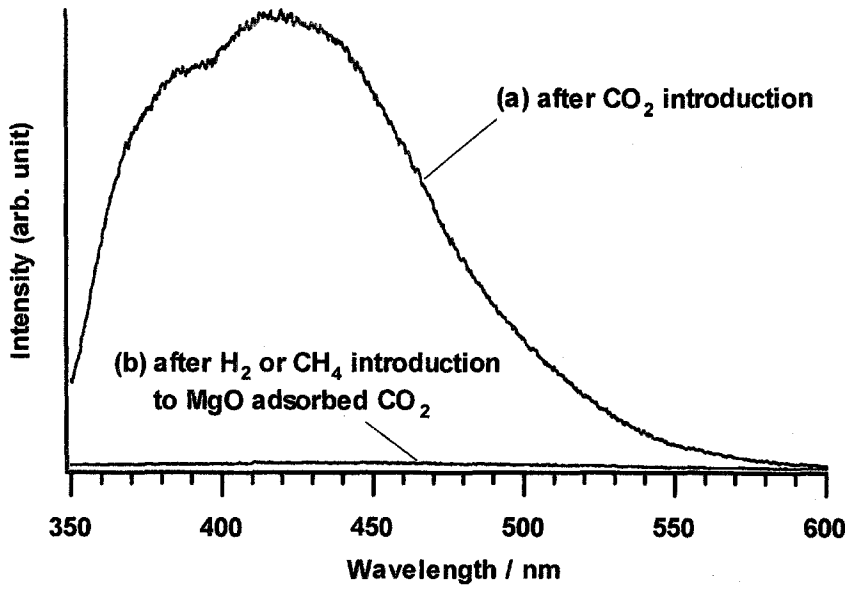

Figure 11 Phosphorescence emission spectra excited at 320 nm of MgO (a) after CO_2 introduction and (b) after H_2 or CH_4 introduction to MgO adsorbed CO_2.

MgO are at 61500 cm^{-1} (7.68 eV). On the other hand, Tench and Pott[51] reported the excitation intensity at 240 nm on MgO, in addition, Coluccia et al.[52-54] and Anpo et al.[55] investigated that the observed luminescence is derived from extrinsic lattice defects such as an F^+ center, an electron trapped at surface anion vacancy. In introducing CO_2 to MgO, the excitation intensity at 250 nm was quenched gradually. Therefore, CO_2 interacts with the extrinsic lattice defects. On the other hand, it is found that an absorption of the excitation wavelength at 320 nm increased in intensity when CO_2 was adsorbed on MgO. We obtained the same conclusion as ZrO_2. This shows that new bands build up between the valence band and conduction band of MgO. In addition, Figure 11 shows phosphorescent emission spectra excited at 320 nm of MgO (a) after CO_2 introduction and (b) after H_2 or CH_4 introduction to MgO-adsorbed CO_2. The broad peak observed at 350-600 nm was quenched after introduction of H_2 or CH_4. Thus, it is identified that the photoactive species derived from the adsorbed CO_2 interacts with H_2 or CH_4 as a reductant.

Electron Paramagnetic Resonance (EPR)

As mentioned above, we investigated whether the surface species derived from CO_2

adsorbed on MgO surface were photoactivated in a low energy. From many studies, the photoactivated CO_2 species on MgO was assigned to CO_2^-. radical species.[38,56-58] Moreover, it was reported that CO_2 interacts with an F^+ center of MgO. We also measured EPR spectra to clarify the photoactivated CO_2 species in the present reaction. Figure 12 shows the EPR spectra of MgO with adsorbed CO_2 species. A signal derived from Mn^{2+} as an impurity appeared as shown in Figure 12(a). This signal did not change although CO_2 was introduced to MgO in the dark. However, sharp signals (g = 1.998, 2.002 and g = 2.007, 2.011, 2.022) of two radical species were observed under photoirradiation. Only one signal (g = 2.001) was monitored when MgO was illuminated in the absence of CO_2. This signal was assigned to color center of MgO. Figure 13 represents the EPR spectra of MgO with adsorbed $^{13}CO_2$ species. Each signal was split into two when $^{13}CO_2$ was adsorbed instead of $^{12}CO_2$. Therefore,

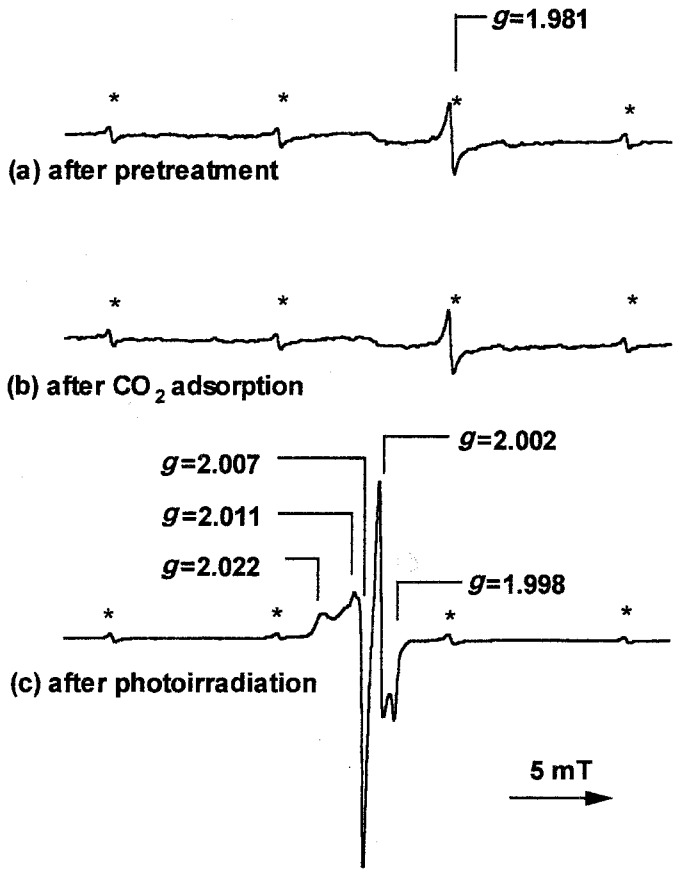

Figure 12 EPR spectra of MgO (a) after pretreatment, (b) after CO_2 adsorption and (c) after photoirradiation. * : Mn^{2+} impurity in MgO.

the signals in Figure 12(c) were not derived from MgO but the CO_2 species adsorbed on MgO. It was reported that g = 1.998, 2002 and g = 2.007, 2.011, 2.022 are assigned to a CO_2^-. radical and a CO_3^-. radical, respectively.[59-67] Our results are also supported by this assignment. In our case, the signals of the CO_2^-. radical and the CO_3^-. radical remained after 1 h although the light illumination was stopped. This indicates that the photoactivated species on MgO is very stable in the dark after photoirradiation. On the other hand, the CO_2^-. radical and CO_3^-. radical, the photoactivated species on MgO, reacts with H_2 or CH_4 as a reductant readily. When H_2 or CH_4 was introduced to MgO in the dark, the signals derived from the CO_2^-. radical and CO_3^-. radical disappeared in short order. In addition, the CO_2^-. radical species vanished more quickly than the CO_3^-. radical species. It is concluded that the CO_2^-. radical is reduced by H_2 or CH_4 to the formate or the acetate rather than the CO_3^-. radical in the present reaction.

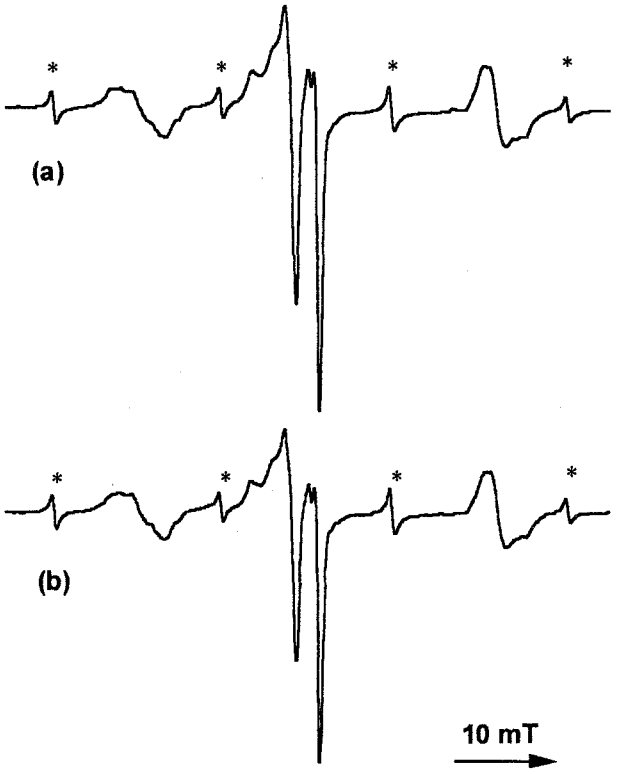

Figure 13 EPR spectra of MgO (a) after $^{13}CO_2$ adsorption under photoirradiation and (b) on standing for 1 h in the dark. * : Mn^{2+} impurity in MgO.

Reaction Mechanism

From these results, we proposed the mechanism of the CO_2 photocatalytic reduction in the presence of H_2 or CH_4 as a reductant as shown in Scheme 1. The two bidentate carbonate are generated on MgO in introducing CO_2 as shown in Chart 1. Species A is the stronger bidentate carbonate than species B. The bidentate carbonates are activated under photoirradiation and are converted to a CO_2^-. radical or a CO_3^-. radical. The CO_3^-. radical derived from species A would be transformed to the bicarbonate, which is inactive for the CO_2 photocatalytic reduction. On the other hand, the CO_2^-. radical species derived from species B is reduced to a surface bidentate formate in the presence of H_2 or CH_4. The surface bidentate formate is very stable on MgO and reduced CO_2 in the gas phase to CO under photoirradiation. In the case of using CH_4 as a reductant, a surface bidentate acetate as well as a surface bidentate formate is generated on MgO. We speculate about the role of the acetate on MgO and suggest the following two possibilities: (1) a surface bidentate acetate is also an active species for CO_2 photocatalytic reduction, and (2) an inactive acetate is transformed to

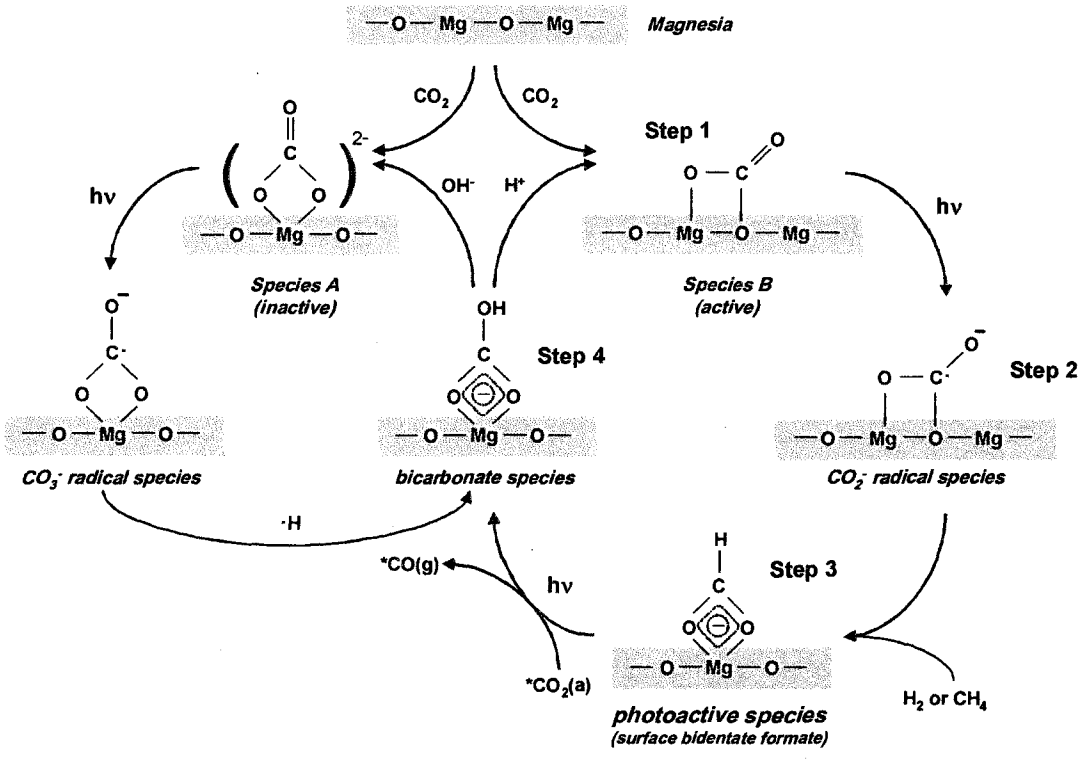

Scheme 1 Mechanism of photocatalytic reduction of CO_2 in the presence of H_2 or CH_4.

an active formate. In the case of the $CH_3CHO + CO_2$ reaction, the activity was lower than that of the $CO_2 + CH_4$ reaction. On the other hand, it was confirmed by FT-IR spectroscopy that a surface formate was formed on MgO when acetaldehyde was introduced to MgO. We cannot assert whether the acetate species is active or not. In conclusion, we observed that the surface bidentate formate is a photoactive species for the CO_2 photocatalytic reduction and will discuss the role of the surface bidentate acetate in a future paper.

Conclusion

In the present study, we uncovered the mechanism of the CO_2 photocatalytic reduction in the presence of H_2 or CH_4 as a reductant. CO_2 adsorbed on MgO is activated to a CO_2^-. radical under photoirradiation and the CO_2^-. radical was reduced to the surface bidentate formate in the presence of H_2 and CH_4 in the dark. It was identified that the photoactive species is the surface bidentate formate. This species which was very stable on MgO were reduced CO_2 in the gas phase to CO under photoirradiation. In addition, it was clarified that the species was derived from the only side-on adsorption-type bidentate carbonate although the two bidentate carbonate were detected by FT-IR spectroscopy. It is isolated that the photocatalytic reaction proceeds over the stable species adsorbed on insulating materials such as MgO. This phenomenon is not explained by the conventional band theory, which is based on the excitation of electrons from the valence band to the conduction band of semiconductor material. We proposed the new concept to the band theory for the photocatalytic reaction.

References

(1) Inoue, T.; Fujishima, A.; Konishi, S.; Honda, K. *Nature* **1979**, *277*, 637.

(2) Hemminger, J. C.; Carr, R.; Somorjai, G. A. *Chem. Phys. Lett.* **1978**, *57*, 100.

(3) Fruge, D. R.; Fong, G. D.; Fong, F. K. *J. Am. Chem. Soc.* **1979**, *101*, 3694.

(4) Halmann, M. *Nature* **1978**, *275*, 115.

(5) Aurian-Blajeni, B.; Halmann, M.; Manassen, J. *Sol. Energy* **1980**, *25*, 165.

(6) Halmann, M.; Katzir, V.; Borgarello, E.; Kiwi, J. *Sol. Energy Mater.* **1984**, *10*, 85.

(7) Halmann, M.; Ulman, M.; Aurianblajeni, B. *Sol. Energy* **1983**, *31*, 429.

(8) Tennakone, K. *Sol. Energy Mater.* **1984**, *10*, 235.

(9) Tennakone, K.; Jayatissa, A. H.; Punchihewa, S. *J. Photochem. Photobiol. A-Chem.* **1989**, *49*, 369.

(10) Chandrasekaran, K.; Thomas, J. K. *Chem. Phys. Lett.* **1983**, *99*, 7.

(11) Anpo, M.; Chiba, K. *J. Mol. Catal.* **1992**, *74*, 207.

(12) Anpo, M.; Yamashita, H.; Ichihashi, Y.; Ehara, S. *J. Electroanal. Chem.* **1995**, *396*, 21.

(13) Anpo, M.; Yamashita, H.; Ikeue, K.; Fujii, Y.; Zhang, S. G.; Ichihashi, Y.; Park, D. R.; Suzuki, Y.; Koyano, K.; Tatsumi, T. *Catal. Today* **1998**, *44*, 327.

(14) Ikeue, K.; Yamashita, H.; Anpo, M.; Takewaki, T. *J. Phys. Chem. B* **2001**, *105*, 8350.

(15) Ikeue, K.; Nozaki, S.; Ogawa, M.; Anpo, M. *Catal. Lett.* **2002**, *80*, 111.

(16) Yamashita, H.; Kamada, N.; He, H.; Tanaka, K.; Ehara, S.; Anpo, M. *Chem. Lett.* **1994**, 855.

(17) Saladin, F.; Forss, L.; Kamber, I. *J. Chem. Soc.-Chem. Commun.* **1995**, 533.

(18) Saladin, F.; Alxneit, I. *J. Chem. Soc.-Faraday Trans.* **1997**, *93*, 4159.

(19) Ogura, K.; Kawano, M.; Yano, J.; Sakata, Y. *J. Photochem. Photobiol. A-Chem.* **1992**, *66*, 91.

(20) Thampi, K. R.; Kiwi, J.; Gratzel, M. *Nature* **1987**, *327*, 506.

(21) Kohno, Y.; Hayashi, H.; Takenaka, S.; Tanaka, T.; Funabiki, T.; Yoshida, S. *J. Photochem. Photobiol. A-Chem.* **1999**, *126*, 117.

(22) Kohno, Y.; Yamamoto, T.; Tanaka, T.; Funabiki, T. *J. Mol. Catal. A-Chem.* **2001**, *175*, 173.

(23) Aliwi, S. M.; Aljubori, K. F. *Sol. Energy Mater.* **1989**, *18*, 223.

(24) Kohno, Y.; Tanaka, T.; Funabiki, T.; Yoshida, S. *Chem. Commun.* **1997**, 841.

(25) Kohno, Y.; Tanaka, T.; Funabiki, T.; Yoshida, S. *Chem. Lett.* **1997**, 993.

(26) Kohno, Y.; Tanaka, T.; Funabiki, T.; Yoshida, S. *J. Chem. Soc., Faraday Trans.* **1998**, *94*, 1875.

(27) Kohno, Y.; Tanaka, T.; Funabiki, T.; Yoshida, S. *Phys. Chem. Chem. Phys.* **2000**, *2*, 2635.

(28) Kohno, Y.; Tanaka, T.; Funabiki, T.; Yoshida, S. *Phys. Chem. Chem. Phys.* **2000**, *2*, 5302.

(29) Kohno, Y.; Ishikawa, H.; Tanaka, T.; Funabiki, T.; Yoshida, S. *Phys. Chem. Chem. Phys.* **2001**, *3*, 1108.

(30) Raman, C. V. *Proc. Indian. Acad. Sci.* **1947**, *26A*, 339.

(31) Raman, C. V. *ibid.* **1961**, *54A*, 205.

(32) Hanna, R. *J. Am. Ceram. Soc.* **1965**, *48*, 376.

(33) Evans, J. V.; Ehateley, T. L. *Trans. Faraday Soc.* **1967**, *63*, 2769.

(34) Jung, H. S.; Lee, J. K.; Kim, J. Y.; Hong, K. S. *J. Colloid Interface Sci.* **2003**, *259*, 127.

(35) Davydov, A. A.; Rubene, N. A.; Budneva, A. A. *Kinet. Katal.* **1979**, *19*, 779.

(36) Fukuda, Y.; Tanabe, K. *Bull. Chem. Soc. Jpn.* **1973**, *46*, 1616.

(37) Tsuji, H.; Shishido, T.; Okamura, A.; Gao, Y. Z.; Hattori, H.; Kita, H. *J. Chem. Soc.-Faraday Trans.* **1994**, *90*, 803.

(38) Yanagisawa, Y.; Takaoka, K.; Yamabe, S.; Ito, T. *J. Phys. Chem.* **1995**, *99*, 3704.

(39) He, M. Y.; Ekerdt, J. G. *J. Catal.* **1984**, *87*, 381.

(40) Busca, G.; Lamotte, J.; Lavalley, J. C.; Lorenzelli, V. *J. Am. Chem. Soc.* **1987**, *109*, 5197.

(41) Shido, T.; Asakura, K.; Iwasawa, Y. *J. Catal.* **1990**, *122*, 55.

(42) Feng, O. Y.; Kondo, J. N.; Maruya, K.; Domen, K. *J. Chem. Soc.-Faraday Trans.* **1997**, *93*, 169.

(43) Martin, C.; Martin, I.; Rives, V. *J. Mol. Catal.* **1992**, *73*, 51.

(44) Wang, G. W.; Hattori, H. *J. Chem. Soc., Faraday Trans. I* **1984**, *80*, 1039.

(45) Peng, X. D.; Barteau, M. A. *Langmuir* **1989**, *5*, 1051.

(46) Xu, C.; Koel, B. E. *J. Chem. Phys.* **1995**, *102*, 8158.

(47) Garcia, A. R.; da Silva, J. L.; Ilharco, L. M. *Surf. Sci.* **1998**, *415*, 183.

(48) Natal-Santiago, M. A.; Hill, J. M.; Dumesic, J. A. *J. Mol. Catal. A-Chem.* **1999**, *140*,

199.

(49) Khaleel, A.; Kapoor, P. N.; Klabunde, K. J. *Nanostruct. Mater.* **1999**, *11*, 459.

(50) Zecchina, A.; Lofthouse, M. G; Stone, F. S. *Faraday Trans. 1* **1975**, *71*, 1476.

(51) Tench, A. J.; Pott, G. T. *Chem. Phys. Lett.* **1974**, *26*, 590.

(52) Coluccia, S.; Deane, A. M.; Tench, A. J. *J. Chem. Soc., Faraday Trans. 1* **1978**, *74*, 2913.

(53) Coluccia, S.; Tench, A. J.; L., S. R. *J. Chem. Soc., Faraday Trans. 1* **1979**, *75*, 1769.

(54) Coluccia, S.; Barton, A.; Tench, A. J. *J. Chem. Soc., Faraday Trans. 1* **1981**, *77*, 2203.

(55) Anpo, M.; Yamada, Y.; Kubokawa, Y.; Coluccia, S.; Zecchina, A.; Che, M. *J. Chem. Soc., Faraday Trans. 1* **1988**, *84*, 751.

(56) Willner, I.; Maidan, R.; Mandler, D.; Durr, H.; Dorr, G; Zengerle, K. *J. Am. Chem. Soc.* **1987**, *109*, 6080.

(57) Fujiwara, H.; Hosokawa, H.; Murakoshi, K.; Wada, Y.; Yanagida, S.; Okada, T.; Kobayashi, H. *J. Phys. Chem. B* **1997**, *101*, 8270.

(58) Kaneco, S.; Shimizu, Y.; Ohta, K.; Mizuno, T. *J. Photochem. Photobiol. A-Chem.* **1998**, *115*, 223.

(59) Lunsford, J. H.; Jayne, J. P. *J. Phys. Chem.* **1965**, *69*, 2182.

(60) Serway, R. A.; Marshall, S. A. *J. Chem. Phys.* **1967**, *46*, 1949.

(61) Serway, R. A.; Marshall, S. A. *J. Chem. Phys.* **1968**, *47*, 868.

(62) Smart, R. S. C.; Slager, T. L.; Little, L. H.; Greenler, R. G. *J. Phys. Chem.* **1973**, *77*, 1019.

(63) Meriaudeau, P.; Vedrine, J. C.; Taarit, Y. B.; Naccache, C. **1975**, *71*, 736.

(64) Kai, A.; Miki, T. *Radiat. Phys. Chem.* **1992**, *40*, 469.

(65) Noethig-Laslo, V.; Brecevic, L. *J. Chem. Soc.-Faraday Trans.* **1998**, *94*, 2005.

(66) Noethig-Laslo, V.; Brecevic, L. *Phys. Chem. Chem. Phys.* **1999**, *1*, 3697.

(67) Noethig-Laslo, V.; Brecevic, L. *Phys. Chem. Chem. Phys.* **2000**, *2*, 5328.

Summary

The author focused on three photocatalytic reactions and determined the reaction mechanism on the basis of characterization of catalyst, reaction analysis by changing the condition and kinetics. The first one is photoassisted selective catalytic reduction of NO with NH_3 in the presence of O_2, the second is selective photo-oxidation of hydrocarbons in the liquid phase and the last is photocatalytic reduction of CO_2 in the presence of H_2 or CH_4 as a reductant. The main results are summarized as follows;

In Part I, the author investigates the photoassisted selective catalytic reduction of NO with ammonia in the presence of oxygen. The reaction mechanism and the electron transfer between TiO_2 and NH_3 adsorbed on TiO_2 were discussed. The intermediate was identified by means of FT-IR and EPR spectroscopy.

In chapter 1, the author describes the photo-assisted selective catalytic reduction (photo-SCR) with NH_3 over Rb-ion-modified silica-supported vanadium oxide (Rb-VS). Rb-VS exhibited the activity for photo-SCR of NO with NH_3 in the presence of oxygen at room temperature. V_2O_5/SiO_2 and SiO_2 did not promote the photo-SCR either in the dark or under photoirradiation. The reaction mechanism over irradiated Rb-VS is different from the conventional NO*x* SCR with ammonia. It is speculated that NO*x* is firstly adsorbed over irradiated Rb-VS in the presence of O_2, followed by adsorption of NH_3.

In chapter 2, the reactivity of TiO_2 for the photo-SCR with NH_3 in the presence of O_2 is described. 83 % of NO conversion and 96 % of N_2 selectivity were achieved in the photo-SCR system over TiO_2 photocatalyst (JRC-TIO-4 equivalent to Degussa P-25) in the conventional fixed bed flow system. In the absence of O_2, N_2O was generated in addition to N_2. In comparison with various TiO_2 photocatalysts, JRC-TIO-1, JRC-TIO-3 and ST-01 demonstrated the most excellent NO conversion. The specific surface area of three samples used in the photo-SCR is almost the same as to be ca. 40 m^2g^{-1}. However, the surface area is not the factor which controls the activity of the photo-SCR because ST-31 exhibited very low activity despite high surface area. On the other hand, the crystal phase of JRC-TIO-3 was

rutile although that of JRC-TIO-1 and ST-01 was detected as anatase by XRD. Therefore, the crystal phase is not also an important factor to affect the activity of the photo-SCR. N_2 was evolved in the gas phase when NO was flowed over TiO_2 pretreated by NH_3 and TiO_2 was illuminated by Xe lamp. It was concluded that the photo-SCR reaction proceeds according to Eley-Rideal mechanism. NO in the gas phase attacks NH_3 adsorbed on the Lewis acid site of TiO_2. The strength and/or quantity of the Lewis acid site related to NH_3 adsorption had an influence on the N_2 evolution. Therefore, the surface acid property of TiO_2 is an important factor to control the N_2 evolution. In addition, the reaction orders of gases (NO, NH_3 and O_2) and light intensity were determined by the kinetic studies. The rate-determining step of the photo-SCR over TiO_2 is the process of decomposition of a NH_2NO intermediate under excess O_2 concentration or that of re-oxidation of Ti^{3+} to Ti^{4+} under O_2 concentration below 2 %.

In chapter 3, the reaction analysis carried out using the closed circulating system and the observation by FT-IR spectroscopy was described. The produced nitrogen gas detected was $^{15}N^{14}N$ on using ^{15}NO and $^{14}NH_3$. Each N atom of a N_2 molecule was originated from NH_3 and NO. As mentioned above, N_2O was generated in the absence of O_2. In this case, $^{15}N_2O$ was detected in the $^{15}NO + {}^{14}NH_3$ reaction. It was concluded that NO plays a role as an oxidant which re-oxidizes Ti^{3+} species to Ti^{4+} species in the absence of O_2. The FT-IR spectroscopy exhibited that NH_3 is adsorbed on the Lewis acid site of TiO_2 in the dark. In addition, it is speculated that the adsorption of NH_3 to TiO_2 results in the formation of Ti-NH_2 and Ti-OH after the cleavage of Ti-O-Ti bond. The bands due to NH_3 adsorbed on the Lewis acid site of TiO_2 decreased in intensity in contact with NO under photoirradiation accompanied by the appearance of the NH_2NO intermediate and the evolution of H_2O. This suggests that NO attacks adsorbed NH_3 to produce the NH_2NO intermediate like Eley-Ridial mechanism and N_2 and H_2O are generated via the decomposition of the NH_2NO intermediate. On the other hand, NO converts to nitrate species via NO_2 in the presence of O_2 when Ti sites are not occupied by NH_3. Nitrate species forms Brønsted acid site and stocks NH_3 species as an ammonium ion. The nitrate species poisons the Ti site and the activity gets lower due to the stability of nitrate species. In conclusion, the NO consumption rate kept high level stably in the fixed bed flow system as described in chapter 2 because the active sites are steadily

covered with adsorbed species.

In chapter 4, the author confirmed the formation of stable NH_2 radical over UV-irradiated TiO_2 by EPR spectroscopy. NH_3 was introduced to TiO_2 and subsequently evacuated, followed by photoirradiation with a 500 W ultrahigh-pressure mercury lamp equipped with UV-33 cut filter. New EPR signals were observed as soon as TiO_2 adsorbing NH_3 was illuminated at 123 K. The author simulated the obtained EPR spectrum of TiO_2 adsorbing $^{14}NH_3$ or $^{15}NH_3$ under photoirradiation and determined the hyperfine tensors of the nitrogen-14 or -15-labeled NH_2 radical. These signals were quite stably present even at 123 K for more than one hour after the irradiation was ceased. In addition, the lines assigned to the NH_2 radical vanished away on introducing NO in the dark, whereas the lines due to the Ti^{3+} species increased in intensity. Taking these results into account, the author can conclude that NO in the gas phase attacks NH_3 adsorbed on TiO_2. In addition, a spin state of NO, a doublet, coincides with that of the NH_2 radical. In conclusion, the author proposed that the electron transfer takes place from the N atom of NH_3 adsorbed on TiO_2 to the Ti atom of TiO_2 bulk. In other words, the electron is trapped on Ti atom and the hole is captured by the NH_2^- species evolved from the fission of NH_3 adsorbed on TiO_2. The stability of the NH_2 radical causes the high reaction cross section with NO and it is quenched just after introduction of NO leaving the Ti^{3+} species.

In Part II, the selective photo-oxidation of various hydrocarbons is described. The author found that V_2O_5/Al_2O_3 exhibited the most high activity in four supports and the cyclohexane photo-oxidation consists of some reactions included the photochemical reactions as well as the photocatalytic reactions. From the results, two important factors for the improvement of photocatalytic system were derived. The author applied these factors to the selective photo-oxidation of other hydrocarbons successfully.

In chapter 5, the author describes the results of photo-oxidation of cyclohexane with gaseous oxygen over various supported vanadium oxides. Cyclohexanol, cyclohexanone and CO_2 were obtained as main products under irradiation of the light, and the formation of trace amount of cyclohexanediol and cyclohexanedione was confirmed. Any products were not

detected in the dark at all, indicating that all the catalyst samples showed photoactivity. Alumina-supported vanadium oxide exhibited specific photocatalytic performance in the selective oxidation of cyclohexane to produce cyclohexanone. No products were formed under photo-irradiation of neither alumina nor V_2O_5. Higher loading of vanadium oxide (above 5 wt.%) on alumina support resulted in reducing activity, suggesting that the active species are stable isolated-VO_4 on alumina.

In chapter 6, the author describes the selective photo-oxidation of cyclohexane over V_2O_5/Al_2O_3 in detail and discussed on the elementary reactions of cyclohexane photo-oxidation. V_2O_5/Al_2O_3 exhibited the high selectivity to partial oxidation compounds (cyclohexanol and cyclohexanone) as compared with TiO_2 in the photo-oxidation of cyclohexane in the liquid phase. The formation scheme of cyclohexanol is different from that of cyclohexanone. It was clarified that the photo-decomposition of ketone (Norrish Type I reaction) contributes to the evolution of cyclohexanol. The features of the reaction are a high selectivity to partial oxidation products and a reasonable ketone/alcohol ratio (K/A ratio). However, by elongation of the photoirradiation time, cyclohexyl hexanoate as a by-product was generated and the K/A ratio decreased gradually. The author clarified that the K/A ratio and the selectivity to the partial oxidation compounds can be controlled by the O_2 concentration and the irradiated wavelength, respectively. The most important factors are

(1) The O_2 concentration should be kept above 30 % to achieve the high K/A ratio.

(2) The irradiated wavelength $\lambda < 300$ nm should be cut off to inhibit the formation of CO_2 and the ester compound as a by-product.

To maintain the high K/A ratio, the author carried out the photo-oxidation of cyclohexane over V_2O_5/Al_2O_3 with keeping the O_2 concentration at 80 %, and to avoid the formation of ketene and CO_2, we cut off light with the wavelengths $\lambda < 330$ nm. No ester by-product was produced under this condition. Further, the evolution of cyclohexanone became dominant and the high K/A ratio was achieved. After 24 h, 0.33 % of the conversion and 87 % of selectivity were achieved with the K/A ratio of 3.8.

In chapter 7, the application of V_2O_5/Al_2O_3 photocatayst to the selective photo-oxidation of other hydrocarbons is described. The author optimized the loading amount

of V_2O_5/Al_2O_3 in the selective photo-oxidation of cyclohexane and cyclopentane. More than 0.22 mmol of isolated VO_4 species of V_2O_5/Al_2O_3 exhibited the highest evolution of the partial oxidation products (alcohol and ketone) in the oxidation of cyclohexane and cyclopentane. The conversion of cyclohexane and the selectivity of the partial oxidation products were achieved to be 0.49 % and 85 % over 0.8 g of 3.5 wt.% V_2O_5/Al_2O_3, respectively, where the K/A ratio was 6.2. In addition, V_2O_5/Al_2O_3 can selectively oxidize various hydrocarbons in the liquid phase. The priority was in the order of tertiary carbon > secondary carbon > primary carbon > benzene ring.

The part III is devoted to the proposition of new concept of photocatalysis. This chapter deals with the photocatalytic reduction of CO_2 in the presence of CH_4 as a reductant. MgO exhibits the activity for the reduction of CO_2 to CO under photoirradiation in the presence of H_2 or CH_4 as a reductant although MgO is an insulating material. The CO evolution by the photocatalytic reaction could not be detected in the gas phase before the amount of introduced CO_2 reached 66 $\mu mol \cdot g\text{-}MgO^{-1}$. Therefore, it was speculated that intermediate of the photocatalytic CO_2 reduction is generated on MgO. The EPR spectra showed that a CO_2 molecule adsorbed on MgO is activated to a CO_2^-. radical under photoirradiation. In addition, the author confirmed by photoluminescence that new accepter level builds up between the valence band and the conduction band of MgO on adsorbing CO_2 to MgO. The CO_2^-. radical was reduced to a surface bidentate formate by H_2 in the dark, on the other hand, to a surface bidentate formate and a surface bidentate acetate by CH_4 in the dark. The author identified the formation of the bidentate formate on introducing HCHO or CH3CHO to MgO. The surface bidentate formate anchors on MgO as a photoactive species and reduces CO_2 in the gas phase to CO because the CO_2 photocatalytic reduction proceeded over MgO adsorbing HCHO or CH_3CHO and because only ^{12}CO was formed in the presence of $^{12}CO_2$ over MgO modified by a ^{13}C-labeled formate under irradiation. The active species was generated from the side-on adsorption-type bidentate carbonate selectively although the two types of bidentate carbonates were detected by FT-IR spectroscopy.

List of publications

Part I

Chapter 1.

1. Photoassisted selective catalytic reduction of NO with ammonia in the presence of oxygen at low temperature
   Tsunehiro Tanaka, Kentaro Teramura, Takuzo Funabiki
   Physical Chemistry Chemical Physics, **2000**, *2*, 2681-2682.

Chapter 2.

2. Photoassisted NO reduction with NH_3 over TiO_2 photocatalyst
   Tsunehiro Tanaka, Kentaro Teramura, Kyoko Arakaki and Takuzo Funabiki
   Chemical Communications, **2002**, 2742-2743.

3. Kinetic study of photo-SCR with NH_3 over TiO_2
   Kentaro Teramura, Tsunehiro Tanaka, Seiji Yamazoe, Kyoko Arakaki and Takuzo Funabiki
   Applied Catalysis B: Environmental, submitted.

Chapter 3.

4. TiO_2/SiO_2 photocatalysts at low levels of loading: preparation, structure and photocatalysis.
   Tsunehiro Tanaka, Kentaro Teramura, Takashi Yamamoto, Sakae Takenaka, Satohiro Yoshida and Takuzo Funabiki
   Journal of Photochemistry and Photobiology A: Chemistry, **2002**, *148*, 277-281.

5. Photoassisted selective catalytic reduction of NO with ammonia in the presence of oxygen over TiO_2
   Kentaro Teramura, Tsunehiro Tanaka and Takuzo Funabiki
   Langmuir, **2003**, *19*, 1209-1214.

Chapter 4.

6. EPR study of photoinduced electron transfer between adsorbent and adsorbed species

in photo-SCR with NH_3
Kentaro Teramura, Tsunehiro Tanaka, Takuzo Funabiki
Chemistry Letters, **2003**, *132*, 1184-1185.

7. Clarification of photoinduced electron transfer between adsorbent and adsorbed species by EPR spectroscopy
Kentaro Teramura, Tsunehiro Tanaka, Takuzo Funabiki
Langmuir, submitted.

Part II

Chapter 5.

8. Photooxidation of Cyclohexane over Alumina-Supported Vanadium Oxide Catalyst
Kentaro Teramura, Tsunehiro Tanaka, Takashi Yamamoto, Takuzo Funabiki
Journal of Molecular Catalysis A: Chemical, **2001**, *165*, 299-301.

Chapter 6.

9. Selective photo-oxidation of neat cyclohexane in the liquid phase over V_2O_5/Al_2O_3
Kentaro Teramura, Tsunehiro Tanaka, Masaya Kani, Tomohiro Hosokawa and Takuzo Funabiki
Journal of Molecular Catalysis A: Chemical, **2004**, *208*, 299-305.

Chapter 7.

10. Selective photo-oxidation of various hydrocarbons in the liquid phase over V_2O_5/Al_2O_3
Kentaro Teramura, Tsunehiro Tanaka, Tomohiro Hosokawa, Tai Ohuchi, Masaya Kani and Takuzo Funabiki
Catalysis Today, in press.

Part III

11. Photocatalytic reduction of CO_2 to CO in the presence of H_2 or CH_4 as a reductant over MgO
Kentaro Teramura, Tsunehiro Tanaka, Haruka Ishikawa, Yoshiumi Kohno and Takuzo

Funabiki
Journal of Physical Chemistry B, in press.

The following papers are not included in this thesis

12. NO Reduction with CO in the Presence of O_2 over Cu/Al_2O_3 (3) -Structural Analysis of Active Species by Means of XAFS and UV/Vis/NIR Spectroscopies-
Takashi Yamamoto, Tsunehiro Tanaka, Sosuke Suzuki, Ryoji Kuma, Kentaro Teramura, Yuan Kou, Takuzo Funabiki and Satohiro Yoshida
Topics in Catalysis, **2002**, *18*, 113-118.